

**A Full 3D Railroad System Model to Investigate Train-Substructure  
Interaction Under Dynamic Load**

by

Ahmed El-Ghandour  
B.Sc. (Cairo University) 2004  
M.Sc. (University of Illinois at Chicago) 2010

Thesis submitted in partial fulfillment of the requirements  
for the degree of Doctor of Philosophy in Civil Engineering  
in the Graduate College of the  
University of Illinois at Chicago, 2017

Chicago, Illinois

Defense Committee:

Craig D. Foster, Chair and Advisor

Didem Ozevin

Eduard Karpov

Mohsen Issa

Thomas Royston, Mechanical Engineering and Bioengineering

Copyright by  
Ahmed El-Ghandour  
2017

To my father, my mother, and my brothers,  
for believing in me, and unconditionally supporting me.

## ACKNOWLEDGMENTS

During my PhD journey I went through many hardships and struggles and I could not succeed without the help of amazing people from whom I received tremendous support to be able to make it to the finish line.

I would like to express my deepest gratitude and appreciation to my supervisor Prof. Craig Foster, who was immensely patient, generous, informative and supportive from day one until the defense day. I learned a lot from Professor Foster not only as a supervisor, but also as a teacher whose classes were very useful and informative. He was certainly the best teacher I had at UIC. Also, as a person, he taught me some personal qualities, that will last with me in my professional and personal life.

I also want to extend my gratitude to Dr. Mohamed Salah, Dr. Mohamed Shalaby, Dr. Mohamed Senousy, and Dr. James Liu for their help and guidance to improve my skills in ANSYS, especially with the APDL knowledge they kindly shared with me. Additionally, I would like to extend my appreciation to my lab mates who cheered me up whenever I was feeling down: Dr. David Weed, Milad Parvaneh, Dr. Mohammad Hosein Motamedi, Dr. Talisa Mohammad Nejad, and Dipika Gongal.

I would like to thank, as well, my committee members, Professor Didem Ozevin, Professor Eduard Karpovi, Professor Mohesen Issa, and Professor Thomas Royston for their time to read my thesis and to be part of my dissertation committee.

## ACKNOWLEDGMENTS (Continued)

I would like to extend my deepest gratitude to my brothers Tamer and Mohamed El-Ghandour, for their support and encouragement. Besides, I would like to thank my dear friends Dr. Ashraf Hamed and Dr. Mohamed Zaher, and Ahmed El-Sawi for their continuous support.

### Contribution of Authors

Chapter 1 is the literature review of the work done in the railroad field and the different models created by different researchers. this chapter shows how my dissertation adds up to the work done in the railroad area, and a big portion of it was published in El-Ghandour, Ahmed I., Martin B. Hamper, and Craig D. Foster. "Coupled finite element and multibody system dynamics modeling of a three-dimensional railroad system." Proceedings of the Institution of Mechanical Engineers, Part F: Journal of Rail and Rapid Transit 230.1 (2016): 283-294. in which I was the first author. Chapter 2 represents the first part of my research work and it was published in the same paper, where I was the main driver of the research. Martin Hamper assisted me in sections 2.3 through 2.5, my supervisor Dr. Craig Foster contributed to the writing of the manuscript. Chapter 3 represents the results of the published paper mentioned above, which was the first half of my research work. Chapter 4 represents the bridge approach problem, including the model and the results. These results will be used in a paper that will be submitted very soon to one of the scientific journals and I will be the first author for it, with contribution of my supervisor Dr. Craig Foster. Chapter 5 represents the conclusion of the work done through the dissertation and the two cases presented. It also includes the future work that can be done to benefit from this work and what kind of problem can be solved using the same line of work.

## TABLE OF CONTENTS

<u>CHAPTER</u>	<u>PAGE</u>
<b>1 INTRODUCTION . . . . .</b>	<b>1</b>
1.1 Background and motivation . . . . .	1
1.2 Modeling using finite element method . . . . .	3
1.3 Modeling using multibody systems . . . . .	6
1.4 Coupling FEM and MBS . . . . .	7
1.5 Bridge approach problem . . . . .	8
1.6 Goal of the work . . . . .	11
1.7 Structure of this dissertation . . . . .	12
<b>2 FINITE ELEMENT MODEL . . . . .</b>	<b>13</b>
2.1 Railroad system components . . . . .	13
2.2 FE model . . . . .	14
2.3 Formulation of the floating frame of reference . . . . .	17
2.4 Contact formulation . . . . .	21
2.5 Equations of motion . . . . .	23
2.6 The nodal elimination for the coupling . . . . .	25
<b>3 VERIFICATION OF THE FE MODEL . . . . .</b>	<b>26</b>
3.1 Supported model . . . . .	31
3.2 Unsupported rail . . . . .	33
<b>4 BRIDGE APPROACH MODEL . . . . .</b>	<b>39</b>
4.1 Modeling the bridge . . . . .	39
4.1.1 FE Model . . . . .	40
4.1.2 Boundary conditions . . . . .	43
4.2 Wave reflection . . . . .	45
4.3 Results . . . . .	51
4.3.1 Vertical displacements . . . . .	52
4.3.2 The wheel/rail contact force . . . . .	62
4.4 Stresses in the substructure . . . . .	67
<b>5 CONCLUSIONS AND FUTURE WORK . . . . .</b>	<b>72</b>
5.1 Conclusions . . . . .	72
5.2 Future work . . . . .	75
<b>APPENDICES . . . . .</b>	<b>78</b>
<b>Appendix A . . . . .</b>	<b>79</b>

## TABLE OF CONTENTS (Continued)

<u>CHAPTER</u>	<u>PAGE</u>
Appendix B . . . . .	101
Appendix C . . . . .	108
Appendix D . . . . .	110
CITED LITERATURE . . . . .	111
VITA . . . . .	117

## LIST OF TABLES

<b><u>TABLE</u></b>		<b><u>PAGE</u></b>
I	Finite element model dimensions and material properties . . . . .	15
II	The mechanical properties of the wheelset. . . . .	29
III	Finite element model dimensions . . . . .	42
IV	Finite element model material properties. . . . .	44

## LIST OF FIGURES

<b>FIGURE</b>		<b>PAGE</b>
1	The 3D FE model. . . . .	16
2	Dimensions of the three substructure layers. . . . .	17
3	Definition of the reference frame. . . . .	19
4	Geometric and FE nodes. . . . .	20
5	An illustration of Recuero's model. . . . .	27
6	An illustration of the FE model. . . . .	28
7	Suspended wheelset used for the dynamic analysis. . . . .	28
8	Displacement at the middle of the flexible section of the rail. . . . .	30
9	Vertical displacement of the rail at the third sleeper when the wheel/rail contact is directly above it, the difference at the peak is approximately 16%. . . . .	32
10	Vertical displacement of the rail at the center of the fourth span when the wheel/rail contact is directly above it, the difference at the peak is approximately 9%. . . . .	33
11	Vertical displacement of the rail at the sixth sleeper when the wheel/rail contact is directly above it, the difference at the peak is approximately 16%. . . . .	34
12	The normal contact force. . . . .	35
13	Vertical displacement of the rail at the third sleeper when the wheel/rail contact is directly above it, unsupported middle sleeper. The difference at the peak is approximately 16%. . . . .	36
14	Vertical displacement of the rail at the center of the fourth span when the wheel/rail contact is directly above it, unsupported middle sleeper. The difference at the peak is approximately 5%. . . . .	37
15	Vertical displacement of the rail at the sixth sleeper when the wheel/rail contact is directly above it, unsupported middle sleeper. The difference at the peak is approximately 29%. . . . .	38
16	The normal contact force, unsupported middle sleeper. . . . .	38
17	Full 3D Finite Element Model of the bridge approach with the following color coding: Blue: Ballast, Red: Sub-ballast, Green: Sub-grade, Yellow: Deck, Orange: Abutment. . . . .	40
18	Side view of the model. . . . .	41
19	Vertical displacements of Node 44, see Figure 24a, inclined case, speed=45m/s (a) No damping (b) Modal damping. . . . .	46
20	Vertical displacements of Node 83, see Figure 24a, inclined case, speed=45m/s (a) No damping (b) Modal damping. . . . .	47
21	Vertical displacements of Node 132, see Figure 24a, inclined case, speed=45m/s (a) No damping (b) Modal damping. . . . .	49

## LIST OF FIGURES (Continued)

<u>FIGURE</u>		<u>PAGE</u>
22	Wheel-rail contact force, speed=45m/s (a) No damping (b) Modal damping. . . . .	50
23	The used two proposed slab designs (a) Rectangular slab (b) Inclined slab. . . . .	52
24	(a) Points of interests on the rail (b) Points on the approach and in the soil. . . . .	53
25	Vertical displacement of Node 44, a general rail point away from the slab effect, see Figure 24a. . . . .	54
26	Vertical displacement of Node 132, a rail point above the slab middle point, see Figure 24a. . . . .	55
27	Vertical displacement of Node 272, a rail point in the middle of the bridge, see Figure 24a. . . . .	56
28	Vertical displacements of Node 164, a rail point on last sleeper before the abutment, see Figure 24b. . . . .	56
29	Vertical displacements of Node 170, the last rail node before the abutment, see Figure 24b. . . . .	57
30	Vertical displacement of Node 176, the first rail point after the beginning of the abutment, see Figure 24b. . . . .	58
31	Vertical displacement of Node 182, a rail point on the first sleeper on the abutment, see Figure 24b. . . . .	58
32	Vertical displacement of Node 83, a rail point on last sleeper before the slab, see Figure 24a. . . . .	60
33	Vertical displacement of Node 101, a rail point on first sleeper of the slab, see Figure 24a. . . . .	60
34	Vertical displacement of a ballast node under the last sleeper before the abutment. . . . .	61
35	Vertical displacement of a subgrade node under the last sleeper before the abutment. . . . .	62
36	Wheel/rail contact force, the inset showing the area near the bridge entrance, speed=30m/s. . . . .	63
37	Wheel/rail contact force, the inset showing the area near the bridge entrance, speed=45m/s. . . . .	64
38	Wheel/rail contact force, the inset showing the area near the bridge entrance, speed=60m/s. . . . .	64
39	Wheel/rail contact force for the no slab case . . . . .	65
40	Wheel/rail contact force for the rectangular slab case . . . . .	65
41	Wheel/rail contact force for the inclined slab case . . . . .	66
42	Wheel/rail contact force, at the beginning of the slab, speed=30m/s. . . . .	67
43	Difference in vertical stress from unloaded case in the ballast above the middle of the slab, see Figure 24a. . . . .	68
44	Difference in vertical stress from unloaded case in the subgrade below the middle of the slab, see Figure 24a. . . . .	69

## LIST OF FIGURES (Continued)

<u>FIGURE</u>		<u>PAGE</u>
45	Difference in vertical stress from unloaded case in the ballast just before the bridge entrance, see Figure 24b. . . . .	70
46	Difference in vertical stress from unloaded case in the subgrade away of the slab effect, see Figure 24a. . . . .	71

## SUMMARY

Since the first day the railroad have been invented, it has become one of the most important methods of transportation for both passengers and goods. Millions of miles of railroads tracks are crossing the land all over the world to facilitate the transportation of passengers and different products. The importance of the railroad raised the interest of many researchers and engineers to try to understand and improve the performance of the rails.

The finite element method (FEM) has been used widely, as a very powerful numerical method, in the literature to model and investigate the performance of the different components of the railroad system. A lot of scientists used the FEM to study different issues associated with the railroad system, such as stresses in the wheel or the rail web, degradation of the ballast, soil settlement, and many other problems.

Beside the FEM, the multi-body systems dynamics (MBS) have been used by many researchers as well as the FEM in the same field. It is very useful tool especially when it comes to the dynamic analysis and investigating the vehicle performance or issues related to the wheel/rail contact. In this work, a detailed model that couples both FEM and MBS in one model is created. This model consists of a full 3D FE model that includes the different components of the railroad system (rails, sleepers, ballast, subballast, subgrade, and fasteners) using beam, solid and spring elements. The FE model is then coupled with the MBS code to extract the output of the dynamic analysis. The model was verified with the results in the literature and showed great performance. The good results of the coupled model provided a strong motivation

## SUMMARY (Continued)

to move forward with another problem, which is the bridge approach problem in this work. A new coupled model was created to investigate the bridge approach problem that arises from the variation of the stiffness below the rail due to the stiff foundation on the bridge and the softer substructure before and after the bridge.

To solve the stiffness variation problem, a concrete slab was implemented under the ballast before the bridge with one end resting on the abutment. Two designs of the slab were studied in this work, namely rectangular and inclined slab. The performance of both slabs was compared with the no slab case, and the results showed great improvement in the vertical displacement, the contact force, and the substructure stresses for both slabs, while the inclined slab showed better performance than the rectangular one as it provides a gradual change in the stiffness in the approach zone.

The results of this work show the effectiveness of the presented coupling technique between the FEM and MBS in one model and the usefulness of the presented models. The bridge model analysis showed the effectiveness of the inclined slab as a recommended solution for the approach zone problem and its impact on the reduction of the vertical displacement, the contact forces, and the stresses.

## CHAPTER 1

### INTRODUCTION

(A big portion of this chapter were previously published as El-Ghandour, Ahmed I., Martin B. Hamper, and Craig D. Foster. "Coupled finite element and multibody system dynamics modeling of a three-dimensional railroad system." Proceedings of the Institution of Mechanical Engineers, Part F: Journal of Rail and Rapid Transit 230.1 (2016): 283-294.)

#### 1.1 Background and motivation

Among the different means of transportation, rail has been the one of the most important, especially over the last two centuries. This importance derives from the economic advantages for both people and cargo transportation, and the comfort and safety factors for passengers. Rail is also one of the most energy-efficient modes of transportation. The railroad industry has witnessed many developments over the past two centuries, including new fuels, improved sleeper designs and materials, higher speeds, and other improvements down to the interior design for comfort of the passengers. These developments, especially with the advent of high-speed trains, were great motivators for studying the effect of the changes on the rail system. The rail system that carries trains consists of rails, sleepers, fasteners, pads, and the substructure.

Rails guide the vehicles that move over them, maintaining continuous contact with these vehicles. The distance between the rails (gage) is maintained by the sleepers also known as cross

ties. Sleepers are also responsible for the transmission of vertical load from the vehicle to the substructure. Fasteners connect the rails to the sleepers and usually include rail pads to help damp vibrations. The substructure of the rails consists of three layers: ballast, subballast, and subgrade. The topmost layer is the ballast, a gravel layer responsible for holding the sleepers in position as well as transferring loads to the other substructure layers. The subballast and subgrade assist in the ballast and rail support (AREMA manual [1], Shabana et al. [2]). All these elements cooperate to transfer the vehicle load to the ground, provide smooth performance, and help to reduce maintenance and wear.

Because of the complex behavior of rail and the cost of experiments, computer modeling has become a useful tool for examining many problems related to rail. Numerous researchers have built different models that can help to investigate and understand various issues associated with railroad engineering. Such problems include unsupported sleepers (Lundqvist and Dahlberg [3], Zhang et al. [4], Zakeri et al. [5], Recuero et al. [6]), derailment (Wang and Li [7], Barbosa [8], Bao et al. [9], Sato et al. [10]), ballast settlement (Huang and Tutumluer [11], Brown et al. [12]), and other problems. The following sections will investigate in more depth the work done by the researchers to benefit from the advanced numerical modeling methods to deal with the complicated problems associated with the railroad industry, and to achieve better performance and to reduce the maintenance cost.

## 1.2 Modeling using finite element method

The finite element method (FEM) has been used by numerous researchers to investigate railroad systems and the associated problems. For example, Biempica et al. [13] examined residual stresses in UIC-60 rails. They used FEM to simulate and analyze the rails and compare the level of stresses with the experimental results. The stress generated due to the wheel-rail contact was also investigated by Monfared [14]. He used a FE model and applied static analysis to predict the regions of highest stresses. These regions can exist on the wheel, rail web, or the contact surface of the rail. Different contact patch shapes were investigated in Monfared's work. Sladkowski and Sitarz [15] used FEM to analyze the interaction between the rail and the wheel. By comparing different wheel and rail profiles, Sladkowski and Sitarz analyzed the stresses developed due to each profile, and investigated the performance of the different combinations of rail and wheel profiles, and the wear in each one.

Krácalík et al. [16] built a 2D finite element model to model the wheel-rail contact. The purpose of that model was to study the stress and strain effect in two models, the first is a twin-disc test and the second is a full-scale wheel-rail test. A crack was added to the models to investigate the effect of the stress and strain on the crack depth in either the wheel or the rail. While 2D was used in [16] to model the wheel-rail contact, a 3D model was developed by Arslan and Kayabaşı [17] to model the wheel-rail contact. The main goal of that study was to have a strong 3D model that has fewer assumptions and more robust meshing compared to other models in the literature. Beside the stresses, FEM has been also used to study strains

in rail webs. Molatefi and Mozafari [18] modeled the rail with FE and used moving loads to represent the contact force. They compared their results with experiments and showed good agreement.

Most researchers modeling rail dynamics have assumed in their work rigid substructures, and therefore the models did not include the deformability of the soil layers, even if they included rail flexibility. Some researchers, however, included the effect of the substructure by simplifying it and modeling it as spring-dampers elements. Xiao et al. [19] and Xiao et al. [20] studied the problem of track support failure. The substructure was modeled in both work using spring-damper elements. The vehicles' dynamic response was investigated in [19] on linear track, while in [20], the vehicle derailment was investigated over a curved track with lack of track support in both models at certain locations. Another work based on the finite element was done by Siew et al [21]. They built a nonlinear finite element model to study the performance of the tangential turnout (the part of the rail where two tracks intersect) and its interaction with the ballast and the sleepers. The model was used to study the turnout critical points for both deflection and forces.

Chen et al. [22] used the FEM to study the fastening systems of the railroad when it is combined with concrete sleepers. Their 3D model included the different element of the fasteners and the interaction with the concrete sleepers. Experimental work was performed to validate the numerical work, and showed the effectiveness of the FE model.

A few researchers have created a full continuum model using the finite element method to model the different layers of the substructure. Chebli et al. [23] created a FE model to investigate the in-situ measurement and the dynamic responses of high-speed trains. FEM was also used by Kumaran et al. [24] to model the different components of the railroad system (rails, sleepers, ballast and subballast) to study the dynamic response of prestressed concrete sleepers and the interaction between the wheels and the rails. Koskinen [25] used FEM to study the substructure effect on the rails, by modeling the bridge, railway and soil.

Beside the main mechanical problems, finite element method was also used to investigate thermal problems that affect some mechanical components in the railroad system. Tarawneh et al. [26] used FEM to build a model that test the thermal performance of railroad bearing pressed onto an axle. To study the inner components of the bearing, the FE model was used to run different thermal scenarios to investigate the bearing performance under different thermal loading. The results showed great agreement with the experimental results, and that the increase of a couple of roller temperature inside the bearing does not affect the external bearing case and the overall performance. Another thermal study that was performed using FEA is carried out by Masoudi et al. [27]. In this work Masoudi et al. built a 3D FE model of the rail to study the residual stresses developed in the rail during the quenching process that occurs during the rail manufacturing. The simulations showed how the stresses are distributed during the quenching and how it may be a cause for crack initiation.

Similar work was done by Nejad [28] but with focus on the wheel instead of the rail. A 3D FE model of the wheel was developed to study the residual stresses induced during the heat

treatment process (quenching and annealing) of the wheel. Another FE model for thermal analysis was constructed by Mohan [29] to study the heat generated due to the friction between the wheel and the rail. The model demonstrates the effect of both thermal and structural loading on the wheel behavior.

In mechanical finite elements, the ballast is usually modeled, as mentioned above, using springs or solid elements. Another method used to model the ballast is the discrete element method (DEM). The discrete element method models each particle of ballast or soil (sometimes as aggregates) separately, using simple contact formulations to describe their interaction. DEM has been used to study the case of the uneven ballast settlement and the displacement of the rail associated with it by Tutumluer [30]. Tutumluer focused on the properties of the ballast such as gradation, aggregate type, and angularity. The study showed that the level of plastic deformation is increased with increasing load. It is important to mention here that the discrete element method, while it can model each ballast particle, it is computationally expensive and has not yet been integrated with a full vehicle model.

### **1.3 Modeling using multibody systems**

Another numerical modeling technique that has been widely used in different engineering fields, including railway engineering, is multibody systems dynamics (MBS). Any system that includes rigid and flexible elements that are kinematically connected using joints can be modeled with a multibody system as discussed in [31]. MBS is an extensively used tool by different researchers in different areas of interests, such as rotor dynamics [32], vehicle analysis [33], and turbine

gearboxes [34], MBS can be used to model human bodies, combustion, automobiles, and robots as well.

MBS is commonly used in the rail industry. The railroad vehicles and the wheel-rail contact are usually the main components modeled by MBS (Shabana et al. [35], Shabana and Sany [36]). Liu and Bruni [37] used MBS to model a single axle wheel set of roller rigs. Their work compared two cases for the rig, one is a standard arrangement of the rig, and the second when a differential gear was included. The results was focused on the contact forces based on a proposed methodology and how both arrangements affect it.

Based on a new nonlinear approach, Recuero et al [38] used the MBS to demonstrate the modeling of rail flexibility using absolute nodal coordinate formulation. The new approach was compared to study similar problem that was modeling using the floating frame of reference approach. Both approaches showed good agreement.

To study the trains derailment mechanism and dynamic responses, the MBS simulation was used by Liang et al. [39]. The model simulated a lateral impact on passenger vehicle on ballasted track. Different sensitivity analyses were performed and the final results showed the importance of design improvement in the train suspension.

#### **1.4 Coupling FEM and MBS**

With the high level of usage of both FEM and MBS in the rail industry over the last few decades, coupling the techniques in the same simulation has proven very valuable for many problems. The benefit of coupling both FEM and MBS is the ability to profit from the advantages of

each technique. For example, using FEM is more efficient for simulating the substructure and the sleepers' elasticity; however, using MBS is more efficient for modeling the contact between the wheel and the rail. In contrast to many studies in the literature, where the researchers either used FEM or MBS to study a specific problem, this coupled model imparts the ability to investigate different scenarios of different components of the rail system with greater accuracy.

A number of researchers have worked on coupling both FEM and MBS to create more accurate and sophisticated models to investigate more complex scenarios. Galvin et al. [40] built a full 3D model to dynamically analyze the interaction between the trains and the track and substructure. The vehicles were modeled using MBS while FEM was used to model the track. The soil was modeled using the boundary element method by building a homogenous half-space model. Tanabe et al. [41] also coupled MBS and FEM in their work. They focused on the dynamic interaction between the train and the substructure in the case of earthquakes. They also studied the behavior after derailment. Using independent dynamic integration algorithms, Ambrósio et al. [42] coupled FEM and MBS to investigate a pantograph-catenary interaction. FEM was used to model the catenary and MBS used to model the pantograph. El-Ghandour et al. [43] studied the effects of substructure stiffness on wheel-rail dynamics, including the problem of unsupported sleepers.

### **1.5 Bridge approach problem**

While many researchers have been attracted to study the above-mentioned problems, bridge approaches and other transitions have attracted particular attention due to the impact to the

rail system and related costs. The difference in the stiffness between bridge abutments and the surrounding soil causes many problems in the railroad industry. The sudden stiffness changes can cause increased stress, which consequently increases settlement near the transition. These differential settlements create a rapid change in the rail height at the bridge approach, which leads to higher forces and increased wear in the track and the wheels. This wear, in turn, creates a need for extra maintenance cost. The main causes of this problem are poor soil compaction, natural settlement under the embankment, and excessive traffic loads. See Briaud et al. [44] for more detailed discussion of these issues.

Several solutions have proposed to mitigate the settlement around transitions. Using a finite element model, Monley and Wu [45] simulated the effect of the geogrid tensile reinforcement that is placed in the approach fill before the abutment. They also studied the effect of including a collapsible inclusion between the tensile reinforcement and the abutments walls. The latter case showed better results compared to the case of only tensile reinforcement due to the effect of inclusion on the lateral load reduction.

Helwany et al. [46] used FEM to study the performance of a geosynthetic-reinforced soil (GRS) bridge abutment and its effect on the foundation soil settlement. The study also included the effect of the soil density combined with the GRS bridge abutment. Their results showed that the GRS bridge abutment performed nicely with dense soil. On the contrary, the case of loose soil showed large level of settlement around the abutment.

Li and Davis [47] conducted another study, in which the field tests were performed on four different bridge approaches in order to determine the causes and the remedies of the track geometry degradation and its link to the sudden change in the track stiffness at the bridge approach. They studied the influence of the stiffnesses of the different layers on the general track stiffness and found that the ballast and subballast have more impact on the track stiffness than the subgrade layer. Adding a rubber mat underneath the concrete ties to improve the damping was recommended as well.

Dahlberg [48] used finite elements to study the degradation of the rail due to the track stiffness variation. Dahlberg's FE model included a transition section in the rail where the stiffness is increased gradually between the two zones with significant difference in the track stiffness values. Also, he tested a case where an under-sleeper pad (elastomeric product) was used as another method to provide a desired stiffness transition zone in the middle of the track. He obtained similar results by gradually increasing the ballast stiffness under each sleeper from the low stiffness zone to the high stiff zone. An optimization analysis was performed to obtain the suitable stiffnesses for each transition zones in the different cases.

Zhang et al. [49] performed a comparison analysis between the conventional geogrid-reinforced and pile-supported embankments, as well as a combined fixed-geogrid-reinforced and pile-supported embankment. The effectiveness of both techniques on the bridge approach settlement was assessed using numerical analysis, and the fixed-geogrid-reinforced technique showed better results on both settlement and lateral displacement.

Another solution that is common between both highways and railroad bridge approach problem is the implementation of slab in the substructure before the bridge. Slabs have been used in highways since the 1970s, and the wedge-shaped transition zone was implemented by the Japanese National Railways in railroad bridges as a solution for the variation of stiffness problem [50]. The purpose of this slab, which can be flat or wedge-shape, is to increase the substructure stiffness in the low stiffness zone before the bridge to provide smoother transition in the stiffness value at the bridge approach. Detailed studies about the slab design and implementation are performed in [51] and [52].

## **1.6 Goal of the work**

The purpose of this work is to build a fully detailed 3D finite element model that represent the different components of the railroad system to investigate the substructure performance under dynamic load by coupling it with the multi-body systems dynamics in the time domain. The analysis in this work is performed using the modal frequencies extracted from the FE model instead of the nodal degrees of freedom, and uses the Floating Frame of Reference (FFR) formulation to obtain the elastic response of the system.

A nodal elimination procedure is performed in this study after applying the modal analysis to provide the MBS code with the rail nodes data, including mode shapes, and stiffness. This elimination technique helps in modeling a complex model including large number of mode shapes. After that, the multibody dynamics analysis is performed, then we reconstruct the full solution in the substructure model as will be explained in the following chapter.

The wheel-rail contact is modeled using MBS. The FEM model includes the rails, fasteners, sleepers, and substructure as deformable bodies. The continuum finite element model allows us to provide a detailed geometry of the substructure in a way that captures the stiffness change across the transition. This coupling technique will be then used to model the bridge approach problem and investigate the suggested solution. To our knowledge, this is the first time that such a coupled formulation has been applied to the problem of bridge approaches.

### **1.7 Structure of this dissertation**

The rest of this dissertation is structured as follows: in Chapter 2, the first finite element model is explained in detail, listing the different components of the model, the model dimensions and materials. The formulations of the floating frame of reference and the contact formulations between the wheel and the rail is also explained in Chapter 2. Chapter 3 includes the verification of the first model and the technique used in this thesis. Chapter 4 shows the work focused on the bridge approach problem. It contains the FE bridge model and its details and the suggested mitigation technique and the results. Finally, Chapter 5 summarizes the conclusion of the thesis work and the main output of the coupling models and the bridge approach problem results, and the suggested future work.

## CHAPTER 2

### FINITE ELEMENT MODEL

(A big portion of this chapter were previously published as El-Ghandour, Ahmed I., Martin B. Hamper, and Craig D. Foster. "Coupled finite element and multibody system dynamics modeling of a three-dimensional railroad system." Proceedings of the Institution of Mechanical Engineers, Part F: Journal of Rail and Rapid Transit 230.1 (2016): 283-294.)

As discussed in the introduction chapter, finite elements method have been widely used in the area of railroad industry to study and analyze different problems with mechanical and thermal nature as well as substructure related problems. It is a very powerful tool that can be used to save the cost of building and testing many prototypes by creating numerical models to be tested in a variety of situations. In the following sections of this chapter, we will explain in detail how the model is created using the FE and how it was coupled with the MBS to benefit from the advantages of both methods to build a more effective coupled model and reduce the computational cost for such large and detailed models.

#### **2.1 Railroad system components**

The railroad system can be divided into three major components: the running vehicle (train), the track, and the substructure. In this work we will use a built-in wheelset in the MBS code to represent the vehicle, while for the track, it is divided in this work to: rails, sleepers, and

fasteners. On the other side, the substructure will be modeled based on three layers, namely the ballast, the subballast, and the subgrade, respectively from top to bottom.

The track components and the soil layers will be modeled using a commercially available FE software package, and the wheelset will be modeled using the MBS code as mentioned above. The following section explains the different types of elements used in the FE model through the rest of this dissertation.

## **2.2 FE model**

A full 3D FE model using beam, solid, and spring elements is created to model the different parts of the system using the FE software, while the dynamic analysis and the contact between the wheels and the rails are modeled using an MBS code. The rails and the sleepers were modeled using 3D beam elements, where the initial part of the rails were modeled as rigid body, while the middle part of the rails and the sleepers are modeled as flexible bodies. The three layers of the substructure: the ballast, the subballast, and the subgrade, are modeled using solid elements. Spring-damper elements were used to model the fasteners between the rails and the sleepers. The main dimensions and material properties needed for the different components of the model are provided in Table I.

In this model, the track is designed to have a rigid section before and after the flexible section. The rigid sections are assumed to have all their degrees of freedom constrained, whereas the deformable section of the rail includes both the rails and the substructure beneath them. As is shown in Figure 1, the deformable rail is connected to the sleepers using spring-damper

TABLE I: Finite element model dimensions and material properties

Description	Symbol	Value	Unit
Length of the rigid rail	$L_{rr}$	40	m
Length of the flexible rail	$L_{fr}$	6.5	m
Gauge length	$G$	1.5113	m
Stiffness of the rail	$E_r$	210e9	N/m <sup>2</sup>
Density of the rail	$\rho_r$	7700	kg/m <sup>3</sup>
Poissons ratio of the rail	$\epsilon_r$	0.3	kg/m <sup>3</sup>
Cross-sectional area of the rail	$A_r$	64.5e-4	m <sup>2</sup>
Second moment of inertia of the rail	$I_{R_{yy}}$	2010e-8	m <sup>4</sup>
Second moment of inertia of the rail	$I_{R_{zz}}$	326e-8	m <sup>4</sup>
Timoshenko shear coefficient for the rail		0.34	
Length of a sleeper Length	$L_s$	2.36	m
Gap between sleepers	$g_s$	0.65	m
Stiffness of a sleepers	$E_s$	64e9	N/m <sup>2</sup>
Density of a sleeper	$\rho_r$	2750	kg/m <sup>3</sup>
Stiffness coefficient of a pad	$K_{pad}$	26.5e7	N/m
Damping coefficient of a pad	$C_{pad}$	4.6e4	N.s/m
Poissons ratio of a sleeper	$\epsilon_s$	0.25	kg/m <sup>3</sup>
Cross-sectional area of a sleeper	$A_s$	513.8e-4	m <sup>2</sup>
Second moment of inertia of a sleeper	$I_{S_{yy}}$	25735e-8	m <sup>4</sup>
Second moment of inertia of a sleeper	$I_{S_{zz}}$	18907e-8	m <sup>4</sup>
Timoshenko shear coefficient for a sleeper		0.83	
Stiffness of the ballast	$E_b$	260e6	N/m <sup>2</sup>
Density of the ballast	$\rho_b$	1300	kg/m <sup>3</sup>
Poissons ratio of the ballast	$\epsilon_b$	0.3	kg/m <sup>3</sup>
Stiffness of the subballast	$E_{sb}$	200e6	N/m <sup>2</sup>
Density of the subballast	$\rho_{sb}$	1850	kg/m <sup>3</sup>
Poissons ratio of the subballast	$\epsilon_{sb}$	0.35	kg/m <sup>3</sup>
Stiffness of the subgrade	$E_{sg}$	200e6	N/m <sup>2</sup>
Density of the subgrade	$\rho_{sg}$	1850	kg/m <sup>3</sup>
Poissons ratio of the subgrade	$\epsilon_{sg}$	0.35	kg/m <sup>3</sup>

elements that are connected to the ballast layer. The substructure layers are constrained on both sides in the longitudinal direction, and the bottom of the subgrade is also constrained. Figure 2 shows the dimensions of the three substructure layers. Modal analysis is used in this study to obtain the mode shapes and natural frequencies of the FE model, which are used as an input to the MBS code before running the dynamic analysis in the time domain.

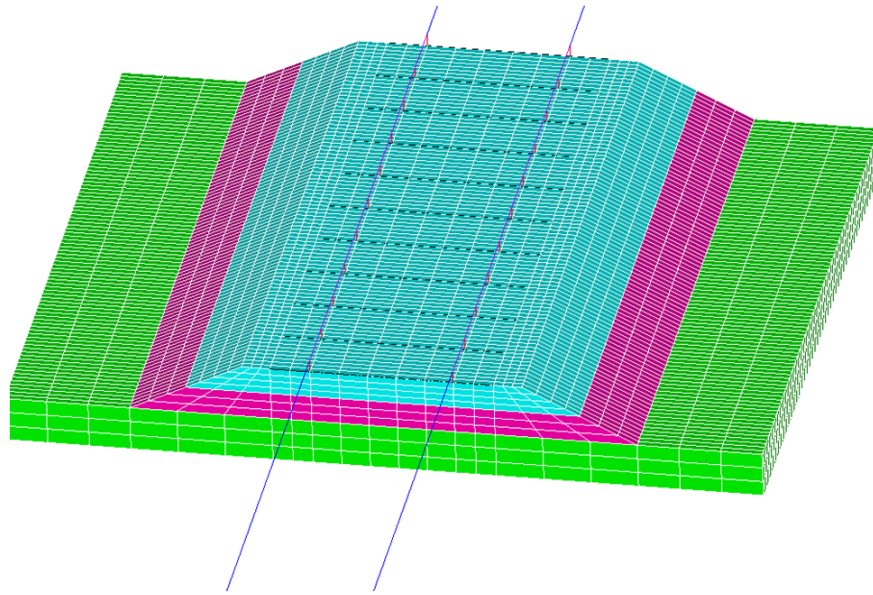


Figure 1: The 3D FE model.

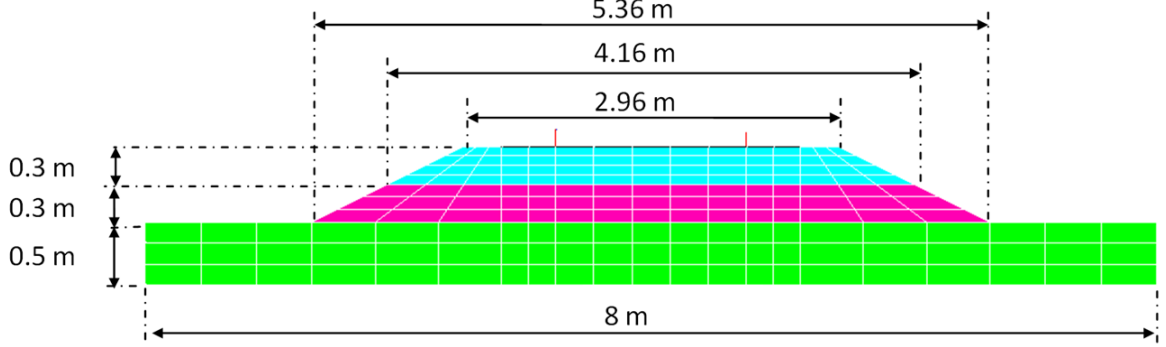


Figure 2: Dimensions of the three substructure layers.

### 2.3 Formulation of the floating frame of reference

In this work, the FFR formulation is used to introduce body flexibility into the equations of motion. The FFR approach takes advantage of the component-mode representation of a FE model, where the model is reduced to a set of desired mode shapes, to decrease the number of degrees of freedom in the system. This reduced model can be then used to evaluate the deformation of flexible bodies in the MBS environment. FFR is ideal for the case of small deformations, such as the case of a typical rail deformation, and is also generalized to allow for large rotations. FFR was applied to modeling rail flexibility in [53] and has been verified by Rathod et al [54]. In this work, it is shown how the deformation of the rails can be taken into account for the prediction of contact points, normal forces and creepages. A detailed account of the contact prediction and evaluation method is provided in this section. Each rail in the used track model is represented by two interdependent models: the geometric model, which

describes the surface of the rail in the contact prediction algorithm, and the FE model, which accounts for the elastic properties of the rail. The rail's geometric model as shown in Figure 3 is defined by the following equation:

$$\mathbf{r}^r = \mathbf{R}^r + \mathbf{A}^r(\overline{\mathbf{R}}^{rp} + \mathbf{A}^{rp}\overline{\overline{\mathbf{U}}}^{rp}) \quad (2.3.1)$$

where  $\mathbf{r}^r$  defines the position of an arbitrary point on the rails surface,  $\mathbf{R}^r$  defines the location of the tracks coordinate system with respect to the global coordinate system,  $\overline{\mathbf{R}}^{rp}$  defines the location of the rail profile's coordinate system with respect to the tracks coordinate system,  $\mathbf{A}^{rp}$  defines the orientation of the profile's coordinate system with respect to the tracks coordinate system and  $\overline{\overline{\mathbf{U}}}^{rp}$  defines a point on the rail surface in the profile frame.  $\overline{\overline{\mathbf{U}}}^{rp}$  is assumed to be defined by a profile curve that describes the contact surface of the rail that is swept along the rail space curve to form a contact surface.

The rail space curve is defined by a series of Absolute Nodal Coordinate Formulation (ANCF) 3D beam elements as described in [55] and may be represented by the following equation:

$$\overline{\mathbf{R}}^{rp}(x^r, y^r, z^r, t) = \mathbf{S}(x^r, y^r, z^r, t)\mathbf{e}^r(t) \quad (2.3.2)$$

where  $\mathbf{S}$  is the matrix of shape functions for the ANCF 3D beam element provided by Shabana in [55],  $\mathbf{e}^r$  is the time-dependent vector of nodal coordinates, which describes the position and first-order spatial derivatives of the rail space curve and  $x^r$ ,  $y^r$  and  $z^r$  are the local coordinates

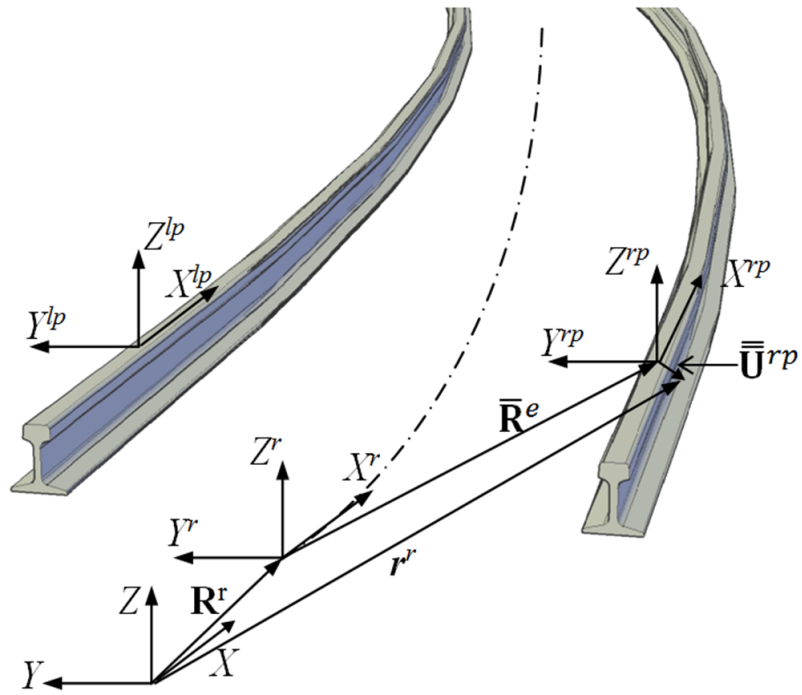


Figure 3: Definition of the reference frame.

defined in the ANCF elements coordinate system. The vector  $\mathbf{e}^r$  must be continuously updated to account for the deformation of the FE model as prescribed by Shabana et al.<sup>30</sup> Note that the nodes of the FE model need not coincide with the nodes of the geometric model as shown in Figure 4.

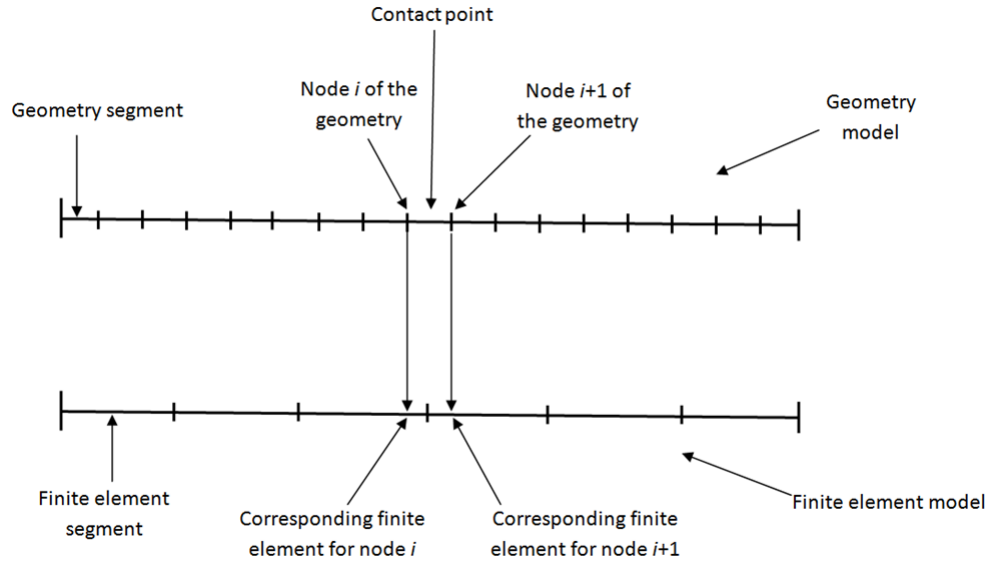


Figure 4: Geometric and FE nodes.

Using the FFR formulation, the FE model of the rail is used to update the ANCF vector of nodal coordinates ( $\mathbf{e}^r$ ). A point on element  $j$  in the FE model of rail  $i$  may be described with the following equation presented in [31]:

$$\mathbf{r}^{ij} = \mathbf{R}^i + \mathbf{A}^i(\bar{\mathbf{u}}_0^{ij} + \bar{\mathbf{u}}_f^{ij}), \quad j = 1, 2, \dots, n_e \quad (2.3.3)$$

where  $\mathbf{R}^i$  defines the position of the track's coordinate system,  $\mathbf{A}^i$  defines the orientation of the track body's coordinate system with respect to the global coordinate system,  $n_e$  is the number of elements in the FE model of rail  $i$ . The vectors  $\bar{\mathbf{u}}_0^{ij}$  and  $\bar{\mathbf{u}}_f^{ij}$  define the position of the point in the reference and deformed configurations respectively and are defined as

$$\bar{\mathbf{u}}_0^{ij} = \mathbf{S}_b^{ij} \mathbf{B}_c^{ij} \mathbf{e}_{bo}^i, \quad \bar{\mathbf{u}}_f^{ij} = \mathbf{S}_b^{ij} \mathbf{B}_c^{ij} \mathbf{B}_r^i \mathbf{B}_m^i \mathbf{q}_f^i \quad (2.3.4)$$

where  $\mathbf{S}_b^{ij}$  is the FE shape function matrix associated with element  $j$ ,  $\mathbf{B}_c^{ij}$  is the Boolean element connectivity matrix,  $\mathbf{e}_{bo}^i$  is the vector of FE nodal coordinates in the non-deformed configuration,  $\mathbf{B}_r^i$  is a matrix of reference conditions used to define the element displacement field,  $\mathbf{B}_m^i$  is the modal matrix obtained from the FE model. This matrix has columns defined by the modes of vibration selected for the analysis and  $\mathbf{q}_f^i$  is the vector of modal coordinates that represent the elastic degrees of freedom in the equations of motion.

## 2.4 Contact formulation

Many methods have been developed in the literature to estimate the contact forces and locations between bodies. Some use simplified procedures to ensure an efficient response. For example, Meli and Pugi [56] use a linear superposition principle to rapidly approximate the contact. In this investigation, the Elastic Contact Formulation for Algebraic Equations (ECFA) approach,

presented in [2], is used to predict the location of the contact point. This 3D non-conformal contact approach does not treat the governing equations as constraints, which allows the wheel to have six degrees of freedom with respect to the rail. Small wheel/rail separations and penetrations are permitted in ECFA. Although less efficient than some other procedures, there are significant gains in accuracy.

Each contact surface is represented in terms of two non-generalized coordinates, referred to as surface parameters. This representation allows the location of any point on a contact surfaced to be defined by only two independent coordinates, which greatly simplifies the contact problem. Using this surface parameterization, the following four equations provided by Shabana et al in [2] are solved iteratively to determine the location of the contact point for a given wheel and rail pair

$$\mathbf{E}(S) = [\mathbf{t}_1^r \cdot \mathbf{r}^{wr} \quad \mathbf{t}_2^r \cdot \mathbf{r}^{wr} \quad \mathbf{t}_1^w \cdot \mathbf{r}^r \quad \mathbf{t}_2^w \cdot \mathbf{r}^r]^T = \mathbf{0} \quad (2.4.1)$$

where  $\mathbf{t}_i^j$  is the tangent vector of surface  $j$  taken with respect to surface parameter  $i$ ,  $\mathbf{r}^{wr}$  is defined as the relative difference in position of the contact point on the wheel with respect to the corresponding point on the rail, and  $\mathbf{n}^r$  is the normal vector of the rail at the contact point. With the set of surface parameters corresponding to the solution of this equation, the penetration between the wheel and rail must be checked to determine if the solution represents contact or a small separation. The penetration is computed as  $\delta = \mathbf{r}^{wr} \cdot \mathbf{n}^r$ , where a negative penetration implies contact, and a positive penetration implies separation. If the penetration

proves that a contact point exists between a given wheel/rail pair, the normal force is computed as  $F^N = -K_H\delta^{3/2} - C\dot{\delta}|\delta|$ , where  $K_H$  is the Hertzian constant,  $C$  is the damping constant and  $\dot{\delta}$  is the time derivative of the wheel/rail penetration. The normal contact force, the location and dimensions of the Hertzian contact ellipse, and the tangential and spin creepages are computed using the procedure outlined in [2].

Subsequently, this data is used to compute the tangential creep forces and the creep spin moment as prescribed by Kalker's nonlinear creep theory as described by Shabana et al in [2]. In order to account for the effect of the deformation of the rail on the prediction of the contact point, one must first determine the element in the rail model that is in contact with the wheel. Following this, the geometry of the rail is updated and used in the computation of the location and dimensions of the Hertzian contact ellipse, as well as the tangential and spin creepages as defined by [57]. The geometry is updated continuously throughout the iterative procedure used to determine the location of the contact point and the associated forces.

## **2.5 Equations of motion**

In this investigation, the augmented form of the equations of motion presented in [31] is implemented. The augmented form of the equations of motion is a constrained approach to the solution of the equations of motion, in which a system of differential and nonlinear algebraic constraint equations are solved simultaneously. The augmented form of the equations of motion may be written as [31]:

$$\begin{bmatrix} \mathbf{m}_{rr} & \mathbf{m}_{rf} \\ \mathbf{m}_{fr} & \mathbf{m}_{ff} \end{bmatrix} \begin{bmatrix} \ddot{\mathbf{q}}_r \\ \ddot{\mathbf{q}}_f \end{bmatrix} = \begin{bmatrix} (\mathbf{Q}_e)_r \\ (\mathbf{Q}_e)_f \end{bmatrix} + \begin{bmatrix} (\mathbf{Q}_v)_r \\ (\mathbf{Q}_v)_f \end{bmatrix} - \begin{bmatrix} \mathbf{C}_{\mathbf{q}_r}^T \\ \mathbf{C}_{\mathbf{q}_f}^T \end{bmatrix} \boldsymbol{\lambda} - \begin{bmatrix} \mathbf{0} \\ \mathbf{K}_{ff}\mathbf{q}_f \end{bmatrix} \quad (2.5.1)$$

In this equation the variables are defined as follows:  $\mathbf{m}_{rr}$  is the inertia matrix that is related to the reference coordinates,  $\mathbf{m}_{rf}$  and  $\mathbf{m}_{fr}$  are inertia matrices that correspond to the dynamic coupling of the elastic and reference coordinates,  $\mathbf{m}_{ff}$  is the inertia matrix that is related to the elastic coordinates,  $\mathbf{q}_r$  is the vector of the generalized rigid-body coordinates,  $\mathbf{q}_f$  is the vector of elastic modal coordinates of the FFR that describe the track and substructure flexibility,  $(Q_e)_r$  and  $(Q_e)_f$  are the vectors of the generalized external forces associated with the rigid and elastic coordinates respectively,  $(Q_v)_r$  and  $(Q_v)_f$  are the vectors of the quadratic velocity inertia forces that are related to the rigid and elastic coordinates respectively,  $\mathbf{q}_r$  and  $\mathbf{q}_f$  are the constraint Jacobian matrices that are related to the rigid and elastic coordinates respectively,  $\boldsymbol{\lambda}$  is the vector of Lagrange multipliers, and  $\mathbf{K}_{ff}$  is the track stiffness matrix. The equations of motion are solved for the generalized accelerations and the Lagrange multipliers. Following this solution, the independent coordinates and velocities are found using the explicit Adams-Bashforth predictor-corrector numerical integration scheme, as described in [58]. Subsequently, the dependent coordinates and velocities are computed and used to produce the Augmented

Form of the equations for the following time step. This procedure continues until such a time that the final time step is completed.

## **2.6 The nodal elimination for the coupling**

In this work, to couple the two codes in efficient way that can help us to build models with more detail, a nodal elimination technique was applied. The nodal elimination technique was performed after the modal analysis to provide the MBS code with the mode shapes, modal mass, and stiffness corresponding to only the nodes of the rails. Since only the rail directly interacts with the MBS code, this technique is a successful way to decrease the size of the arrays in the input file provided to the MBS code and reduce the number of degrees of freedom in the model.

This reduction in the size of the modal arrays allows for developing much more complicated models with a very large number of nodal degrees of freedom prior to the nodal reduction. At the same time, the number of extracted mode shapes should be chosen to ensure the coverage of enough modes for the analysis. Since the load is both concentrated and moving, a high number of mode shapes is generally needed. The model is linear, and this make the modal analysis is very suitable method as it is computationally inexpensive.

After running the dynamic analysis on the MBS code, the main outputs of the rails are extracted, mainly the modal displacements and the contact forces, and then using a Matlab code, the displacement and force values of the whole structure are reconstructed using the modal vectors and displacements.

## CHAPTER 3

### VERIFICATION OF THE FE MODEL

(A big portion of this chapter were previously published as El-Ghandour, Ahmed I., Martin B. Hamper, and Craig D. Foster. "Coupled finite element and multibody system dynamics modeling of a three-dimensional railroad system." *Proceedings of the Institution of Mechanical Engineers, Part F: Journal of Rail and Rapid Transit* 230.1 (2016): 283-294.)

The model created in this work is fully 3D and all the various components are presented as described in the preceding chapter. The FE model will be coupled as will be explained below with the MBS code to have an effective model that benefits from the two methods. As the coupled model will be used later for more complex problems, the verification of the coupled model should be demonstrated. To this end, Recuero's model [6] is compared with the model produced in this investigation.

The model used in Recuero's work, which is illustrated in Figure 5, uses beam elements for the rails and sleepers, and the substructure is represented by a series of springs under the sleepers. The model created in this investigation, which is illustrated in Figure 6, includes three substructure layers modeled using eight-node solid elements with fasteners modeled using spring-damper elements. As we are trying to verify our model with respect to Recuero's, we use the exact track properties of Recuero's model, which includes the rails and the sleepers.

However, the substructure (ballast, subballast, and subgrade) is modeled differently with more details.

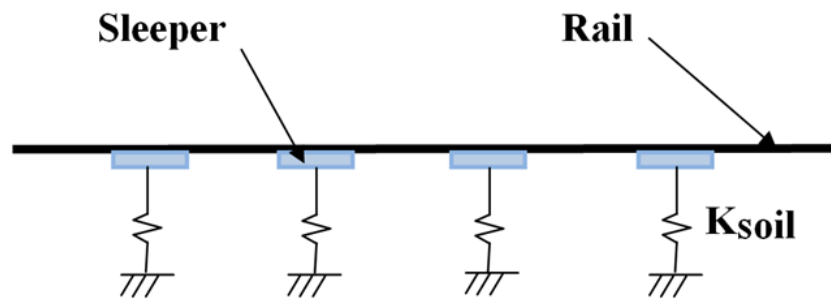


Figure 5: An illustration of Recuero's model.

The dynamic analysis was performed using MBS code SAMS/2000 [59]. The MBS code is provided with information from the FE model such as mode shapes, modal matrix, mass matrix and stiffness matrix, which are extracted from the modal analysis of the FE model. The suspended wheelset shown in Figure 7 was used for the dynamic analysis to represent the train. The wheelset information is listed in Table II.

For the verification purpose, we ran two examples. The first compares the two models with all the sleepers included, whereas in the second the middle sleeper is unsupported. It is important to note that the spring elements beneath the middle sleeper are removed in both models to

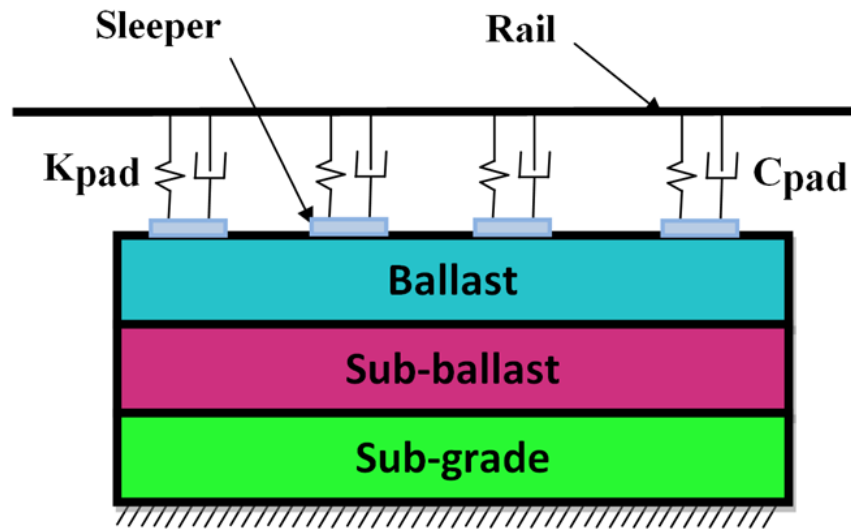


Figure 6: An illustration of the FE model.

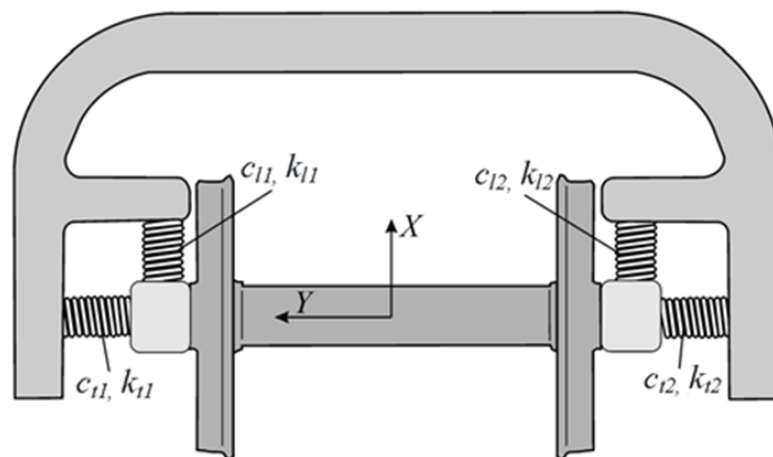


Figure 7: Suspended wheelset used for the dynamic analysis.

model the unsupported case. Before comparing the results from the model presented in this work and Recuero's model, it is important to check that a sufficient number of modes were included. A convergence test on the total number of modes was performed for this purpose.

TABLE II: The mechanical properties of the wheelset.

<b>Description</b>	<b>Value</b>	<b>Unit</b>
Mass	1568	kg
$I_{xx}$	656	kg.m <sup>2</sup>
$I_{yy}$	168	kg.m <sup>2</sup>
$I_{zz}$	656	kg.m <sup>2</sup>
$k_{l1}=k_{l2}$	13500	N/m
$k_{t1}=k_{t2}$	25000	N/m
$c_{l1}=c_{l2}$	1000	N.s/m
$c_{t1}=c_{t2}$	0	N.s/m

A large number of mode shapes were extracted to account for the fact that the load applied to the rail is both very concentrated and moving. Generally, many modes are required to accurately resolve the response of a body to highly concentrated forces. In the case of wheel/rail dynamics, the number of modes is compounded by the fact that the concentrated load is changing position. The selected modes had the lowest frequencies, with care being taken to ensure that different types of mode shapes were covered. The shapes included deformation in all three spatial directions and also twisting modes. Different numbers of mode shapes were tested to ensure the convergence as shown in Figure 8. This figure shows the vertical displacement as a function

of time at the middle of the flexible section as predicted by the given numbers of modes. We can see that convergence is achieved around 350 modes, but the difference between 300 and 350 modes is very small, about 0.24%, therefore the results in the rest of this paper will be based on the 300-mode model. We note here that Recuero's model uses 18 modes for each case, which may be adequate for their analysis given the simpler substructure model.

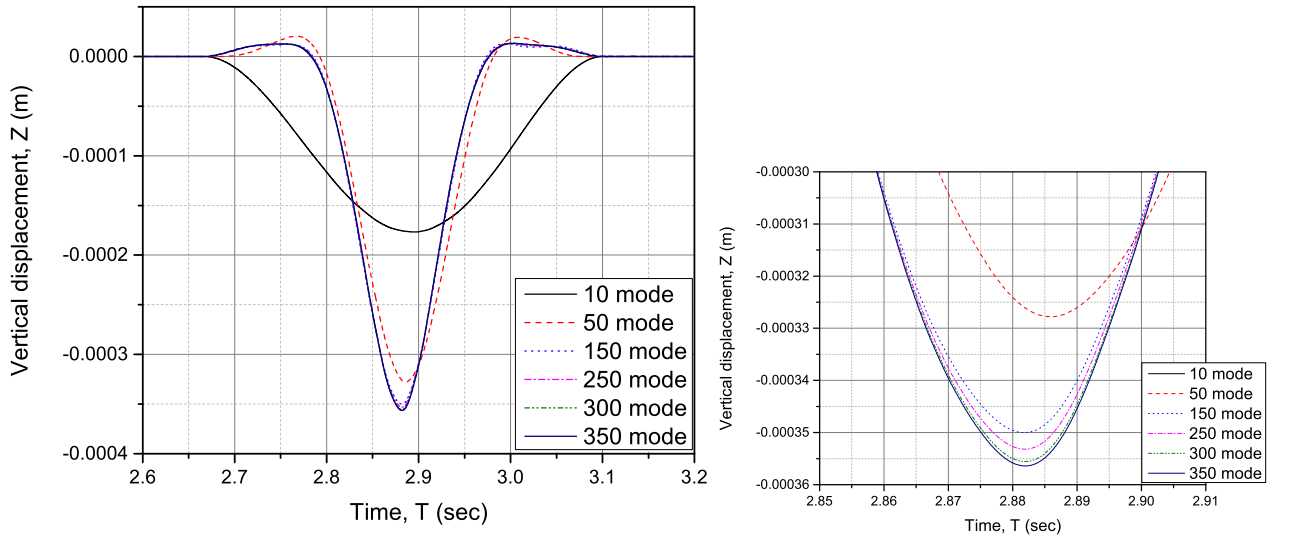


Figure 8: Displacement at the middle of the flexible section of the rail.

### 3.1 Supported model

As previously described, the model includes two rigid sections with a deformable section located between them. The deformable section in this problem includes 11 supported sleepers. The vertical displacement (deformation) of the rail is studied at three longitudinal locations along the track. The three positions are: the third sleeper, as shown in Figure 9, the center of the fourth span (between the fourth and fifth sleepers) as shown in Figure 10, and at the middle of the deformable section (the sixth sleeper), as shown in Figure 11. The percentage difference between the peaks of the two models is included in the captions. We also calculated the difference between the maximum depression and maximum rise, as this distance can often be more critical than the absolute depression. The percentage difference between the two models for Figure 9 to Figure 11 are 14, 6 and 13%, respectively.

The results show that the two models have the same trend at the three positions, with some difference in the peak values. Some difference is expected as a result of the differences in the models assumptions, for example, the effect of the three layers, and the complexity of the presented FE model compared with the model in the literature. In particular, the Poisson effects in the soil create a slight elevation of the rail on either side of the area of the maximum depression. This elevation is known as rail lift-off from sleepers and the proposed model is able to capture it more clearly than the simple spring-damper model. With the chosen material parameters for the ballast, subballast and subgrade, the model with solid elements is slightly stiffer than the spring elements used to model the ballast in the literature paper. A model

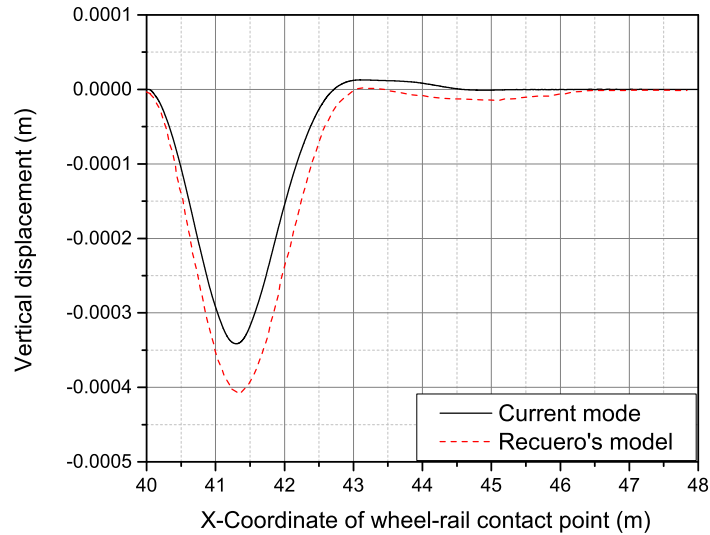


Figure 9: Vertical displacement of the rail at the third sleeper when the wheel/rail contact is directly above it, the difference at the peak is approximately 16%.

using uncoupled springs for the substructure does not capture this phenomenon to the same extent. In addition to the displacements, the model also shows good agreement with the model from the literature in the contact force, as shown in Figure 12. This figure shows the same trend, though the amplitude is not exact, which is likely due to differences in the way in which the two models incorporate damping of the substructure. The current model seems to have a somewhat smoother response, although this may also be related to the number of modes used.

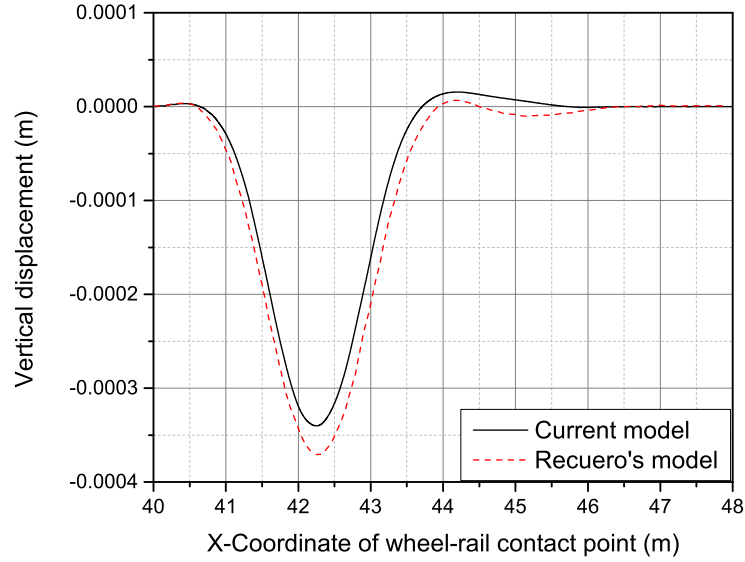


Figure 10: Vertical displacement of the rail at the center of the fourth span when the wheel/rail contact is directly above it, the difference at the peak is approximately 9%.

### 3.2 Unsupported rail

In this section, the support of the sleeper in the middle of the deformable rail, sleeper number 6, is removed. In Recuero's model the springs underneath the rail at that position are removed, whereas in the model presented in this work the fasteners between the rail and the sixth sleeper are removed. The vertical displacements are compared for the two models in the same three positions mentioned in the preceding section. Figure 13 to Figure 15 show the same performance of the supported rail case. The vertical difference between the maximum rise and the minimum peak (the depression) is measured here as well, and the percentage difference

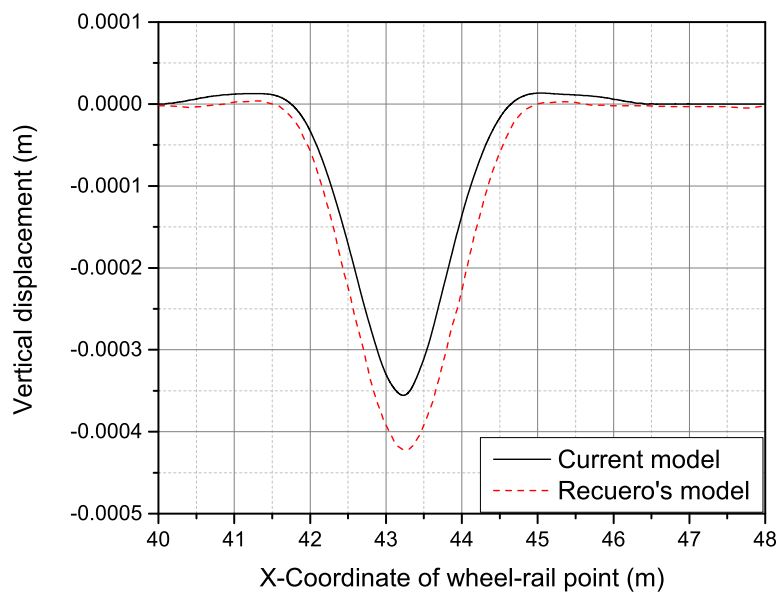


Figure 11: Vertical displacement of the rail at the sixth sleeper when the wheel/rail contact is directly above it, the difference at the peak is approximately 16%.

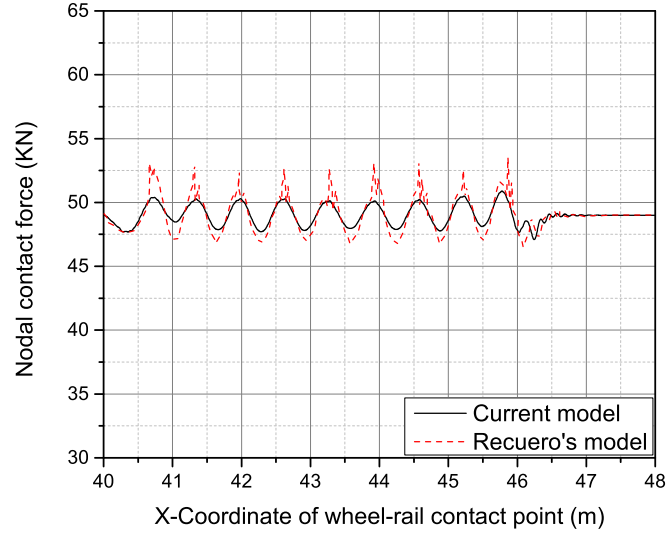


Figure 12: The normal contact force.

between the two models for Figures 13 to 15 are: 10.6, 4, and 26.6%, respectively. The results plotted in the figures show that the presented model has a good agreement with the previously published model. The trend is the same in both cases, and the differences between the peaks are acceptable.

The difference between the two models can be explained by the fact that the model in this work includes a much more detailed description of the track substructure than Recuero's model, and again that the substructure in the current model is slightly stiffer. As in the previous subsection, a similar rise in the rails outside the area of depression is observed. Again, we compare the normal contact force between the two models, as shown in Figure 16. As expected, the behavior

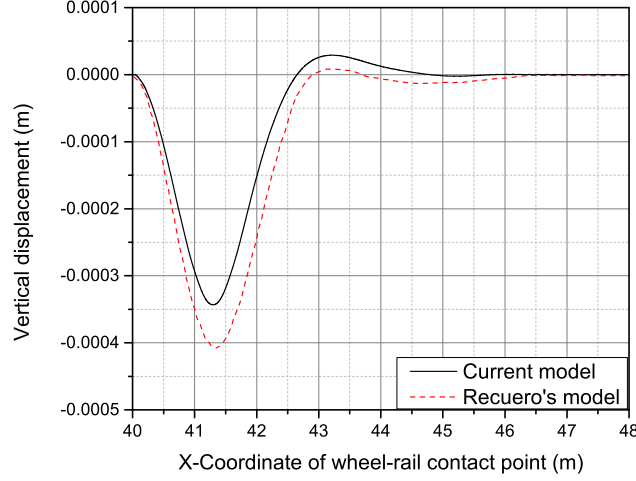


Figure 13: Vertical displacement of the rail at the third sleeper when the wheel/rail contact is directly above it, unsupported middle sleeper. The difference at the peak is approximately 16%.

of the two models due to the missing sleeper in the middle is different. The proposed model includes the fasteners, and the other sleepers are supported with solid elements, which damp the vibration differently than the simple springs used in the literature to model the soil. Another reason for this difference is that Recuero's model uses fewer modes, whereas our model uses a large number of mode shapes. This larger number of modes creates a more flexible response, which tends to soften force peaks. The results presented in this and the previous subsection show reasonable agreement with the literature. The figures show better agreement at the center of the span between two sleepers than at the sleepers. This difference is due to the fact that both models have no support at these points, while the support underneath the sleepers is

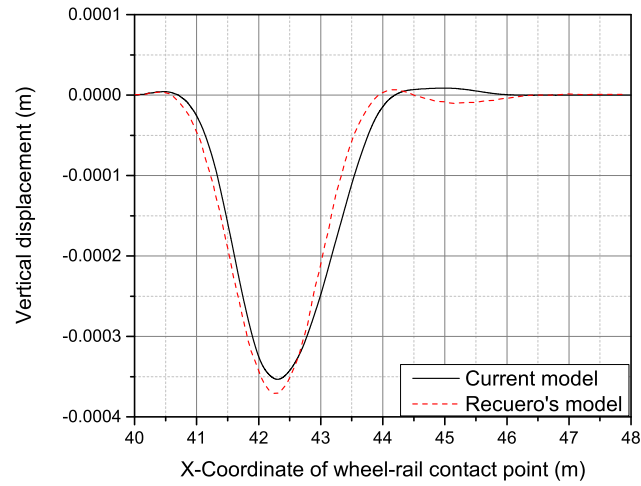


Figure 14: Vertical displacement of the rail at the center of the fourth span when the wheel/rail contact is directly above it, unsupported middle sleeper. The difference at the peak is approximately 5%.

handled differently in the two models. The differences in the peaks vary between 5 and 16%, except at the center of the case with an unsupported sleeper, where it was 29%. This difference is due to the difference in stiffness and the number of mode shapes included.

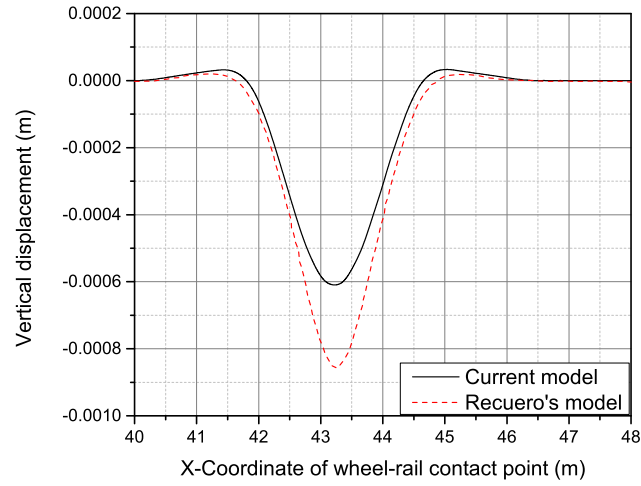


Figure 15: Vertical displacement of the rail at the sixth sleeper when the wheel/rail contact is directly above it, unsupported middle sleeper. The difference at the peak is approximately 29%.

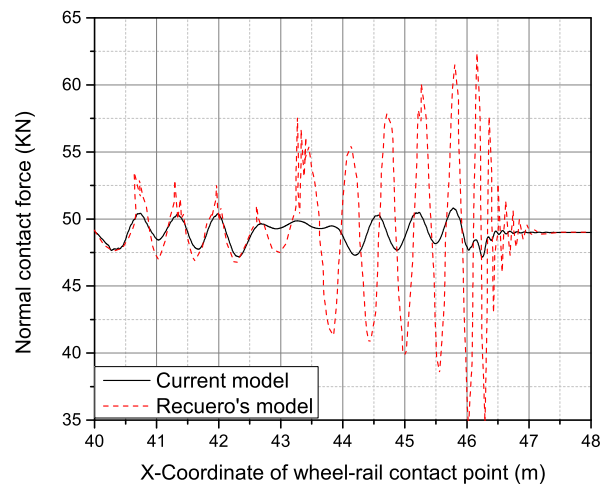


Figure 16: The normal contact force, unsupported middle sleeper.

## CHAPTER 4

### BRIDGE APPROACH MODEL

The coupling work between FEM and MBS presented in the previous chapters shows the effectiveness of the employed technique and how it helps in achieving realistic results, as verified in Chapter Three. The method also saves the computational time and allows us to build more complicated models with more details and fewer assumptions.

In this chapter, we take the work a step further to study more complicated model and study a realistic problem. Here, we apply the coupling technique to a full 3D bridge model to investigate the bridge approach problem. The bridge approach problem, as described in Chapter One, arises due to the stiffness variation between the substructure that supports the rails before and after the bridge compared to the stiffness of the bridge structure that supports the rails above the bridge. In this chapter we construct a model to examine this problem and a possible solution.

#### 4.1 Modeling the bridge

In this section we detail the FE model for the bridge approach problem. Here, finite element modeling is used to model the different components of the problem, including rails, sleepers, and substructure as well as the bridge components. Using beam, solid and spring elements, a full 3D model is created. Both dynamic analysis and wheel-rail contact forces are modeled

using the MBS code used in the previous chapters. The finite element model, including material properties, dimensions and used elements, is described in the following subsection.

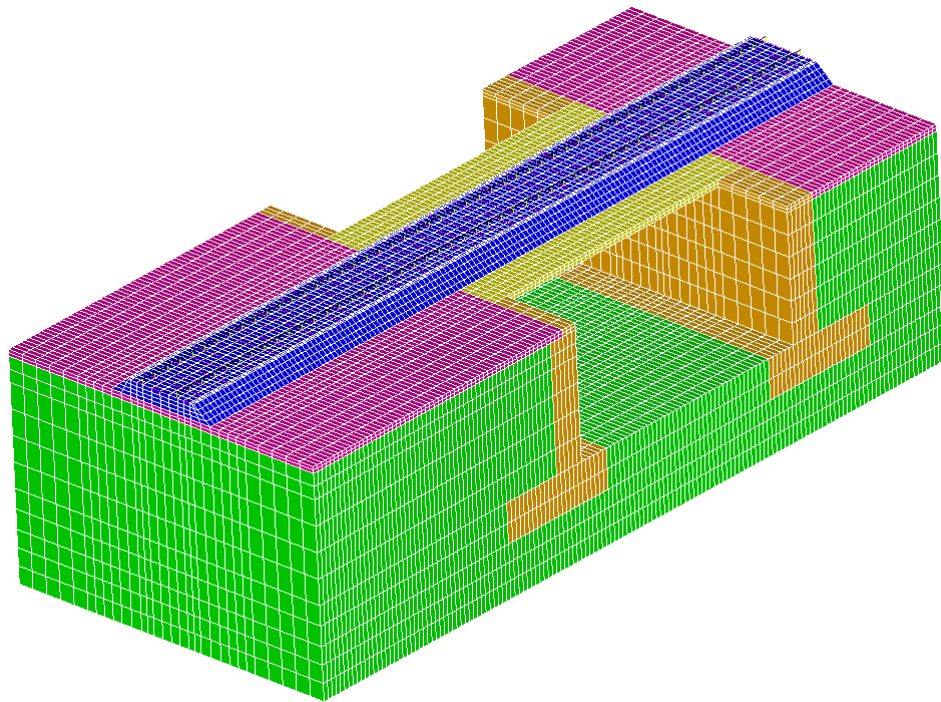


Figure 17: Full 3D Finite Element Model of the bridge approach with the following color coding: Blue: Ballast, Red: Sub-ballast, Green: Sub-grade, Yellow: Deck, Orange: Abutment.

#### 4.1.1 FE Model

In this work, the commercial FE software ANSYS has been used to model the components of the bridge system. Figure 17 and Figure 18 show the full model and its side view respectively.

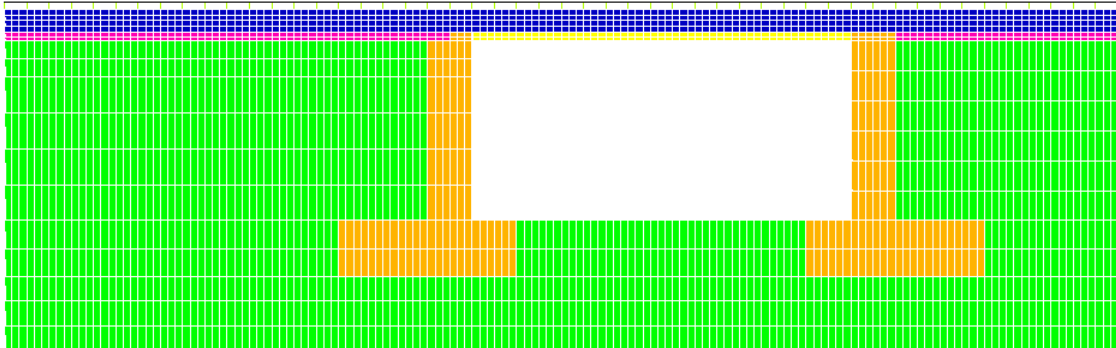


Figure 18: Side view of the model.

The model consists of rails that are connected to the sleepers using the fasteners. The sleepers are resting on the ballast layer that is rested on the subballast before and after the bridge, and resting on the deck in the bridge zone. The deck is resting on concrete beams that are supported by the abutments. The subballast and the abutments are resting on the subgrade layer. For this investigation, a concrete slab is modeled below the ballast layer with one end is resting on the abutment.

For the elements selection, beam elements were used to model the rails, the sleepers and the concrete beams, while solid elements were used to model the substructure layers (ballast, subballast, and subgrade), bridge deck, slab, and abutments.

The fasteners between the sleepers and the rails are modeled using spring-damper elements. Table III shows the main dimensions of the model while Table IV shows the material properties of the different materials used in the bridge model.

TABLE III: Finite element model dimensions

Description	Symbol	Value	Unit
Rail length	$L_r$	30	m
Gauge length	$G$	1.5113	m
Rail cross section area	$A_r$	64.5e-4	m <sup>2</sup>
Rail second moment of inertia	$I_{R_{yy}}$	2010e-8	m <sup>4</sup>
Rail second moment of inertia	$I_{R_{zz}}$	326e-8	m <sup>4</sup>
Concrete beam length	$b_l$	12	m
Concrete beam width	$b_w$	0.3	m
Concrete beam depth	$b_d$	0.75	m
Sleeper Length	$L_s$	2.6	m
Gap between sleepers	$g_s$	0.6	m
Sleeper cross section area	$A_s$	513.8e-4	m <sup>2</sup>
Sleeper second moment of inertia	$I_{S_{yy}}$	25735e-8	m <sup>4</sup>
Sleeper second moment of inertia	$I_{S_{zz}}$	18907e-8	m <sup>4</sup>
Ballast Depth	$B_d$	0.6	m
Sub-ballast Depth	$SB_d$	0.25	m
Sub-grade Depth	$SG_d$	8.5	m

The modal decomposition and nodal elimination used in the previous model, in Chapter 3, are applied here as well. Basically, a modal analysis is performed for the whole bridge model to extract the mode shapes, eigenvalues, mass matrix and stiffness matrix of the whole system. The part of these matrices associated with the rail nodes are extracted separately and provided to the MBS code as the main input. Then, the dynamic analysis is performed in the MBS code where the contact between the wheels and the rails is taken in consideration. After running the dynamic analysis, the modal displacements and the contact forces are extracted from the MBS code, and then used as input to a Matlab code to reconstruct the nodal deformation of the whole system based on the whole system mode shapes and eigenvalues, which will be used

to visualize the model deformation, strain and elastic stresses. The analysis done in the rest of this chapter are based on running speed of 30 m/s and stiffness proportional damping except where noted. The same wheelset used in Chapter 3 is used for the bridge model as well.

#### **4.1.2 Boundary conditions**

Defining suitable boundary conditions is essential in any FE model. In this bridge model rail is modeled using beam elements with their beginning and end nodes are fully constrained. The bottom face of the model, subgrade layer, is fixed in all directions, while the nodes that fall on any of the four sides are constrained in the direction perpendicular to that surface that contains these nodes.

The common nodes between the sleepers and ballast are constrained for the rotational degrees of freedom as the solid elements only have translational degrees of freedom while the beam elements have six degrees of freedom, three translational and three rotational. Also, the rotational degrees of freedom of the common nodes between the spring elements and the beam elements of the rail are constrained.

TABLE IV: Finite element model material properties.

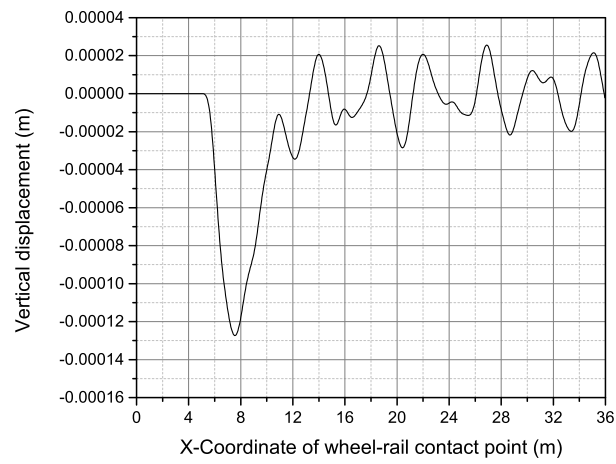
Description	Symbol	Value	Unit
Rail stiffness	$E_r$	210e9	N/m <sup>2</sup>
Rail density	$\rho_r$	7700	kg/m <sup>3</sup>
Rail Poisson's ratio	$\epsilon_r$	0.3	
Sleeper stiffness	$E_s$	64e9	N/m <sup>2</sup>
Sleeper density	$\rho_s$	2750	kg/m <sup>3</sup>
Sleeper Poisson's ratio	$\epsilon_s$	0.25	
Concrete beam stiffness	$E_{bm}$	31e9	N/m <sup>2</sup>
Concrete beam density	$\rho_{bm}$	2500	kg/m <sup>3</sup>
Concrete beam Poisson's ratio	$\epsilon_{bm}$	0.2	
Deck stiffness	$E_d$	31e9	N/m <sup>2</sup>
Deck density	$\rho_d$	2500	kg/m <sup>3</sup>
Deck Poisson's ratio	$\epsilon_d$	0.25	
Ballast stiffness	$E_b$	260e6	N/m <sup>2</sup>
Ballast density	$\rho_b$	1300	kg/m <sup>3</sup>
Ballast Poisson's ratio	$\epsilon_b$	0.3	
Sub-ballast stiffness	$E_{sb}$	200e6	N/m <sup>2</sup>
Sub-ballast density	$\rho_{sb}$	1850	kg/m <sup>3</sup>
Sub-ballast Poisson's ratio	$\epsilon_{sb}$	0.35	
Sub-grade stiffness	$E_{sg}$	200e6	N/m <sup>2</sup>
Sub-grade density	$\rho_{sg}$	1850	kg/m <sup>3</sup>
Sub-grade Poisson's ratio	$\epsilon_{sg}$	0.3	
Abutment stiffness	$E_a$	20e9	N/m <sup>2</sup>
Abutment density	$\rho_a$	2500	kg/m <sup>3</sup>
Abutment Poisson's ratio	$\epsilon_a$	0.3	
Slab stiffness	$E_{sl}$	31e9	N/m <sup>2</sup>
Slab density	$\rho_{sl}$	2500	kg/m <sup>3</sup>
Slab Poisson's ratio	$\epsilon_{sl}$	0.25	
Fastener stiffness	$K_f$	70e8	N/m

## 4.2 Wave reflection

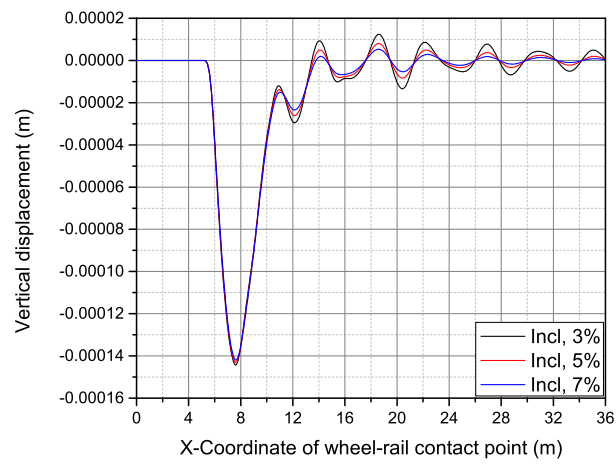
In some FE models, the model boundaries can cause artificial wave reflection. These reflections affect the outputs of the models and can mislead the conclusions. In this section, we test our model for wave reflections and how to eliminate it if it exists, so it will not affect the results in the rest of the chapter.

We started by expanding the model in the Three directions to minimize the boundary effects. Then we tested the model for the reflections without adding any damping to the model, including the material damping. One method to eliminate the wave reflection is to apply damping to the model, which is useful for both static and dynamic analysis. In this section, modal damping was used to damp any undesired excitation in the system. We tested the model for three modal damping values which are 3%, 5%, and 7%. In the following figures we compare the results for the two cases where there is no damping and where modal damping is applied. The analysis in this section are based on running speed of 45 m/s and the case of inclined slab (this will be discussed in the next section)

In Figure 19, the nodal vertical displacement of node 44 is presented. We can see that the model still have some wave reflections, as the displacements is still oscillating even though the contact between the wheel and the rail is already done, even with the expansion of the model size. The same performance can be seen at different locations, Node 83 and node 132, where the wave reflections exist where no damping is applied, and they are eliminated with applying the modal damping, see Figure 20 and Figure 21. We can see that the reflections are eliminated at all

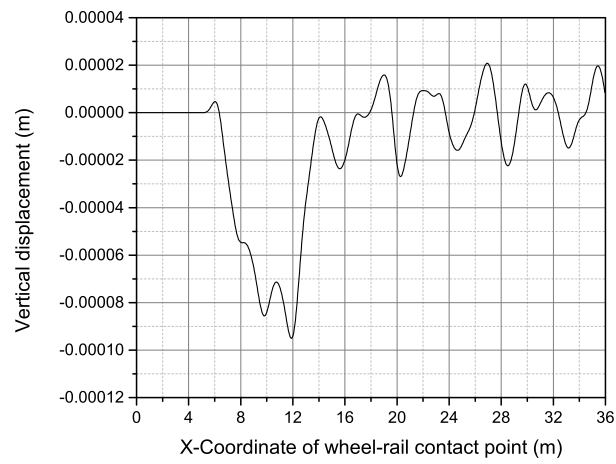


(a)

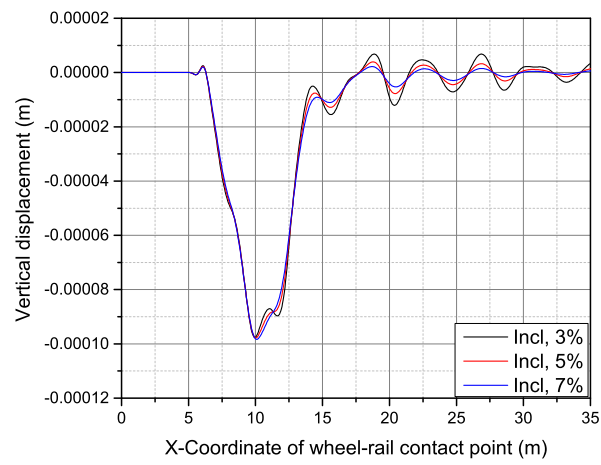


(b)

Figure 19: Vertical displacements of Node 44, see Figure 24a, inclined case, speed=45m/s (a) No damping (b) Modal damping.



(a)



(b)

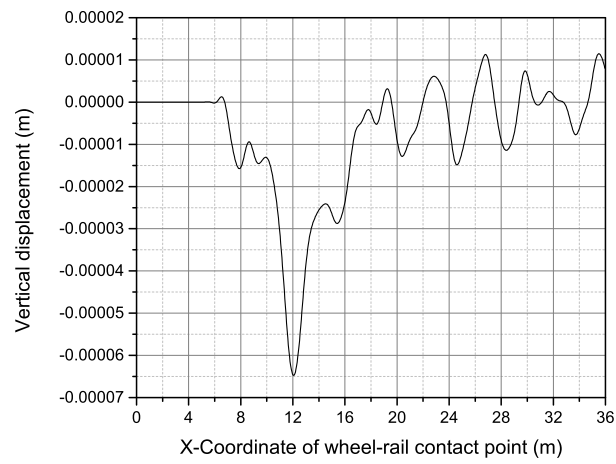
Figure 20: Vertical displacements of Node 83, see Figure 24a, inclined case, speed=45m/s (a) No damping (b) Modal damping.

locations when the modal damping is applied, even with smallest case of 3%. The rest of vibrations seen here are just the normal vibration from the dynamic loading which is decaying with time as seen in all the figures.

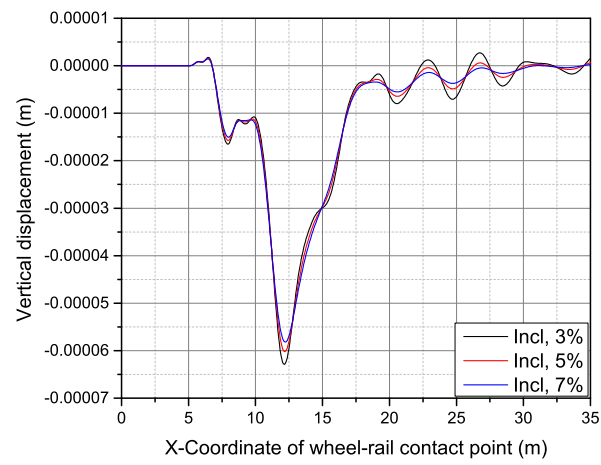
Beside the displacement, the wheel-rail contact force were examined for the wave reflections.

As shown in Figure 22 the wave reflection can be seen in the wheel-rail contact force as well when no damping is applied, and it is eliminated when the modal damping is applied.

Based on the results in this section, we can continue the rest of this chapter knowing that the model does not have reflection problem. Again, in the rest of this chapter all the simulations are based on stiffness proportional damping as mentioned before, which as seen below also have no wave reflection problems.

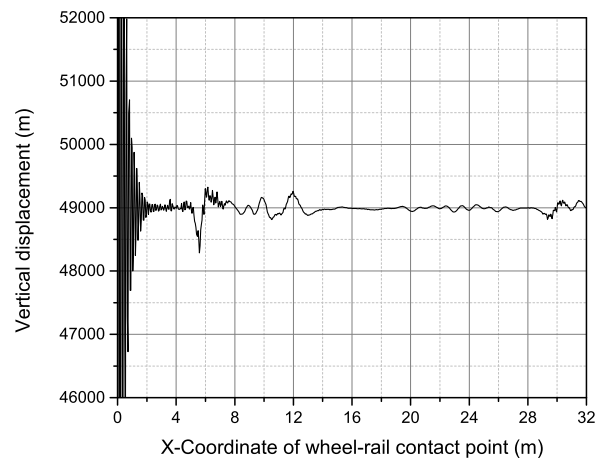


(a)

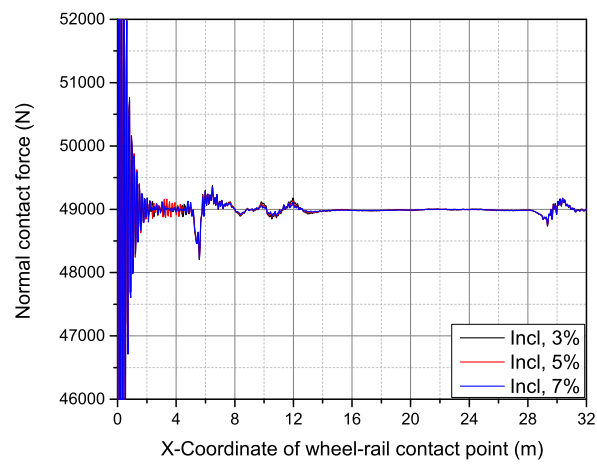


(b)

Figure 21: Vertical displacements of Node 132, see Figure 24a, inclined case, speed=45m/s (a) No damping (b) Modal damping.



(a)



(b)

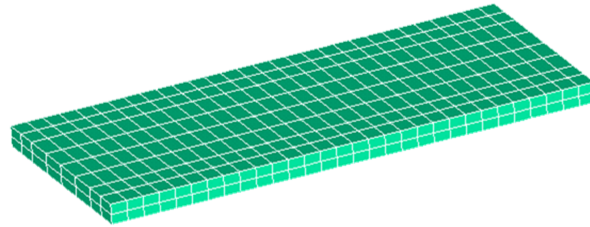
Figure 22: Wheel-rail contact force, speed=45m/s (a) No damping (b) Modal damping.

### 4.3 Results

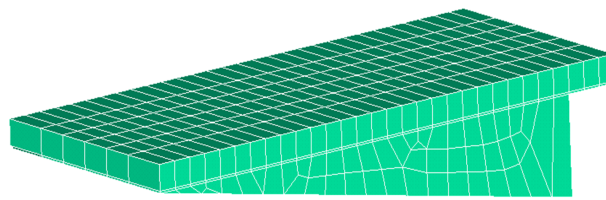
In this section, the main outputs of interest of the model are presented. We focus on the vertical displacements, contact forces, and stress. The bridge approach problem, as discussed above, is mainly the problem of settlement due to high stresses caused by a sudden change in stiffness in the supporting layer under the rail at the entrance and the exit of the bridge. We investigate a potential solution by placing a concrete slab under the ballast layer that can rest on the edge of the abutment to minimize the settlement by decreasing the gradient of the stiffness variation.

The use of slab is not common in the railroad industry, therefore, we started with a slab design close to a slab used in the highway bridge design found in the literature [60].

Two slab designs are presented to investigate the effect of each of them: a rectangular slab and inclined slab, as shown in Figure 23. The locations and the node numbers on the rail and soil where the vertical displacements are presented in Figures 24a and 24b. The rectangular slab has a length of 6m, and width of 2.6m, and thickness of 0.25m. On the other hand, the inclined slab has the same length and width while the thickness increases from 0.25m to 1.2m.



(a) Rectangular slab



(b) Inclined slab

Figure 23: The used two propped slab designs (a) Rectangular slab (b) Inclined slab.

#### 4.3.1 Vertical displacements

The following figures compare different results for three cases: no slab, rectangular slab, and inclined slab at the approach zone. In Figure 25, the vertical displacements of a general node on the rail away from the slab effect is presented for the three cases, and as expected the three models show similar performance as the effect of the bridge approach is minimal at that distance.

In Figure 26, the vertical displacement of a node in the middle of the slab is examined. Here, the effect of the slab in each of the three models is very clear.

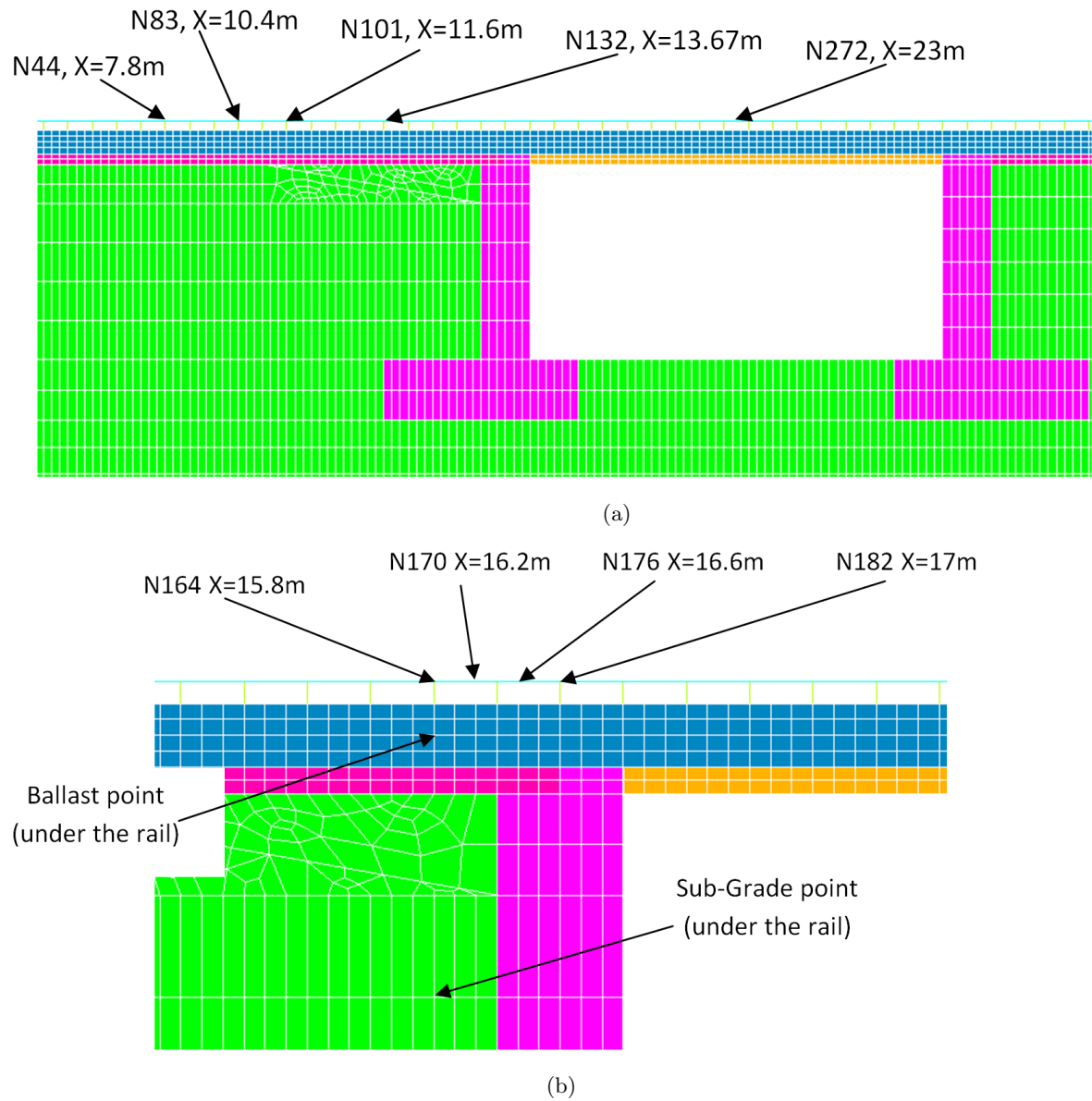


Figure 24: (a) Points of interests on the rail (b) Points on the approach and in the soil.

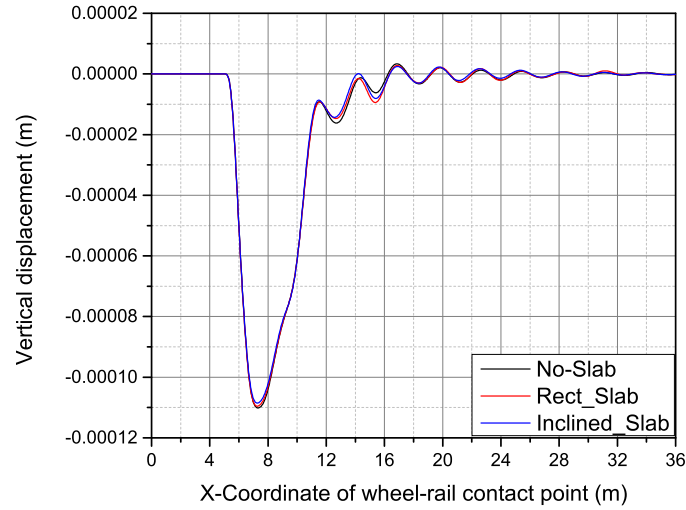


Figure 25: Vertical displacement of Node 44, a general rail point away from the slab effect, see Figure 24a.

As anticipated, the highest value of vertical displacement is associated with the case of no slab, while it decreases by 19% with the rectangular slab, and by nearly 52% with the inclined slab.

Figure 27 presents another point located far from the effect of the bridge approach zone, in the middle of the bridge, and it shows identical performance for the three cases as predicted.

In Figure 28 to Figure 31, rail points at the bridge approach zone are presented. Figure 28 shows the vertical displacement of the rail node above the last sleeper before the abutment, while Figure 29 shows the vertical displacement for the last rail node before the abutment. Continuing on the track, Figure 30 shows the vertical displacement for the first rail node above

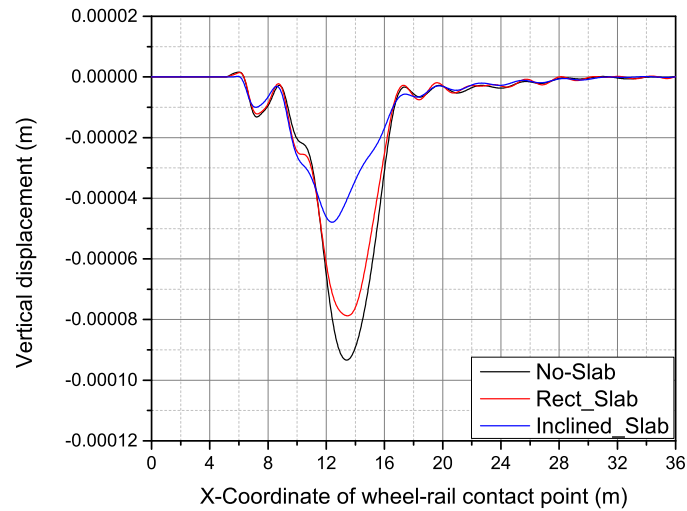


Figure 26: Vertical displacement of Node 132, a rail point above the slab middle point, see Figure 24a.

the abutment while Figure 31 shows the vertical displacement of the rail node above the first sleeper above the abutment.

These four figures show clearly the effect of the two slabs on the reduction of the vertical displacement of the rail, compared to the no slab case. As shown in Figure 28, the rail node above the last sleeper before the abutment, the use of the rectangular slab and the inclined slab reduce the vertical displacement by about 44% and 71% respectively compared to the no slab case.

In Figure 29, the last rail node before the abutment, the use of the rectangular slab and the inclined slab reduce the vertical displacement by about 46% and 68%, respectively, compared

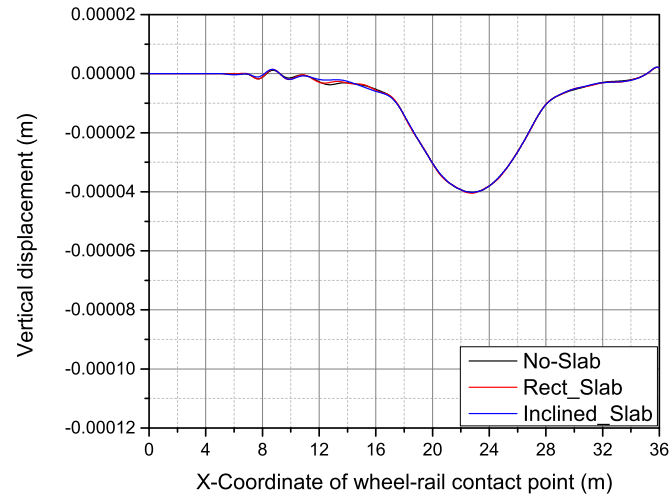


Figure 27: Vertical displacement of Node 272, a rail point in the middle of the bridge, see Figure 24a.

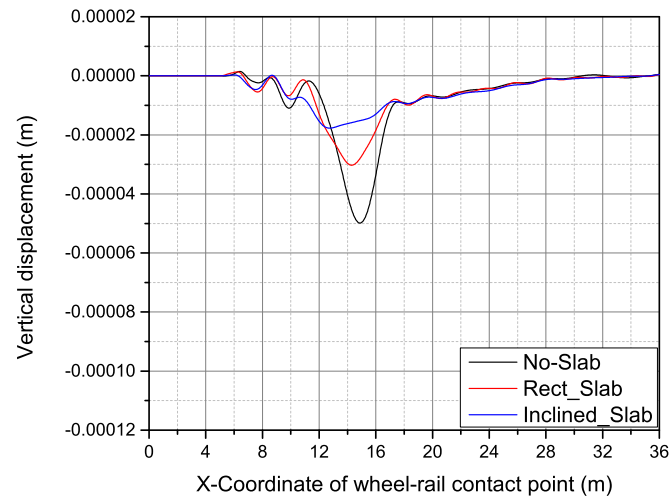


Figure 28: Vertical displacements of Node 164, a rail point on last sleeper before the abutment, see Figure 24b.

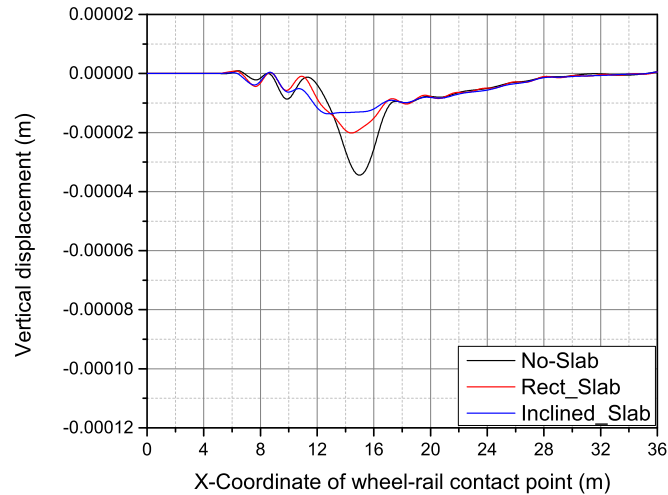


Figure 29: Vertical displacements of Node 170, the last rail node before the abutment, see Figure 24b.

to the no slab case. The same trend of reduction is also shown in Figure 30, the rail node above the first sleeper above the abutment. The use of the rectangular slab and the inclined slab reduced the vertical displacement by about 45% and 58%, respectively, compared to the no slab case. In Figure 31, the rail node above the first sleeper above the abutment, the use of the rectangular slab and the inclined slab reduced the vertical displacement by about 30% and 34% respectively compared to the no slab case.

The above figures and the associated percentages in the vertical displacements reduction show the effectiveness of the implementation of both the rectangular and the inclined slabs in the bridge approach zone, especially the inclined slab, which has a higher vertical displacement

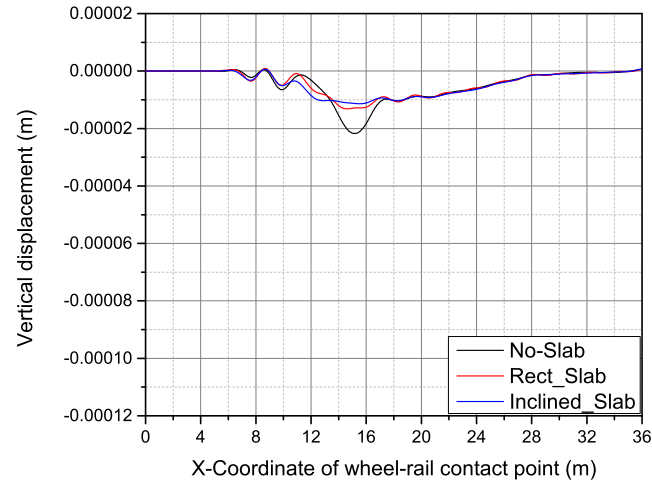


Figure 30: Vertical displacement of Node 176, the first rail point after the beginning of the abutment, see Figure 24b.

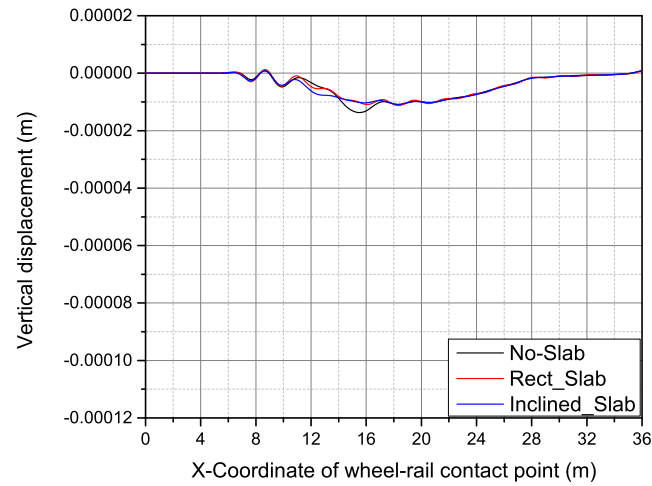


Figure 31: Vertical displacement of Node 182, a rail point on the first sleeper on the abutment, see Figure 24b.

reduction. By comparing the displacements between Figure 28 and Figure 30, which represents the last sleeper before the abutment and the first sleeper above the abutment, respectively, we can see clearly how the slabs reduce the vertical “jump” in the rail displacement when the vehicle cross the entrance of the bridge. Quantitatively, the no slab case has 75% change in the height of the vertical displacement, and 60% in the rectangular slab case, while it is only 43% in the inclined slab case. However, we should pay attention to the absolute values before and after the abutment to recognize that the 43% is from a smaller vertical displacement for the inclined slab case compared to the no slab case, where the vertical displacement before the abutment was a relatively higher value.

It is also important to mention here that the effect of the slabs starts from the beginning of the slab section, not only before the abutment at the bridge approach zone. As seen in Figure 32, the vertical displacement of the rail node above the last sleeper before the beginning of the slab is presented, and we can see it shows already slight difference between the three cases due to the effect of the implemented slabs. However, in Figure 33, which shows the vertical displacement of the rail node above the first sleeper on the slab, we can see clearly the effect of the different slab designs on the system performance via the variation in the displacement peak values even where the slab effect is just starting.

Besides the rail nodes, the results of few points in the ballast and subgrade are also presented. In Figure 34, the vertical displacement of a node in the ballast under the last sleeper before the abutment is presented. We can see how the vertical displacement in the ballast is decreased with the use of the slabs, with a reduction of 33% for the rectangular slab, and 62% for the inclined

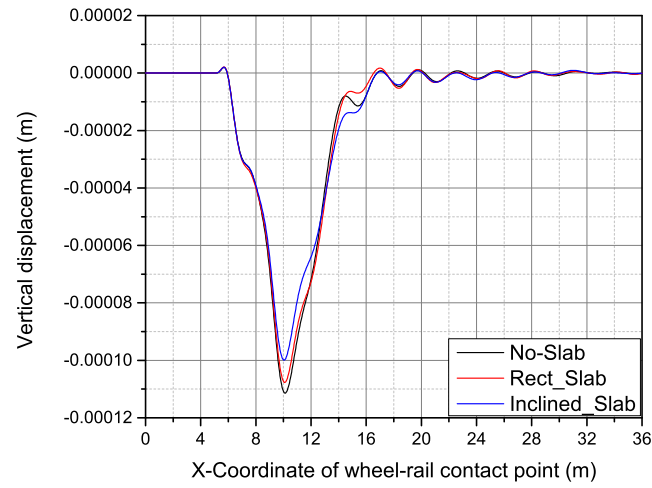


Figure 32: Vertical displacement of Node 83, a rail point on last sleeper before the slab, see Figure 24a.

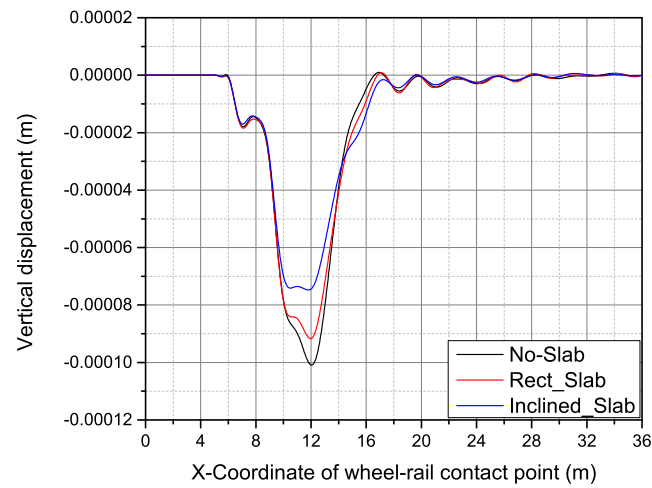


Figure 33: Vertical displacement of Node 101, a rail point on first sleeper of the slab, see Figure 24a.

slab. In Figure 35, which presents the vertical displacement of a node on the subgrade under the last sleeper before the abutment, we can see similar behavior is repeated. The rectangular slab shows a reduction of 33% while the inclined slab shows a reduction of about 40% in the vertical displacement compared to the case of no slab.

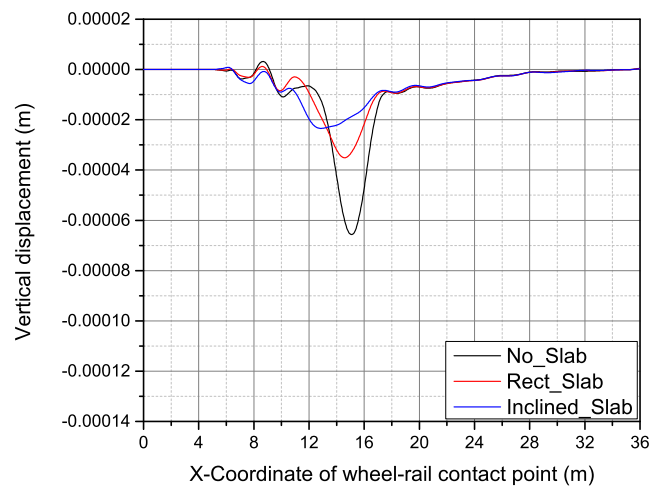


Figure 34: Vertical displacement of a ballast node under the last sleeper before the abutment.

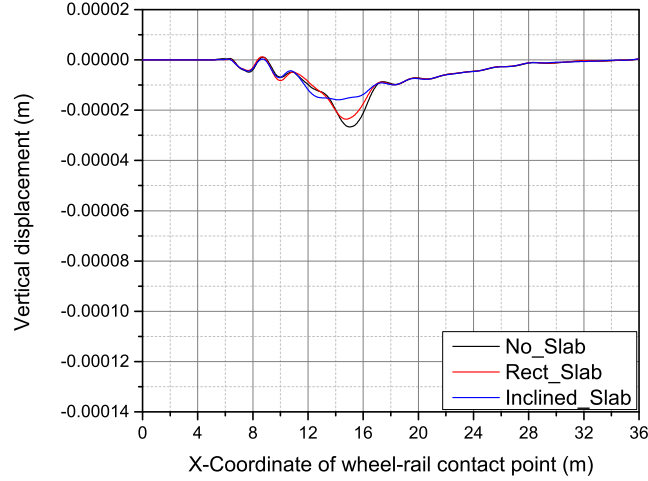


Figure 35: Vertical displacement of a subgrade node under the last sleeper before the abutment.

#### 4.3.2 The wheel/rail contact force

The wheel/rail contact force is also a significant factor to investigate in this study, as it is an indicator of ride quality and also has its impact on the track structure. Figure 36 compares the contact force for the three models, no slab, rectangular slab, and inclined slab, with a wheelset running with a speed of 30 m/s. As we can see in the figure, the model with no slab has the highest jump in the contact force value as the wheelset approaches the bridge entrance zone, around  $X=16\text{m}$ , while having a rectangular slab reduces the peak of the jump, and the case of inclined slab shows an even smoother variation compared to the other cases.

It is important to mention here that the magnitude of the force depends on the velocities of the train. Therefore, similar runs were performed at higher speeds to check the model performance

regarding this point. As shown in Figure 37 and Figure 38, we can see the results show greatly improved performance and the same trend of the lower speed is achieved with a running vehicle with speeds of 45 m/s and 60 m/s, respectively. These results show the effectiveness of the model performance at different speeds as well as the effectiveness of the two slabs, especially the inclined one, compared to the no slab case. Even at higher speed, the slabs will reduce contact forces and improve rider comfort.

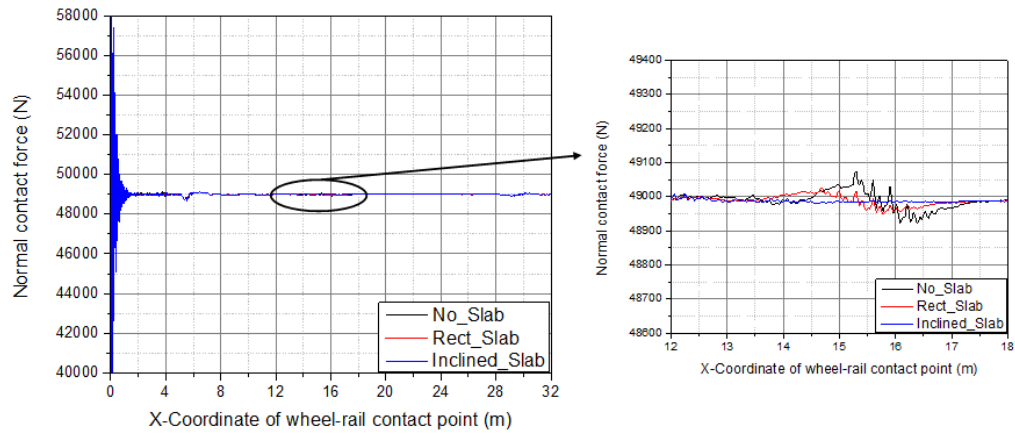


Figure 36: Wheel/rail contact force, the inset showing the area near the bridge entrance, speed=30m/s.

For clearer comparison, Figure 39 to Figure 41 show the performance of each case at four different speeds and how the slabs perform at the bridge approach zone. The speeds used here are 15, 30, 45, and 60 m/s.

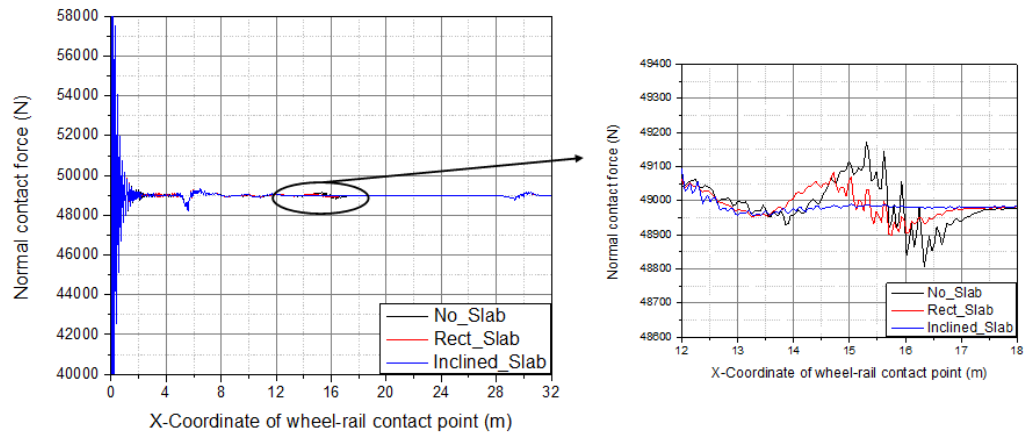


Figure 37: Wheel/rail contact force, the inset showing the area near the bridge entrance, speed=45m/s.

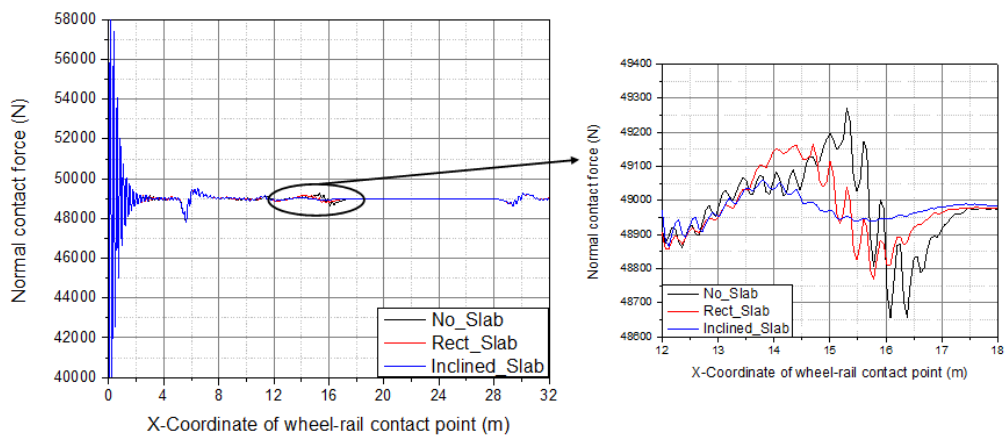


Figure 38: Wheel/rail contact force, the inset showing the area near the bridge entrance, speed=60m/s.

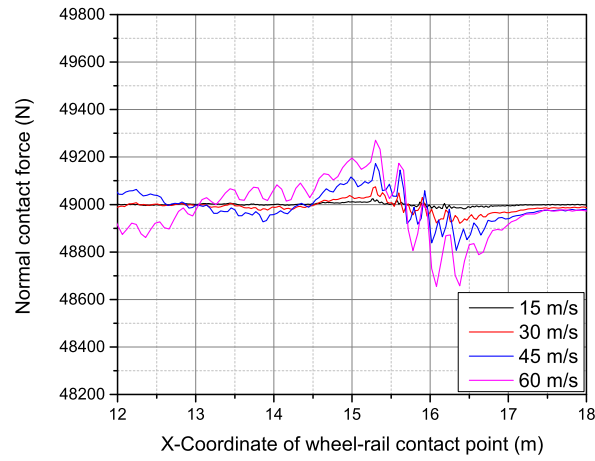


Figure 39: Wheel/rail contact force for the no slab case

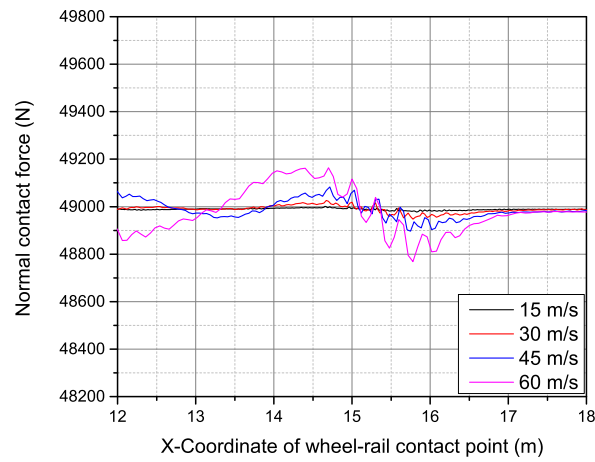


Figure 40: Wheel/rail contact force for the rectangular slab case

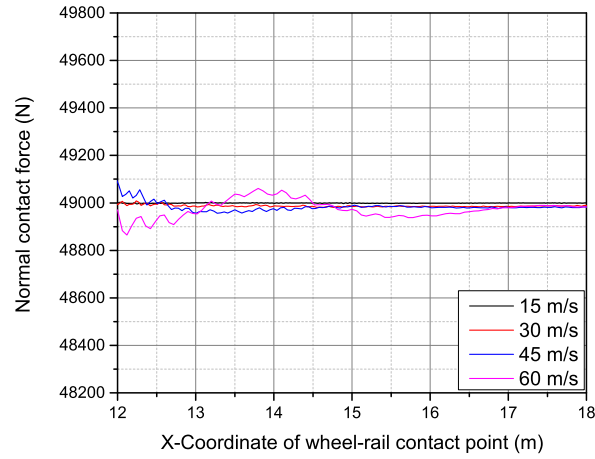


Figure 41: Wheel/rail contact force for the inclined slab case

It is important to point out that using the slab did not shift jump in the contact force from the bridge entry to the beginning of the slab. As shown in Figure 42, the contact force for the three cases are almost the same at the beginning of the slab, as the slab depth is initially small.

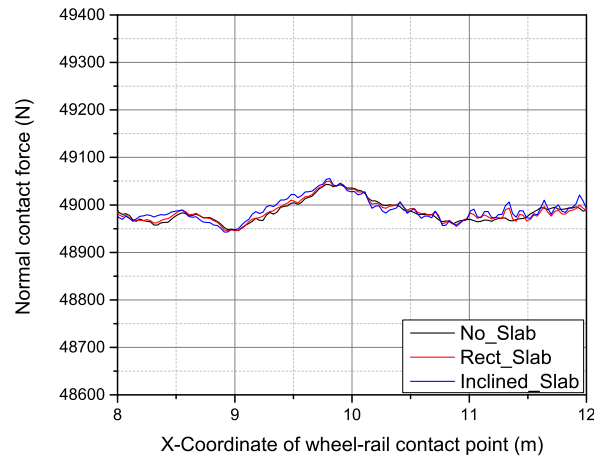


Figure 42: Wheel/rail contact force, at the beginning of the slab, speed=30m/s.

#### 4.4 Stresses in the substructure

The previous sections showed the improved performance of the models with the implemented slab when it comes to the displacements and the contact forces. We also wish to investigate the stresses in the substructure to see how the implementation of the slabs affects the stresses in the soil. High stresses can lead to settlement of the soil, exacerbating the issues associated with bridge approaches. In the rest of this section, the stresses are compared for the three cases. The plotted stresses are the change in the stress from the static stress caused by gravity, which means that the gravity effect was excluded for the three cases, and this is why the graphs start at zero stress.

By checking the stresses in the ballast layer above the middle point of the slab, we can see that the implementation of the slabs does not have a strong affect on the stress compared to the no slab case, as shown in Figure 43.

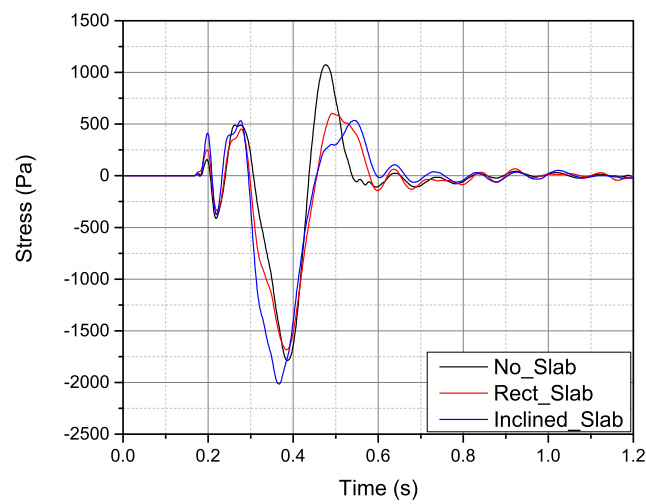


Figure 43: Difference in vertical stress from unloaded case in the ballast above the middle of the slab, see Figure 24a.

On the other hand, the results shown in Figure 44 represents the stresses in the subgrade below the middle of the slab. As shown, the stress magnitude is reduced with the implementation of the slabs, especially with the inclined slab.

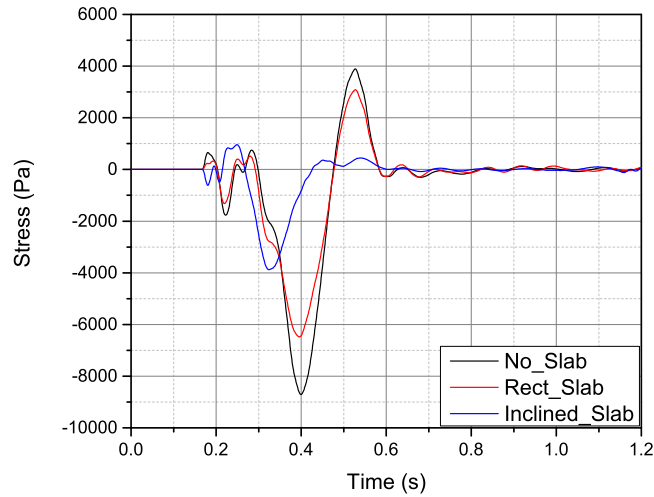


Figure 44: Difference in vertical stress from unloaded case in the subgrade below the middle of the slab, see Figure 24a.

Another point of interest is the ballast at the bridge entrance, as this is the main area where the stiffness suddenly change from soft to stiff leading to the the bridge approach problems mentioned before. As shown in Figure 45, by comparing the stress of the three cases, we can see that the case of the rectangular slab acts in very similar way of the no slab case, which can be explained as the change in the stiffness at that point, very close to the bridge entrance, is acting in similar way for both the rectangular and the no slab cases, even though the difference is not the same. However, the stress of the inclined slab case show a significant reduction in the stress level in the ballast layer, as the sudden change in the stiffness problem is eliminated.

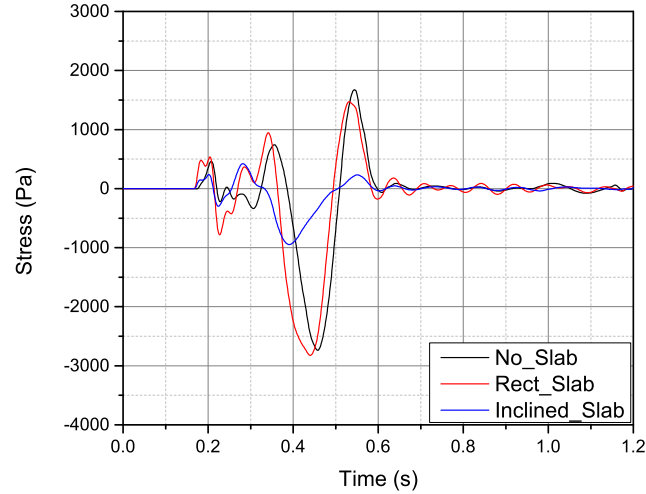


Figure 45: Difference in vertical stress from unloaded case in the ballast just before the bridge entrance, see Figure 24b.

Finally, we check the stress at a point away from the effect of the slab, as we did with the displacements, we can see that the models are working as expected, as the stresses are the same as shown in Figure 46

The results presented in this chapter show the robustness of the FE model, as well as the coupling technique presented through the work. The implementation of the slabs at the bridge entrance zone show great effectiveness on all the investigated outputs: vertical displacement, contact force and vertical stress. The inclined slab, as expected, performed more effectively than the rectangular slab, and showed high reduction in the three mentioned outputs compared to both cases. It can be concluded from the results presented here that constructing a concrete

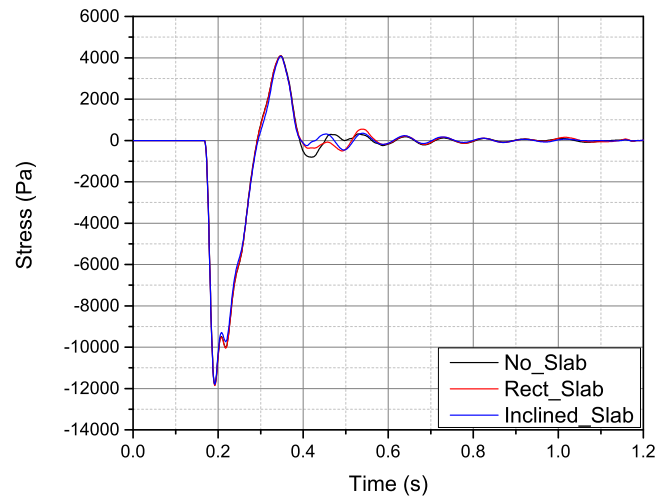


Figure 46: Difference in vertical stress from unloaded case in the subgrade away of the slab effect, see Figure 24a.

slab at the entrance/exit of the bridge, can lead to significant reduction in the settlement and the developed problems as it reduce the suddenness of stiffness change and hence stresses in the substructure.

## CHAPTER 5

### CONCLUSIONS AND FUTURE WORK

#### 5.1 Conclusions

Due to the different problems associated with the railroad industry, many researchers have directed their knowledge and tools to try to search for solutions. In this work, finite element analysis and multibody system dynamics were used to model and investigate the railroad system. We started with a generic model of a regular track to use it to implement the suggested methodology. This methodology is based on coupling the FEM and MBS in the same model. the coupling process starts by building a full 3D model using the FEM and extract the modal information of the whole system.

These modal information includes the mode shapes, the modal frequencies, and damping values. Nodal elimination is then applied as the modal components associated to the rails only are extracted and provided to the MBS code, where the dynamic analysis is performed.

The dynamic analysis includes the wheel/rail contact, as the vehicle is represented using a wheelset and the rails are modeled using beam elements. The main output of the MBS analysis are the modal displacement of the rails and the contact forces between the wheel and the rails over the analysis time. The modal displacements are used as an input to a Matlab code to reconstruct the nodal displacements of the whole system, which later is used as input to

ANSYS (to visualize the nodal deformation and calculate the strains and the elastic stresses). The model was verified as it was compared with the literature and showed great agreement for both displacements and forces for two scenarios.

The comparison between the FE model and the literature, as shown in Chapter 3, was performed for two main cases. The first is the normal track with no defects, while the second case included an unsupported sleeper in the middle of the model. The results included the vertical displacements of the rail nodes at different locations including points above the sleepers and between the sleepers as well. Also, the contact force between the wheel and the rail was presented. The results showed great agreement between the FE model and the literature. The new model did show some coupling in the deformation between sleepers that previous model were unable to capture. Before the modal decomposition was applied, a convergence test was performed for the effect of the number of mode shapes to guarantee that the used number of mode shapes were sufficient and does not affect the result negatively.

After the methodology was verified, the work took a further step to benefit from the coupling technique by investigating a more practical and complicated problem, which is the bridge approach problem. The bridge approach problem is a common problem in the railroad industry. This problem appears at the bridge entrance and exit due to the sudden stiffness variation between the foundation stiffness before and after the bridge. This sudden stiffness variation causes soil settlement, which leads to a change in the rail level. This rail change in level causes a sudden impact which develops high level of contact force, faster wear of rail surface, and discomfort for passengers.

A full 3D bridge model was built using FE and coupled with the MBS code in the same way as in the first part of this work. The purpose of that model was to study the effectiveness of constructing a concrete slab below the ballast at the bridge approach zone. The purpose of these slab is to create a more gradual change in the stiffness, improve ride quality, reduce the wear in the wheel and the rail surface, and reduce the maintenance cost. We compared three cases: no slab, rectangular slab, and inclined slab. The rectangular slab has a constant thickness, while the inclined slab has a linearly increasing thickness to linearly increase the stiffness from the soft soil stiffness to the stiff bridge.

The work investigated the model performance regarding the vertical displacement of the rail nodes as well as the soil nodes. The results show great improvement in the performance with both slabs especially, as expected, with the inclined slab. We can see in Chapter 4, the vertical displacements were reduced considerably at different locations and show smoother level of change from the soil to the bridge. The contact forces were investigated as well, and the results show a good reduction in the force peak at the entrance of the bridge when the slabs were used, and, again, the inclined slab showed better performance. The effect of train speed was taken in consideration for the contact forces analysis, and the results showed that the model performed in well even at higher speeds. The analysis also showed that the implementation of the slab did not simply move the force peak from the abutment to the beginning of the slab.

Another important factor to investigate in this study was the stress in the soil besides the vertical displacements and the contact forces. High stresses can cause increase soil settlement and degradation of the material. The implementation of slab has an effect on the performance

of the soil, especially the subgrade, this why it was necessary to look at the stress values. The stresses figures show how the stress in the the models with the implemented slabs have been reduced in the subgrade layer below the slabs, which show the effectiveness of the presented methodology and the FE model used and also the effectiveness of the used slabs. The stress in the ballast was not affected greatly by the slab.

In general, The results discussed in Chapters Three and Four show clearly the effectiveness of the coupling technique, presented in this work, between FEM and MBS codes where the model is created using FEM and then the main outputs of the modal analysis is provided to the MBS code and then apply the nodal elimination process which can save significant amount of time and makes us able to study more complicated models with more details. The results also show the effectiveness of the slab implementation at the bridge entrance and how it has a clear effect on the vertical displacements (for rails and soil), the wheel/rail contact force and the stress level in the subgrade at the bridge approach zone.

## **5.2 Future work**

The work performed in this dissertation covers mainly the coupling between the FEM and MBS to benefit from the advantages of each method in one model in a way that helps to build a complicated model but with much less simulation time. The coupling was implemented in two successful models including the investigation of the bridge approach problem. However, there is still a space for further work that can be done to profit from the coupled model developed here and to be applied on different cases.

For instance, the model can be used to investigate a problem such as the vibration in the surrounding structures around the railroad track. The interaction between the train and the rails produces vibrations in the surrounding area, especially with high speed trains, which could be felt in the buildings close to the rail if the vibrations level is high enough or the building are close enough to the rails. The work done here can be directed to build a sophisticated model that contains the different components of the rail system including the surrounding buildings and benefit from the fact that the suggested approach can save time for the model that includes a lot of details. This work can be used to help in finding solutions that eliminate or at least reduce the vibration level in areas surrounding a train track. The model could simulate different approaches to damp these vibrations below the acceptable level.

The case of the bridge approach problem itself could be used for further analysis as well. For example, an optimization process could be performed on the slab design by using the coupled FE/MBS model to decide the most suitable slab material and dimensions or even the shape of the slab to increase the reduction in the contact forces and the vertical deformation to reduce the settlement or at least slow it down, and provide more comfortable rides and save the maintenance cost. As the FE model is parametric based, it could be easily used in automated optimization process with using good coding to run the model with variable inputs for each run.

More advanced analysis could be applied as well in future models, such as using plastic material model instead of elastic one to have deeper investigation regarding the soil performance under

different speeds or loading. Also, to perform non-linear analysis to even make the model a robust one that has the minimum number of assumptions and simplifications.

In general, the methodology used in this work showed its efficiency and can have different applications in different engineering fields not only limited to the railroad, especially with systems of a complicated nature and when the coupling between FEM and MBS is needed so time could be saved and assumptions could be minimized.

## APPENDICES

## Appendix A

### THE APDL FE MODEL

This is the ANSYS-APDL code used to build the inclined model. It is a parametric code that can be edit by changing the parameters at the top of the code. The code also include the modal analysis, and to save space, the part where the data extracted from SAMS and modified using Matlab is also added at the end.

```

fini
/clear
/prep7
!- - - - -
ET,1,BEAM188 !--- The Rail, the sleepers
ET,2,SOLID185 !--- The Soil layers and the concrete parts
ET,9,COMBIN14 !--- The spring elements connecting rails and sleepers
ET,10,COMBIN14 !--- The spring elements connecting rails and sleepers
ET,11,COMBIN14
!- - - - -
KEYOPT,9,1,0
KEYOPT,9,2,1      !---  Ux
KEYOPT,9,3,0
KEYOPT,10,1,0
KEYOPT,10,2,2     !---  Uy
KEYOPT,10,3,0
KEYOPT,11,1,0
KEYOPT,11,2,3     !---  Uz
KEYOPT,11,3,0
!- - - - -
SECTYPE,1, BEAM, I, , 0      ! rail
SECOFFSET, CENT
SECDATA,0.1524,0.07,0.19,0.0165,0.045,0.0175,0,0,0,0,0,0
!*
SECTYPE,2, BEAM, QUAD, , 0   ! sleeper
SECOFFSET, CENT

```

## Appendix A (Continued)

```
SECDATA,-0.135,-0.11,.135,-.11,.090,.11,-.090,.11,8,10,0,0
```

```
SECTYPE, 3, BEAM, RECT, , 0 ! beam
```

```
SECOFFSET, CENT
```

```
SECDATA,0.3,0.75,0,0,0,0,0,0,0,0,0
```

```
R,9,70e9,5e5, !--- the data of spring in x-dirction
```

```
R,10,70e9,5e5, !--- the data of spring in y-dirction
```

```
R,11,70e9,5e5, !--- the data of spring in z-dirction
```

```
!----- the material info for the corresponding element -----!
```

```
MP,EX,1,210e9 !--- the data of the rails
```

```
MP,PRXY,1,0.30
```

```
MP,ALPD,1,0
```

```
MP,BETD,1,1e-6
```

```
MP,DENS,1,7700
```

```
!*
```

```
MP,EX,55,210e10 !--- RIGID RAIL
```

```
MP,ALPD,55,0
```

```
MP,BETD,55,1e-6
```

```
MP,DENS,55,7700
```

```
!*
```

```
MP,EX,2,64e9 !--- the data of the sleepers
```

```
MP,PRXY,2,0.25
```

```
MP,ALPD,2,0
```

```
MP,BETD,2,10e-4
```

```
MP,DENS,2,2570
```

```
!*
```

```
MP,EX,3,31e9 !--- the data of the beams
```

```
MP,PRXY,3,0.20
```

```
MP,ALPD,3,0
```

```
MP,BETD,3,10e-4
```

```
MP,DENS,3,2500
```

```
!*
```

```
MP,EX,4,260e6 !--- the data of the ballast
```

```
MP,PRXY,4,0.25
```

```
MP,ALPD,4,0
```

```
MP,BETD,4,12e-4
```

```
MP,DENS,4,1300
```

```
!*
```

```
MP,EX,5,200e06 !--- the data of the sub_ballast
```

```
MP,PRXY,5,0.2
```

```
MP,ALPD,5,0
```

## Appendix A (Continued)

```

MP,BETD,5,15e-4
MP,DENS,5,1850
!*
MP,EX,6,200e6      !--- the data of the sub_grade
MP,PRXY,6,0.2
MP,ALPD,6,0
MP,BETD,6,15e-4
MP,DENS,6,1850
!*
MP,EX,7,31e9          !--- the data of the deck
MP,PRXY,7,0.25
MP,ALPD,7,0
MP,BETD,7,8e-4
MP,DENS,7,2500
!*
MP,EX,8,20e9          !--- the data of the abutments
MP,PRXY,8,0.30
MP,ALPD,8,0
MP,BETD,8,10e-4
MP,DENS,8,2500
!*
MP,EX,9,50E9  !--- spring x
MP,PRXY,9,0.1
MP,ALPD,9,0
MP,BETD,9,1e-6
!*
MP,EX,10,50E9 !--- spring y
MP,PRXY,10,0.1
MP,ALPD,10,0
MP,BETD,10,1e-6
!*
MP,EX,11,50E9  !--- spring z
MP,PRXY,11,0.1
MP,ALPD,11,0
MP,BETD,11,1e-6
!*
MP,EX,22,31e9          !--- SLAB
MP,PRXY,22,0.25
MP,ALPD,22,0
MP,BETD,22,10e-4
MP,DENS,22,2500
!*

```

## Appendix A (Continued)

```

!*****      the main variables to be used through the model      *****!
R_Gage=2*0.75565 !--- the rail gage based on SAMS
rigid=5
Rail_out=12
Rail_bridge=12 !--- Rail length ON the bridge
Tot_R_len=Rail_out+Rail_bridge+6 !--- Rail length
Slap_L=6          !--- Slap length

Length_1= Rail_out-2.4
Length_2=2.4
Length_3=1.2
Length_4=1.2
Length_5=Rail_bridge-4.8

DBS=0.6
N_S=Tot_R_len/DBS+1
NE_S=3
NE_X=(N_S-1)*NE_S
E_L=Tot_R_len/NE_X

NE_O=(Rail_out/DBS)*NE_S
NE_B=(Rail_bridge/DBS)*NE_S

B_End=Rail_out+Rail_bridge

Middle_Y=4!(must be even in this model)
S_OUT_Y_Ele=2
B_OUT_Y_Ele=2
D_OUT_Y_Ele=2
A_OUT_Y_Ele=2
SB_OUT_Y_Ele=5! 6

B_Depth_Z_Ele1=4
B_Depth_Z_Ele2=2
D_Depth_Z_Ele=2! 3
SB_Depth_Z_Ele=2! 3
Rubber_Depth_Z_Ele=1
Deck_W=5.84
Abut_W=7.3
outlayerlength=3
Lowerdepth=1.5
LDSG=2

```

## Appendix A (Continued)

```

SB_X_FIRST=NE_0-4*NE_S
SB_X_second=4*NE_S
DS_X_deck=2*NE_S
!!!BA_X_middle=NE_B-4*NE_S
vert1=6
vert2=2
vert3=3

!TOLERANCE=0.001/2
!/NERR,5,10000000,
!-----(( CREATING THE RAILS ))-----!
! LEFT SECTION, Before the bridge !
TYPE,1
MAT,55
secnum,1
k,1,0,-R_Gage/2,0.06924,,,,
k,2,rigid,-R_Gage/2,0.06924,,,,
L,1,2
Lesize,1,,,1,,,,,0
lmesh,1

TYPE,1
MAT,1
secnum,1
*GET,KPr,KP,,COUNT, , , ,
k,3,rigid+E_L/3,-R_Gage/2,0.06924,,,,
L,2,3
Lesize,2,,,1,,,,,0
lmesh,2
LGEN,NE_0*3,2, , ,E_L/3, , ,1,0
! The Bridge section !
*GET,nx1,kp,,count,,,,
nx2=nx1+1
k,nx2,rigid+Rail_out+E_L/3, -R_Gage/2,0.06924,,,,
l,nx1,nx2
*get,nl,line,,count
Lesize,nl,,,1,,,,,0
lmesh,nl
LGEN,(NE_B)*3+(6/DBS)*NE_S*3,nl, , ,E_L/3, , ,1,0
!-----!
TYPE,1
MAT,55

```

## Appendix A (Continued)

```

secnum,1
*GET,KPr,KP,,COUNT, , , ,
*get,nls44,line,,count
k,KPr+1,Tot_R_len+2*Rigid, -R_Gage/2,0.06924
L,KPr,KPr+1
Lesize,nls44+1,,,1,,,,0
lmesh,nls44+1
*get,nls2,line,,count
*get,nend,node,,count
!----- CREATING THE LEFT RAIL -----!
LGEN,2,1,nls2 , , , R_Gage, , ,0 !--- creating the left rail
*get,nend2,node,,count
!--- Creating the surfaces that will be extruded to create the model ---!
*GET,k,kp,,count,,,
K,k+1,rigid,-1.46,-0.135,!-0.135
K,k+2,rigid,-1.3,-0.135,
K,k+3,rigid,-R_Gage/2,-0.135,
K,k+4,rigid, R_Gage/2,-0.135,
K,k+5,rigid, 1.3,-0.135,
K,k+6,rigid,1.46,-0.135,
K,k+7,rigid,-1.81,-0.435,
K,k+8,rigid,-1.3,-0.435,
K,k+9,rigid,-R_Gage/2,-0.435,
K,k+10,rigid, R_Gage/2,-0.435,
K,k+11,rigid, 1.3,-0.435,
K,k+12,rigid,1.81,-0.435,
k,k+13,rigid,-Abut_W/2-outlayerlength,-0.735,
k,k+14,rigid,-Abut_W/2,-0.735,
K,k+15,rigid,-Deck_W/2,-0.735,
K,k+16,rigid,-2.16,-0.735,
K,k+17,rigid,-1.3,-0.735,
K,k+18,rigid,-R_Gage/2,-0.735,
K,k+19,rigid, R_Gage/2,-0.735,
K,k+20,rigid, 1.3,-0.735,
K,k+21,rigid, 2.16,-0.735,
K,k+22,rigid, Deck_W/2,-0.735,
k,k+23,rigid,Abut_W/2,-0.735,
k,k+24,rigid,Abut_W/2+outlayerlength,-0.735,
k,k+25,rigid,-Abut_W/2-outlayerlength,-0.985,
k,k+26,rigid,-Abut_W/2,-0.985,
K,k+27,rigid,-Deck_W/2,-0.985,
K,k+28,rigid,-2.16,-0.985,

```

## Appendix A (Continued)

K,k+29,rigid,-1.3,-0.985,  
 K,k+30,rigid,-R\_Gage/2,-0.985,  
 K,k+31,rigid, R\_Gage/2,-0.985,  
 K,k+32,rigid, 1.3,-0.985,  
 K,k+33,rigid, 2.16,-0.985,  
 K,k+34,rigid, Deck\_W/2,-0.985,  
 k,k+35,rigid,Abut\_W/2,-0.985,  
 k,k+36,rigid,Abut\_W/2+outlayerlength,-0.985,  
 k,k+37,rigid,-Abut\_W/2-outlayerlength,-0.985-(4.8/5) ,  
 k,k+38,rigid,-Abut\_W/2,-0.985-(4.8/5) ,  
 K,k+39,rigid,-Deck\_W/2,-0.985-(4.8/5) ,  
 K,k+40,rigid,-2.16,-0.985-(4.8/5) ,  
 K,k+41,rigid,-1.3,-0.985-(4.8/5) ,  
 K,k+42,rigid,-R\_Gage/2,-0.985-(4.8/5) ,  
 K,k+43,rigid, R\_Gage/2,-0.985-(4.8/5) ,  
 K,k+44,rigid, 1.3,-0.985-(4.8/5) ,  
 K,k+45,rigid, 2.16,-0.985-(4.8/5) ,  
 K,k+46,rigid, Deck\_W/2,-0.985-(4.8/5) ,  
 k,k+47,rigid,Abut\_W/2,-0.985-(4.8/5) ,  
 k,k+48,rigid,Abut\_W/2+outlayerlength,-0.985-(4.8/5) ,  
 k,k+49,rigid,-Abut\_W/2-outlayerlength,-5.805,  
 k,k+50,rigid,-Abut\_W/2,-5.805,  
 k,k+51,rigid,-Deck\_W/2,-5.805,  
 k,k+52,rigid,-2.16,-5.805,  
 k,k+53,rigid,-1.3,-5.805,  
 k,k+54,rigid,-R\_Gage/2,-5.805,  
 k,k+55,rigid,R\_Gage/2,-5.805,  
 k,k+56,rigid,1.3,-5.805,  
 k,k+57,rigid,2.16,-5.805,  
 k,k+58,rigid,Deck\_W/2,-5.805,  
 k,k+59,rigid,Abut\_W/2,-5.805,  
 k,k+60,rigid,Abut\_W/2+outlayerlength,-5.805,  
 k,k+61,rigid,-Abut\_W/2-outlayerlength,-5.805-Lowerdepth,  
 k,k+62,rigid,-Abut\_W/2,-5.805-Lowerdepth,  
 k,k+63,rigid,-Deck\_W/2,-5.805-Lowerdepth,  
 k,k+64,rigid,-2.16,-5.805-Lowerdepth,  
 k,k+65,rigid,-1.3,-5.805-Lowerdepth,  
 k,k+66,rigid,-R\_Gage/2,-5.805-Lowerdepth,  
 k,k+67,rigid,R\_Gage/2,-5.805-Lowerdepth,  
 k,k+68,rigid,1.3,-5.805-Lowerdepth,  
 k,k+69,rigid,2.16,-5.805-Lowerdepth,  
 k,k+70,rigid,Deck\_W/2,-5.805-Lowerdepth,

## Appendix A (Continued)

k,k+71,rigid,Abut\_W/2,-5.805-Lowerdepth,  
 k,k+72,rigid,Abut\_W/2+outlayerlength,-5.805-Lowerdepth,  
 k,k+73,rigid,-Abut\_W/2-outlayerlength,-5.805-Lowerdepth-LDSG,  
 k,k+74,rigid,-Abut\_W/2,-5.805-Lowerdepth-LDSG,  
 k,k+75,rigid,-Deck\_W/2,-5.805-Lowerdepth-LDSG,  
 k,k+76,rigid,-2.16,-5.805-Lowerdepth-LDSG,  
 k,k+77,rigid,-1.3,-5.805-Lowerdepth-LDSG,  
 k,k+78,rigid,-R\_Gage/2,-5.805-Lowerdepth-LDSG,  
 k,k+79,rigid,R\_Gage/2,-5.805-Lowerdepth-LDSG,  
 k,k+80,rigid,1.3,-5.805-Lowerdepth-LDSG,  
 k,k+81,rigid,2.16,-5.805-Lowerdepth-LDSG,  
 k,k+82,rigid,Deck\_W/2,-5.805-Lowerdepth-LDSG,  
 k,k+83,rigid,Abut\_W/2,-5.805-Lowerdepth-LDSG,  
 k,k+84,rigid,Abut\_W/2+outlayerlength,-5.805-Lowerdepth-LDSG,  
 k,k+85,rigid+B\_End,-Abut\_W/2-outlayerlength,-0.735,  
 k,k+86,rigid+B\_End,-Abut\_W/2,-0.735,  
 K,k+87,rigid+B\_End,-Deck\_W/2,-0.735,  
 K,k+88,rigid+B\_End,-2.16,-0.735,  
 K,k+89,rigid+B\_End,-1.3,-0.735,  
 K,k+90,rigid+B\_End,-R\_Gage/2,-0.735,  
 K,k+91,rigid+B\_End, R\_Gage/2,-0.735,  
 K,k+92,rigid+B\_End, 1.3,-0.735,  
 K,k+93,rigid+B\_End, 2.16,-0.735,  
 K,k+94,rigid+B\_End, Deck\_W/2,-0.735,  
 k,k+95,rigid+B\_End,Abut\_W/2,-0.735,  
 k,k+96,rigid+B\_End,Abut\_W/2+outlayerlength,-0.735,  
 k,k+97,rigid+B\_End,-Abut\_W/2-outlayerlength,-0.985,  
 k,k+98,rigid+B\_End,-Abut\_W/2,-0.985,  
 K,k+99,rigid+B\_End,-Deck\_W/2,-0.985,  
 K,k+100,rigid+B\_End,-2.16,-0.985,  
 K,k+101,rigid+B\_End,-1.3,-0.985,  
 K,k+102,rigid+B\_End,-R\_Gage/2,-0.985,  
 K,k+103,rigid+B\_End, R\_Gage/2,-0.985,  
 K,k+104,rigid+B\_End, 1.3,-0.985,  
 K,k+105,rigid+B\_End, 2.16,-0.985,  
 K,k+106,rigid+B\_End, Deck\_W/2,-0.985,  
 k,k+107,rigid+B\_End,Abut\_W/2,-0.985,  
 k,k+108,rigid+B\_End,Abut\_W/2+outlayerlength,-0.985,  
 k,k+109,rigid+B\_End,-Abut\_W/2-outlayerlength,-5.805,  
 k,k+110,rigid+B\_End,-Abut\_W/2,-5.805,  
 k,k+111,rigid+B\_End,-Deck\_W/2,-5.805,  
 k,k+112,rigid+B\_End,-2.16,-5.805,

## Appendix A (Continued)

k,k+113,rigid+B\_End,-1.3,-5.805,  
 k,k+114,rigid+B\_End,-R\_Gage/2,-5.805,  
 k,k+115,rigid+B\_End,R\_Gage/2,-5.805,  
 k,k+116,rigid+B\_End,1.3,-5.805,  
 k,k+117,rigid+B\_End,2.16,-5.805,  
 k,k+118,rigid+B\_End,Deck\_W/2,-5.805,  
 k,k+119,rigid+B\_End,Abut\_W/2,-5.805,  
 k,k+120,rigid+B\_End,Abut\_W/2+outlayerlength,-5.805,

a,k+1,k+7,k+8,k+2  
 a,k+2,k+8,k+9,k+3  
 a,k+3,k+9,k+10,k+4  
 a,k+4,k+10,k+11,k+5  
 a,k+5,k+11,k+12,k+6  
 a,k+7,k+16,k+17,k+8  
 a,k+8,k+17,k+18,k+9  
 a,k+9,k+18,k+19,k+10  
 a,k+10,k+19,k+20,k+11  
 a,k+11,k+20,k+21,k+12  
 a,k+13,k+25,k+26,k+14  
 a,k+14,k+26,k+27,k+15  
 a,k+15,k+27,k+28,k+16  
 a,k+16,k+28,k+29,k+17  
 a,k+17,k+29,k+30,k+18  
 a,k+18,k+30,k+31,k+19  
 a,k+19,k+31,k+32,k+20  
 a,k+20,k+32,k+33,k+21  
 a,k+21,k+33,k+34,k+22  
 a,k+22,k+34,k+35,k+23  
 a,k+23,k+35,k+36,k+24  
 a,k+25,k+37,k+38,k+26  
 a,k+26,k+38,k+39,k+27  
 a,k+27,k+39,k+40,k+28  
 a,k+28,k+40,k+41,k+29  
 a,k+29,k+41,k+42,k+30  
 a,k+30,k+42,k+43,k+31  
 a,k+31,k+43,k+44,k+32  
 a,k+32,k+44,k+45,k+33  
 a,k+33,k+45,k+46,k+34  
 a,k+34,k+46,k+47,k+35  
 a,k+35,k+47,k+48,k+36  
 a,k+37,k+49,k+50,k+38

## Appendix A (Continued)

a,k+38,k+50,k+51,k+39  
 a,k+39,k+51,k+52,k+40  
 a,k+40,k+52,k+53,k+41  
 a,k+41,k+53,k+54,k+42  
 a,k+42,k+54,k+55,k+43  
 a,k+43,k+55,k+56,k+44  
 a,k+44,k+56,k+57,k+45  
 a,k+45,k+57,k+58,k+46  
 a,k+46,k+58,k+59,k+47  
 a,k+47,k+59,k+60,k+48  
 a,k+49,k+61,k+62,k+50  
 a,k+50,k+62,k+63,k+51  
 a,k+51,k+63,k+64,k+52  
 a,k+52,k+64,k+65,k+53  
 a,k+53,k+65,k+66,k+54  
 a,k+54,k+66,k+67,k+55  
 a,k+55,k+67,k+68,k+56  
 a,k+56,k+68,k+69,k+57  
 a,k+57,k+69,k+70,k+58  
 a,k+58,k+70,k+71,k+59  
 a,k+59,k+71,k+72,k+60  
 a,k+61,k+73,k+74,k+62  
 a,k+62,k+74,k+75,k+63  
 a,k+63,k+75,k+76,k+64  
 a,k+64,k+76,k+77,k+65  
 a,k+65,k+77,k+78,k+66  
 a,k+66,k+78,k+79,k+67  
 a,k+67,k+79,k+80,k+68  
 a,k+68,k+80,k+81,k+69  
 a,k+69,k+81,k+82,k+70  
 a,k+70,k+82,k+83,k+71  
 a,k+71,k+83,k+84,k+72  
 a,k+85,k+97,k+98,k+86  
 a,k+86,k+98,k+99,k+87  
 a,k+87,k+99,k+100,k+88  
 a,k+88,k+100,k+101,k+89  
 a,k+89,k+101,k+102,k+90  
 a,k+90,k+102,k+103,k+91  
 a,k+91,k+103,k+104,k+92  
 a,k+92,k+104,k+105,k+93  
 a,k+93,k+105,k+106,k+94  
 a,k+94,k+106,k+107,k+95

## Appendix A (Continued)

```

a,k+95,k+107,k+108,k+96
a,k+97,k+109,k+110,k+98
a,k+98,k+110,k+111,k+99
a,k+99,k+111,k+112,k+100
a,k+100,k+112,k+113,k+101
a,k+101,k+113,k+114,k+102
a,k+102,k+114,k+115,k+103
a,k+103,k+115,k+116,k+104
a,k+104,k+116,k+117,k+105
a,k+105,k+117,k+118,k+106
a,k+106,k+118,k+119,k+107
a,k+107,k+119,k+120,k+108
!---- MESHING THE VERTICAL LINES:
*get,lv1,line,905,leng,,
lsl,s,length,,lv1
LESIZE,ALL,,B_Depth_Z_Ele1,,1,,0
*get,lv2,line,907,leng,,
lsl,s,length,,lv2
LESIZE,ALL,,B_Depth_Z_Ele1,,1,,0
*get,lv12,line,921,leng,,
lsl,s,length,,lv12
LESIZE,ALL,,B_Depth_Z_Ele2,,1,,0
*get,lv22,line,923,leng,,
lsl,s,length,,lv22
LESIZE,ALL,,B_Depth_Z_Ele2,,1,,0
*get,lv3,line,932,leng,,
lsl,s,length,,lv3
LESIZE,ALL,,D_Depth_Z_Ele,,1,,0
*get,lv5,line,961,leng,,
lsl,s,length,,lv5
LESIZE,ALL,,vert1*2/6,,1,,0
*get,lv5,line,984,leng,,
lsl,s,length,,lv5
LESIZE,ALL,,vert1*4/6,,1,,0
*get,lv6,line,1007,leng,,
lsl,s,length,,lv6
LESIZE,ALL,,vert2,,1,,0
*get,lv7,line,1030,leng,,
lsl,s,length,,lv7
LESIZE,ALL,,vert3,,1,,0
*get,lv17,line,1087,leng,,
lsl,s,length,,lv17

```

## Appendix A (Continued)

```

LESIZE,ALL, , ,6, ,1, , ,0
!----- MESHING THE HORIZONTAL LINES:
*get,lh1,line,935,leng,,
lsl,s,length,,lh1
LESIZE,ALL, , ,SB_OUT_Y_Ele, ,1, , ,0
*get,lh2,line,938,leng,,
lsl,s,length,,lh2
LESIZE,ALL, , ,A_OUT_Y_Ele, ,1, , ,0
*get,lh3,line,941,leng,,
lsl,s,length,,lh3
LESIZE,ALL, , ,D_OUT_Y_Ele, ,1, , ,0
*get,lh4,line,908,leng,,
lsl,s,length,,lh4
LESIZE,ALL, , ,B_OUT_Y_Ele, ,1, , ,0
*get,lh5,line,906,leng,,
lsl,s,length,,lh5
LESIZE,ALL, , ,B_OUT_Y_Ele, ,1, , ,0
*get,lh5,line,922,leng,,
lsl,s,length,,lh5
LESIZE,ALL, , ,B_OUT_Y_Ele, ,1, , ,0
*get,lh6,line,911,leng,,
lsl,s,length,,lh6
LESIZE,ALL, , ,S_OUT_Y_Ele, ,1, , ,0
*get,lh7,line,914,leng,,
lsl,s,length,,lh7
LESIZE,ALL, , ,Middle_Y, ,1, , ,0
ET,100,SHELL181
amesh,all
lsl,all
!----- (( creating The sleepers )) -----!
TYPE,1
MAT,2
secnum,2

*GET,K1,KP,,COUNT, , , ,
K,K1+1,rigid,-1.3,-0.135,
K,K1+2,rigid,-R_Gage/2,-0.135,
K,K1+3,rigid, R_Gage/2,-0.135,
K,K1+4,rigid, 1.3,-0.135,

*get,Nlines,line,,count
LSTR, K1+1, K1+2

```

## Appendix A (Continued)

```

LSTR, K1+2, K1+3
LSTR, K1+3, K1+4

S_1=Nlines+1
S_2=Nlines+2
S_3=Nlines+3

lssel,s,line,,S_1
Lesize,S_1,,,S_OUT_Y_Ele,,,,,0
lssel,s,line,,S_3
Lesize,S_3,,,S_OUT_Y_Ele,,,,,0
lssel,s,line,,S_2
Lesize,S_2,,,Middle_Y,,,,,0

lssel,s,line,,S_1,S_3
lmesh,all
lgen,N_S, all,,,DBS,,,,,0
allsel
!*
nummrg,node
numcmp,node
!*
!-----!
! EXTRUDING THE BALST !
!-----!
TYPE, 2
MAT,4 ! extruding the ballast
extopt,esize,(Tot_R_len)/DBS*NE_S,0
extopt,aclear,1
asel,s,area,,1,10
vext,all,,,Tot_R_len
!*
MAT,5 ! extruding the subballast
extopt,esize, (Rail_out)/DBS*NE_S
extopt,aclear,1
asel,s,area,,11,14
asel,a,area,,18,21
vext,all,,,Rail_out
!*
extopt,esize, (6)/DBS*NE_S
extopt,aclear,1
asel,s,area,,66,76

```

## Appendix A (Continued)

```

vext,all,,,6
!*
extopt,esize,(Rail_out-Slap_L)/DBS*NE_S,0
extopt,aclear,1
asel,s,area,,15,17
vext,all,,,Rail_out-Slap_L
!*
MAT,22      ! extruding the Slab
extopt,esize,(Slap_L/DBS)*NE_S,0
asel,s,area,,204
asel,a,area,,209,213,4
vext,all,,,Slap_L
!*
allsel
*get,ks4,kp,,count
k,ks4+1,rigid+Rail_out-Slap_L,-1.3,-0.985
k,ks4+2,rigid+Rail_out-0.6,-1.3,-0.985
k,ks4+3,rigid+Rail_out-0.6,-1.3,-0.985-(4.8/5)
k,ks4+4,rigid+Rail_out-Slap_L,-1.3,-0.985-(4.8/5)
!*
*get,ar1,area,,count
a,ks4+1,ks4+2,ks4+3
a,ks4+1,ks4+3,ks4+4
!*
lsl,s,length,,(4.8/5)
lesize,all,,,2,,1,,0
lsl,s,length,,(Slap_L-0.6)
lesize,all,,,((Slap_L-0.6)/DBS)*NE_S,,1,,0

lsl,s,line,,1450
lesize,all,,,15
!*
ET,100,SHELL181
asel,s,area,,ar1+1,ar1+2
amesh,all
!*
TYPE,      2
extopt,esize,S_OUT_Y_Ele,0
extopt,aclear,1
asel,s,area,,230
vext,all,,,1.3-R_Gage/2
!*

```

## Appendix A (Continued)

```

extopt,esize,Middle_Y,0
asel,s,area,,232
vext,all,,,R_Gage
!*
extopt,esize,S_OUT_Y_Ele,0
asel,s,area,,236
vext,all,,,1.3-R_Gage/2
allsel
!*
MAT,7      ! extruding the deck
extopt,esize,(Rail_bridge)/DBS*NE_S,0
asel,s,area,,130,138,4
asel,a,area,,217
asel,a,area,,222,226,4
asel,a,area,,142
asel,a,area,,147,151,4
vext,all,,,Rail_bridge
!*
!*
MAT,6      ! extruding the sub-grade
extopt,esize,S_OUT_Y_Ele,0
extopt,aclear,1
asel,s,area,,231
vext,all,,,1.3-R_Gage/2
!*
extopt,esize,Middle_Y,0
asel,s,area,,283
vext,all,,,R_Gage
!*
extopt,esize,S_OUT_Y_Ele,0
asel,s,area,,287
vext,all,,,1.3-R_Gage/2
extopt,esize,B_OUT_Y_Ele,0
asel,s,area,,230,231
vext,all,,,-(2.16-1.3)
!*
extopt,esize,D_OUT_Y_Ele,0
asel,s,area,,295,299,4
vext,all,,,-(Deck_W/2-2.16)
!*
extopt,esize,A_OUT_Y_Ele,0
asel,s,area,,302,306,4

```

## Appendix A (Continued)

```

vext,all,,,-(Abut_W/2-Deck_W/2)
!*
extopt,esize,SB_OUT_Y_Ele,0
asel,s,area,,309,313,4
vext,all,,,-(Abut_W/2+outlayerlength-Abut_W/2)
!*
extopt,esize,B_OUT_Y_Ele,0
asel,s,area,,240
asel,a,area,,291
vext,all,,, (2.16-1.3)
!*
extopt,esize,D_OUT_Y_Ele,0
asel,s,area,,323,327,4
vext,all,,, (Deck_W/2-2.16)
!*
extopt,esize,A_OUT_Y_Ele,0
asel,s,area,,331,335,4
vext,all,,, (Abut_W/2-Deck_W/2)
!*
extopt,esize,SB_OUT_Y_Ele,0
asel,s,area,,339,343,4
vext,all,,, (Abut_W/2+outlayerlength-Abut_W/2)
!*
extopt,esize,(Rail_out-Slap_L)/DBS*NE_S,0
extopt,aclear,1
asel,s,area,,22,32
vext,all,,,Rail_out-Slap_L
!*
extopt,esize,(Rail_out-0.6)/DBS*NE_S,0
extopt,aclear,1
asel,s,area,,33,43
vext,all,,,Rail_out-0.6
!*
extopt,esize,(Rail_out-2.4-0.6)/DBS*NE_S,0
extopt,aclear,1
asel,s,area,,44,54
vext,all,,,Rail_out-2.4-0.6
!*
Mat,8          ! The abutments
extopt,esize,(0.6)/DBS*NE_S,0
asel,s,area,,234,242,4
asel,a,area,,297,318,7

```

## Appendix A (Continued)

```

asel,a,area,,325,349,8
asel,a,area,,400
asel,a,area,,405,441,4
vext,all,,0.6
!*
extopt,esize,(0.6)/DBS*NE_S,0
asel,s,area,,490
asel,a,area,,495,531,4
asel,a,area,,535
asel,a,area,,540,576,4
vext,all,,0.6
!*
extopt,esize,(1.2)/DBS*NE_S,0
asel,s,area,,77,87
vext,all,,-1.2
!*
extopt,esize,SB_Depth_Z_Ele,0
asel,s,area,,608,624,16
asel,a,area,,674,714,40
vext,all,,,,0.25
!*
extopt,esize,(4.8)/DBS*NE_S,0
asel,s,area,,445
asel,a,area,,450,486,4
vext,all,,,4.8      !2.4+1.2+1.2
!*
MAT,6
extopt,esize,(Rail_bridge-4.2)/DBS*NE_S,0
asel,s,area,,735
asel,a,area,,740,776,4,4
vext,all,,,Rail_bridge-4.2
!*
extopt,esize,(6)/DBS*NE_S,0
extopt,aclear,1
asel,s,area,,77,87
vext,all,,,6
allsel
!*
Mat,8      ! The abutments
extopt,esize,(4.8)/DBS*NE_S,0
asel,s,area,,780
asel,a,area,,785,821,4

```

## Appendix A (Continued)

```

vext,all,,,4.8
allsel
!*
Mat,6
extopt,esize,(6-2.4)/DBS*NE_S,0 ,0
asel,s,area,,870
asel,a,area,,875,911,4
vext,all,,, (6-2.4)
!*
extopt,esize,Tot_R_len/DBS*NE_S,0 ,0
asel,s,area,,55,65
vext,all,,,Tot_R_len
allsel
nummrg,node
numcmp,node
!----- CREATING THE five beams
TYPE,1
MAT,3
secnum,3
!*
*GET,k0,kp,,count,,,
k,k0+1,rigid+Rail_out, -Deck_W/2,-0.985,,,
k,k0+2,rigid+Rail_out+E_L,-Deck_W/2,-0.985,,,
k,k0+3,rigid+Rail_out, -1.3,-0.985,,,
k,k0+4,rigid+Rail_out+E_L,-1.3,-0.985,,,
k,k0+5,rigid+Rail_out,0,-0.985,,,
k,k0+6,rigid+Rail_out+E_L,0,-0.985,,,
k,k0+7,rigid+Rail_out, 1.3,-0.985,,,
k,k0+8,rigid+Rail_out+E_L, 1.3,-0.985,,,
k,k0+9,rigid+Rail_out, Deck_W/2,-0.985,,,
k,k0+10,rigid+Rail_out+E_L, Deck_W/2,-0.985,,,
!*
*get,LB,line,,count,,
L,k0+1,k0+2
L,k0+3,k0+4
L,k0+5,k0+6
L,k0+7,k0+8
L,k0+9,k0+10
Lesize,LB+1,LB+5,,1,,,,,0
LMESH,LB+1,LB+5
LGEN,NE_B,LB+1,LB+5, ,E_L, , , ,0
!----- Creating the fastnerssprings -----!

```

## Appendix A (Continued)

```

type,9
mat,9
real,9

lsel,all
*get,k1,kp,,count
K,k1+1,rigid,-0.75565,0.06924,
K,k1+2,rigid,-0.75565,-0.135,
K,k1+3,rigid, 0.75565,0.06924,
K,k1+4,rigid, 0.75565,-0.135,
L,k1+1,k1+2,1,,,
L,k1+3,k1+4,1,,,
*get,l1,line,,count,,
LMESH,l1-1,l1
LGEN,N_S,l1-1,l1, ,DBS, , , ,0
!----- y -----!
type,10
mat,10
real,10
*get,k2,kp,,count
K,k2+1,rigid,-0.75565,0.06924,
K,k2+2,rigid,-0.75565,-0.135,
K,k2+3,rigid, 0.75565,0.06924,
K,k2+4,rigid, 0.75565,-0.135,
L,k2+1,k2+2,1,,,
L,k2+3,k2+4,1,,,
*get,l2,line,,count,,
LMESH,l2-1,l2
LGEN,N_S,l2-1,l2, ,DBS, , , ,0
!----- Z -----!
type,11
mat,11
real,11
*get,k3,kp,,count
K,k3+1,rigid,-0.75565,0.06924,
K,k3+2,rigid,-0.75565,-0.135,
K,k3+3,rigid, 0.75565,0.06924,
K,k3+4,rigid, 0.75565,-0.135,
L,k3+1,k3+2,1,,,
L,k3+3,k3+4,1,,,
*get,l3,line,,count,,
LMESH,l3-1,l3

```

## Appendix A (Continued)

```

LGEN,N_S,13-1,13, ,DBS, , ,0
!-----APPLYING INITIAL CONDITIONS -----!
allsel
nummrg,node
numcmp,node
numcmp,elem

nsel,all
IC,all,all,0,0
!----- APPLYING THE BOUNDARY CONDITIONS -----!
allsel
nsel,s,loc,y,Abut_W/2+outlayerlength
nsel,a,loc,y,-Abut_W/2-outlayerlength
D,all,UY,0
allsel
!*
nsel,s,loc,X,rigid
nsel,a,loc,X,Tot_R_len+rigid
D,all,UX,0
!*
allsel
nsel,s,loc,Z,-5.805-Lowerdepth-LDSG
D,all,UX,0
D,all,UY,0
D,all,UZ,0
allsel

nsel,s,node,,1,2
nsel,a,node,,nend-1,nend+2
nsel,a,node,,nend2-1,nend2
D,all,UX,0
D,all,UY,0
D,all,UZ,0
D,all,ROTX,0
D,all,ROTY,0
D,all,ROTZ,0
allsel

nsel,s,node,,2,452,9
nsel,a,node,,455,905,9
D,all,ROTX,0
!D,all,ROTy,0

```

## Appendix A (Continued)

```

!D,all,ROTz,0
allsel

esel,s,mat,,2
nsle
D,all,ROTX,0
D,all,ROTY,0
D,all,ROTZ,0
allsel

esel,s,mat,,3
nsle
D,all,ROTX,0
D,all,ROTY,0
D,all,ROTZ,0
allsel

/dbc,u,,0
/pnum,mat,1
/num,1
eplot
!          SOLUTION          !
!--  MODAL ANALYSIS  --!
/solu
allsel
outres,all,all
ANTYPE,MODAL
MODOPT,LANB,300
MXPAND,300
SOLVE
FINISH
! For applying the dsplacements from SAMS to ANSYS:
!          SOLUTION          !
/solu
n_Col=6          !number of columns in the data sheet
to_skip=0        !number of lines to skip
num_tim_step=1200 !number of time steps
Num_Nodes=65522  !number of nodes in the model

/INQUIRE,numlines,LINES,Nodal_coord,csv
to_read=numlines-to_skip
!

```

## Appendix A (Continued)

```

*DEL,bc_table,,NOPR
! Number of rows reduced by one:
*DIM,bc_table,TABLE,to_read-1,n_Col-1          ! table array to hold data
*TREAD,bc_table,Nodal_coord,csv,,to_skip

! Move data to numerical Array
*DEL,bc_array,,NOPR
*DIM,bc_array,ARRAY,to_read,n_Col

*do,j,1,n_Col
*vfun,bc_array(1,j),copy,bc_table(0,j-1)      ! Shift down and right
*enddo

*do,j,1,num_tim_step
*do,i,1,Num_Nodes,
D,i,UX,bc_array(i+Num_nodes*(J-1),1)
D,i,UY,bc_array(i+Num_nodes*(J-1),2)
D,i,UZ,bc_array(i+Num_nodes*(J-1),3)
D,i,ROTX,bc_array(i+Num_nodes*(J-1),4)
D,i,ROTY,bc_array(i+Num_nodes*(J-1),5)
D,i,ROTZ,bc_array(i+Num_nodes*(J-1),6)
*enddo
/solu
Time,j
allsel
solve
OUTRES,all,all
save
*enddo
FINISH

```

## Appendix B

### APDL ANSYS TO SAMS CODE

This code ANSYS -APDL that is used to extract the needed data for SAMS from the Modal analysis on ANSYS

```

NumExportModes = 500
StartMode = 1
!-----!
EndMode = StartMode + NumExportModes - 1
/POST1
*cfopen, FEM_Output, txt, ,

! Output NumNodes
*get, NumNodes, NODE, 0, COUNT
*vwrite, 'NumNodes'
(a8)
*vwrite, NumNodes
(f8.0)
*vwrite, 'NumModes'
(a8)
*vwrite, NumExportModes
(f6.0)
! the following is the density of each part,
! these values varies depnds on the used model.
!---- the beam elemnts parts: Rails, sleepers, and Beams
MassDensity_P1= 7700
MassDensity_P2= 2570
MassDensity_P3= 2500
!---- the soil layers: Ballast, Sub-ballast, sub_grade, Deck, Abutment
MassDensity_P4= 1800
MassDensity_P5= 1850
MassDensity_P6= 1850
MassDensity_P7= 2500
MassDensity_P8= 2500

```

## Appendix B (Continued)

```

MassDensity_P22= 2600
!---- the spring elemnts :
MassDensity_P9= 0
MassDensity_P10= 0
MassDensity_P11= 0
MassDensity_P12= 0
MassDensity_P13= 0
MassDensity_P14= 0
MassDensity_P15= 0
MassDensity_P16= 0
MassDensity_P17= 0
MassDensity_P18= 0
MassDensity_P19= 0
MassDensity_P20= 0
MassDensity_P21= 0
! Output nodal positions
*vwrite, 'Node Pos'
(a8)
*get, StartNode, NODE, 0, NUM, MIND
NodeI = StartNode

EnumI = 1
*dowhile, NodeI
NodeX = nx(NodeI)
NodeY = ny(NodeI)
NodeZ = nz(NodeI)

*vwrite, EnumI, NodeI, NodeX, NodeY, NodeZ
(2f8.0, 3e25.16)

NodeI = ndnext(NodeI)
EnumI = EnumI + 1
*enddo

! Output frequencies
*vwrite, 'Freqs'
(a5)

*do, ModeI, StartMode, EndMode
*get, ModeFreq, MODE, ModeI, FREQ
*vwrite, ModeI, ModeFreq
(f6.0, e24.16)

```

## Appendix B (Continued)

```

*enddo
! Output all mode shapes
*vwrite, 'Mode Sha', 'pe'
(a8, a2)

!Skip to the first displacements that represent
!the first mode that is desired to be output.
SET, FIRST
*if, StartMode, NE, 1, then
*do, ModeI, 1, StartMode-1
SET, NEXT
*enddo
*endif

*do, ModeI, StartMode, EndMode
*vwrite, 'Mode ', ModeI
(a5, f5.0)
! Output one mode shape
NodeI = StartNode
!For each node, output its mode shape
EnumI = 1
*dowhile, NodeI
DispX = ux(NodeI)
DispY = uy(NodeI)
DispZ = uz(NodeI)
RotX  = rotx(NodeI)
RotY  = roty(NodeI)
RotZ  = rotz(NodeI)

*vwrite, EnumI, NodeI, DispX, DispY, DispZ, RotX, RotY, RotZ
(2f8.0, 6e25.16)

NodeI = ndnext(NodeI)
EnumI = EnumI + 1
*enddo
SET, NEXT
*enddo
! Compute nodal masses
!Allocate mem for nodes
*get, NodeMaxI, NODE, 0, NUM, MAXD
*dim, NodalMass, , NodeMaxI

```

## Appendix B (Continued)

```

! initializing the nodal mass.
*do, NodeI, 1, NodeMaxI
NodalMass(NodeI) = 0
*enddo
!Compute mass of each elem and add mass to each node in the elem
!_____ MODIFY _____!
*get, ElemI, ELEM, 0, NUM, MIND
*dowhile, ElemI

*get, ElemVol, elem, ElemI, VOLU

*if,ElemI,GE,1,AND,ElemI,LE,726,then
*if,ElemI,GE,1,AND,ElemI,LE,360,then
MassDensity=MassDensity_P1
*elseif,ElemI,GE,361,AND,ElemI,LE,726,then
MassDensity=MassDensity_P2
*endif

Node1 = nelem(ElemI, 1)
Node2 = nelem(ElemI, 2)

PartialMass = ElemVol*MassDensity/2

NodalMass(Node1) = NodalMass(Node1) + PartialMass
NodalMass(Node2) = NodalMass(Node2) + PartialMass

*elseif,ElemI,GE,727,AND,ElemI,LE,34662,then

*if,ElemI,GE,727,AND,ElemI,LE,7926,then
MassDensity=MassDensity_P4
*elseif,ElemI,GE,7927,AND,ElemI,LE,11766,then
MassDensity=MassDensity_P5
*elseif,ElemI,GE,11767,AND,ElemI,LE,12486,then
MassDensity=MassDensity_P7
*elseif,ElemI,GE,12487,AND,ElemI,LE,18822,then
MassDensity=MassDensity_P6
*elseif,ElemI,GE,18823,AND,ElemI,LE,20646,then
MassDensity=MassDensity_P8
*elseif,ElemI,GE,20647,AND,ElemI,LE,21798,then
MassDensity=MassDensity_P6
*elseif,ElemI,GE,21799,AND,ElemI,LE,22566,then
MassDensity=MassDensity_P8

```

## Appendix B (Continued)

```

*elseif,ElemI,GE,22567,AND,ElemI,LE,34662,then
MassDensity=MassDensity_P6
*endif

Node1 = nelem(ElemI, 1)
Node2 = nelem(ElemI, 2)
Node3 = nelem(ElemI, 3)
Node4 = nelem(ElemI, 4)
Node5 = nelem(ElemI, 5)
Node6 = nelem(ElemI, 6)
Node7 = nelem(ElemI, 7)
Node8 = nelem(ElemI, 8)

PartialMass = ElemVol*MassDensity/8

NodalMass(Node1) = NodalMass(Node1) + PartialMass
NodalMass(Node2) = NodalMass(Node2) + PartialMass
NodalMass(Node3) = NodalMass(Node3) + PartialMass
NodalMass(Node4) = NodalMass(Node4) + PartialMass
NodalMass(Node5) = NodalMass(Node5) + PartialMass
NodalMass(Node6) = NodalMass(Node6) + PartialMass
NodalMass(Node7) = NodalMass(Node7) + PartialMass
NodalMass(Node8) = NodalMass(Node8) + PartialMass

*elseif,ElemI,GE,34663,AND,ElemI,LE,59551,then

*if,ElemI,GE,34663,AND,ElemI,LE,35442,then
MassDensity=MassDensity_P3
*elseif,ElemI,GE,35443,AND,ElemI,LE,35564,then
MassDensity=MassDensity_P9
*elseif,ElemI,GE,35565,AND,ElemI,LE,35686,then
MassDensity=MassDensity_P10
*elseif,ElemI,GE,35687,AND,ElemI,LE,35808,then
MassDensity=MassDensity_P11
*elseif,ElemI,GE,35809,AND,ElemI,LE,35878,then
MassDensity=MassDensity_P12
*elseif,ElemI,GE,35879,AND,ElemI,LE,338955,then
MassDensity=MassDensity_P13
*elseif,ElemI,GE,38956,AND,ElemI,LE,42032,then
MassDensity=MassDensity_P14
*elseif,ElemI,GE,42033,AND,ElemI,LE,45109,then
MassDensity=MassDensity_P15

```

## Appendix B (Continued)

```

*elseif,ElemI,GE,45110,AND,ElemI,LE,47267,then
MassDensity=MassDensity_P16
*elseif,ElemI,GE,47268,AND,ElemI,LE,49425,then
MassDensity=MassDensity_P17
*elseif,ElemI,GE,49426,AND,ElemI,LE,51583,then
MassDensity=MassDensity_P18
*elseif,ElemI,GE,51584,AND,ElemI,LE,53741,then
MassDensity=MassDensity_P16
*elseif,ElemI,GE,53742,AND,ElemI,LE,55899,then
MassDensity=MassDensity_P17
*elseif,ElemI,GE,55900,AND,ElemI,LE,58057,then
MassDensity=MassDensity_P18
*elseif,ElemI,GE,58058,AND,ElemI,LE,58306,then
MassDensity=MassDensity_P19
*elseif,ElemI,GE,58307,AND,ElemI,LE,58555,then
MassDensity=MassDensity_P20
*elseif,ElemI,GE,58556,AND,ElemI,LE,58804,then
MassDensity=MassDensity_P21
*elseif,ElemI,GE,58805,AND,ElemI,LE,59053,then
MassDensity=MassDensity_P19
*elseif,ElemI,GE,59054,AND,ElemI,LE,59302,then
MassDensity=MassDensity_P20
*elseif,ElemI,GE,59303,AND,ElemI,LE,59551,then
MassDensity=MassDensity_P21
*endif

Node1 = nelem(ElemI, 1)
Node2 = nelem(ElemI, 2)
PartialMass = ElemVol*MassDensity/2
NodalMass(Node1) = NodalMass(Node1) + PartialMass
NodalMass(Node2) = NodalMass(Node2) + PartialMass

*endif
ElemI = elnext(ElemI)
*enddo

! Output nodal masses
*vwrite, 'Node Mas', 's'
(a8, a1)
NodeI = StartNode
EnumI = 1
*dowhile, NodeI

```

## Appendix B (Continued)

```
SingleMass = NodalMass(NodeI)
*vwrite, EnumI, NodeI, SingleMass
(2f8.0, e25.16)
```

```
NodeI = ndnext(NodeI)
EnumI = EnumI + 1
*enddo
*cfclos
FINISH
```

## Appendix C

### OBTAINING THE DEFORMATION FOR THE WHOLE MODEL

This Matlab file was used to rebuild the nodal displacement for the whole model

```

NN=65522; % Total number of nodes in the system
NNR=906;  % Number of nodes on the rails
NM=500;   % Number of mode shapes
DOF=6;    % number of nodal DOF
%---- CHECK you entered the needed data above ---%
%--- Reading the Modal coordinates data (q) ---%
fid_1 = fopen('Sams_modal_disp.dat','r');
[cn,count1]=fscanf(fid_1,'%f %f %f %f %f %f %f %f %f',[NM+1,inf]);
Q=cn';
q=Q(:,2:end); % FOR ALL TIME STEPS (timesteps X number of modes)

%--- Reading the Frequencies (f) ---%
fid_11 = fopen('Freqs.txt','r');
[cn1,count2]=fscanf(fid_11,'%f %f',[2,NM]);
f=cn1(2,:); % frequencies
Omeg=f*2*pi;
for i=1:N
    q(:,i)=q(:,i)/Omeg(i);
end
%--- Reading the mode shapes of the whole system ---%
fid_2 = fopen('MODE_SHAPES.txt','r');
% This file was extuded as FEM_Output but only for mode shapes
[cn,count1]=fscanf(fid_2,'%f %f %f %f %f %f %f %f %f',[DOF+2,inf]);
MODES=cn';

PHI=MODES(:,3:end); %--- The all modes for the whole system (NN*NM)X DOF
phi=PHI';
phi=phi(:);

modes_modif=zeros(NN*DOF,NM);
for i=1:N
    modes_modif(:,i)=phi(1+NN*DOF*(i-1):NN*DOF+NN*DOF*(i-1)); % NDOFXNM

```

## Appendix C (Continued)

```

end


TS=length(Q); % the number of time steps
U=zeros(NN*TS,DOF); % Initializing U

for i=1:TS;
u=modes_modif*q(i,:);
u1=reshape(u,DOF,NN);
U(1+NN*(i-1):NN+NN*(i-1),:)=u1;
end;
%-----%
%----- Writing U for a file -----%
%-----%
csvwrite('Nodal_coord.csv',U);
fclose('all');

```


## Appendix D

### PAPER COPYRIGHT PERMISSION



**RightsLink®**

[Home](#)
[Account Info](#)
[Help](#)
[Live Chat](#)



**Title:** Coupled finite element and multibody system dynamics modeling of a three-dimensional railroad system :

**Author:** Ahmed I El-Ghandour, Martin B Hamper, Craig D Foster

**Publication:** Proceedings of the Institution of Mechanical Engineers, Part F: Journal of Rail and Rapid Transit

**Publisher:** SAGE Publications

**Date:** 01/01/2016

Copyright © 2016, © SAGE Publications

Logged in as:  
Ahmed El

[Logout](#)

#### Gratis Reuse

- Without further permission, as the Author of the journal article you may:
  - post the accepted version (version 2) on your personal website, department's website or your institution's repository. You may NOT post the published version (version 3) on a website or in a repository without permission from SAGE.
  - post the accepted version (version 2) of the article in any repository other than those listed above 12 months after official publication of the article.
  - use the published version (version 3) for your own teaching needs or to supply on an individual basis to research colleagues, provided that such supply is not for commercial purposes.
  - use the accepted or published version (version 2 or 3) in a book written or edited by you. To republish the article in a book NOT written or edited by you, permissions must be cleared on the previous page under the option 'Republish in a Book/Journal' by the publisher, editor or author who is compiling the new work.
- When posting or re-using the article electronically, please link to the original article and cite the DOI.
- All other re-use of the published article should be referred to SAGE. Contact information can be found on the bottom of our '[Journal Permissions](#)' page.

[BACK](#)
[CLOSE WINDOW](#)

Copyright © 2016 Copyright Clearance Center, Inc. All Rights Reserved. [Privacy statement](#), [Terms and Conditions](#).  
Comments? We would like to hear from you. E-mail us at [customercare@copyright.com](mailto:customercare@copyright.com)

**CITED LITERATURE**

## Bibliography

- [1] American Railway Engineering and Maintenance-of-Way Association, 2009.
- [2] Shabana, A. A., Zaazaa, K. E., and Sugiyama, H.: Railroad vehicle dynamics: A computational approach. Taylor & Francis CRC, Boca Raton, FL, 2007.
- [3] Lundqvist, A. and Dahlberg, T.: Load impact on railway track due to unsupported sleepers. Journal of Rail and Rapid Transit, Proceedings of the Institution of Mechanical Engineers, Part F: J, 219(2):67–77, 2005.
- [4] Zhang, S., Xiao, X., Wen, Z., and Jin, X.: Effect of unsupported sleepers on wheel/rail normal load. Soil Dynamics and Earthquake Engineering, 28(8):662 – 673, 2008.
- [5] Zakeri, J. A., Fattahi, M., and Ghanimoghadam, M. M.: Influence of unsupported and partially supported sleepers on dynamic responses of train–track interaction. Journal of Mechanical Science and Technology, 29(6):2289–2295, 2015.
- [6] Recuero, A. M., Escalona, J. L., and Shabana, A. A.: Finite-element analysis of unsupported sleepers using three-dimensional wheel-rail contact formulation. Proceedings of the Institution of Mechanical Engineers, Part K: Journal of Multi-body Dynamics, 225(2):153–165, June 2011.
- [7] Wang, W. and xian Li, G.: Development of high-speed railway vehicle derailment simulation part i: A new wheel/rail contact method using the vehicle/rail coupled model. Engineering Failure Analysis, 24:77 – 92, 2012.
- [8] Barbosa, R. S.: A 3d contact force safety criterion for flange climb derailment of a railway wheel. Vehicle System Dynamics, 42(5):289–300, 2004.
- [9] Bao, T., Han, M., Chen, C., and Chen, S.: Study on the relationship between lateral offset of the center of gravity of goods c70 gondola and the derailment coefficient. In International Conference on Mechatronics, Electronic, Industrial and Control Engineering (MEIC 2015), 2015.
- [10] Sato, Y., Matsumoto, A., Ohno, H., Oka, Y., and Ogawa, H.: Wheel/rail contact analysis of tramways and {LRVs} against derailment. Wear, 265(910):1460 – 1464, 2008. Contact Mechanics and Wear of Rail/Wheel Systems - {CM2006}.
- [11] Huang, H. and Tutumluer, E.: Discrete element modeling for fouled railroad ballast. Construction and Building Materials, 25(8):3306 – 3312, 2011.
- [12] Brown, S., Kwan, J., and Thom, N.: Identifying the key parameters that influence geogrid reinforcement of railway ballast. Geotextiles and Geomembranes, 25(6):326 – 335, 2007.

## Appendix D (Continued)

- [13] Biempica, C. B., del Coz Daz, J., Nieto, P. G., and Snchez, I. P.: Nonlinear analysis of residual stresses in a rail manufacturing process by {FEM}. Applied Mathematical Modelling, 33(1):34 – 53, 2009.
- [14] Monfared, V.: Contact stress analysis in rolling bodies by finite element method (fem) statically. Journal of Mechanical Engineering and Automation, 2012.
- [15] Sladkowski, A. and Sitarz, M.: Analysis of wheelrail interaction using {FE} software. Wear, 258(78):1217 – 1223, 2005. Contact Mechanics and Wear of Rail/Wheel Systems.
- [16] Krácal, M., Trummer, G., and Daves, W.: Application of 2d finite element analysis to compare cracking behaviour in twin-disc tests and full scale wheel/rail experiments. Wear, 346347:140 – 147, 2016.
- [17] Arslan, M. A. and Kayabaşı, O.: 3-d railwheel contact analysis using {FEA}. Advances in Engineering Software, 45(1):325 – 331, 2012.
- [18] Molatefi, H. and Mozafari, H.: Analysis of new method for vertical load measurement in the barycenter of the rail web by using {FEM}. Measurement, 46(8):2313 – 2323, 2013.
- [19] XB, X., ZF, W., XS, J., and XZ, S.: Effects of track support failures on dynamic response of high speed tracks. International Journal of Nonlinear Sciences and Numerical Simulation, 8(4):615–630, 2007.
- [20] Xiao, X., Jin, X., Deng, Y., and Zhou, Z.: Effect of curved track support failure on vehicle derailment. Vehicle System Dynamics, 46(11):1029–1059, 2008.
- [21] Sae Siew, J., Mirza, O., and Kaewunruen, S.: Nonlinear finite element modelling of railway turnout system considering bearer/sleeper-ballast interaction. Structures, 2015.
- [22] Chen, Z., Shin, M., Wei, S., Andrawes, B., and Kuchma, D. A.: Finite element modeling and validation of the fastening systems and concrete sleepers used in north america. Proceedings of the Institution of Mechanical Engineers, Part F: Journal of Rail and Rapid Transit, 2014.
- [23] Chebli, H., Clouteau, D., and Schmitt, L.: Dynamic response of high-speed ballasted railway tracks: 3d periodic model and in situ measurements. Soil Dynamics and Earthquake Engineering, 28(2):118 – 131, 2008.
- [24] Kumaran, G., Menon, D., and Nair, K. K.: Dynamic studies of railtrack sleepers in a track structure system. Journal of Sound and Vibration, 268(3):485 – 501, 2003.
- [25] Koskinen, M.: Modeling of soil-structure interaction between railway bridge and soil. In ABAQUS Users' Conference, 2005.
- [26] Tarawneh, C. M., Fuentes, A. A., Kypuros, J. A., Navarro, L. A., Vaipan, A. G., and Wilson, B. M.: Thermal modeling of a railroad tapered-roller bearing using finite element analysis. Thermal Science and Engineering Applications, 4(3), 2012.

## Appendix D (Continued)

- [27] Masoudi, N. R., Shariati, M., and Farhangdoost, K.: 3d finite element simulation of residual stresses in uic60 rails during the quenching process. Thermal Science, (00):13–13, 2016.
- [28] Nejad, R. M.: Using three-dimensional finite element analysis for simulation of residual stresses in railway wheels. Engineering Failure Analysis, 45:449 – 455, 2014.
- [29] Mohan, P. M.: Analysis of railway wheel to study thermal and structural behaviour. International Journal of Scientific & Engineering Research, 2012.
- [30] Tutumluer, E.: Discrete element modeling of railroad ballast settlement. Doctoral dissertation, University of Illinois, 2007.
- [31] Shabana, A. A.: Dynamics of multibody systems. Cambridge University Press, 2005.
- [32] Ibrahimbegović, A., Mamouri, S., Taylor, R. L., and Chen, A. J.: Finite element method in dynamics of flexible multibody systems: Modeling of holonomic constraints and energy conserving integration schemes. Multibody System Dynamics, 4(2):195–223, 2000.
- [33] Busch, M. and Schweizer, B.: Coupled simulation of multibody and finite element systems: an efficient and robust semi-implicit coupling approach. Archive of Applied Mechanics, 82(6):723–741, 2011.
- [34] Heege, A., Betran, J., and Radovic, Y.: Fatigue load computation of wind turbine gearboxes by coupled finite element, multi-body system and aerodynamic analysis. Wind Energy, 10(5):395–413, 2007.
- [35] Shabana, A. A., Tobaa, M., Sugiyama, H., and Zaazaa, K. E.: On the computer formulations of the wheel/rail contact problem. Nonlinear Dynamics, 40(2):169–193, 2005.
- [36] Shabana, A. A. and Sany, J. R.: A survey of rail vehicle track simulations and flexible multibody dynamics. Nonlinear Dynamics, 26(2):179–212, 2001.
- [37] Liu, B. and Bruni, S.: A method for testing railway wheel sets on a full-scale roller rig. Vehicle System Dynamics, 53(9):1331–1348, 2015.
- [38] Recuero, A. M., Aceituno, J. F., Escalona, J. L., and Shabana, A. A.: A nonlinear approach for modeling rail flexibility using the absolute nodal coordinate formulation. Nonlinear Dynamics, 83(1):463–481, 2016.
- [39] Ling, L., Dhanasekar, M., Thambiratnam, D. P., and Sun, Y. Q.: Lateral impact derailment mechanisms, simulation and analysis. International Journal of Impact Engineering, 94:36 – 49, 2016.
- [40] Galvín, P., Romero, A., and Domínguez, J.: Fully three-dimensional analysis of high-speed train–track–soil–structure dynamic interaction. Journal of Sound and Vibration, 329(24):5147 – 5163, 2010.

## Appendix D (Continued)

- [41] Tanabe, M., Wakui, H., Sogabe, M., Matsumoto, N., and Tanabe, Y.: A combined multi-body and finite element approach for dynamic interaction analysis of high-speed train and railway structure including post-derailment behavior during an earthquake. IOP Conference Series: Materials Science and Engineering, 10(1):012144, 2010.
- [42] Ambrósio, J., Pombo, J., Rauter, F., and Pereira, M.: Multibody Dynamics: Computational Methods and Applications, chapter A Memory Based Communication in the Co-simulation of Multibody and Finite Element Codes for Pantograph-Catenary Interaction Simulation, pages 231–252. Dordrecht, Springer Netherlands, 2009.
- [43] El-Ghandour, A. I., Hamper, M. B., and Foster, C. D.: Coupled finite element and multibody system dynamics modeling of a three-dimensional railroad system. Proceedings of the Institution of Mechanical Engineers, Part F: Journal of Rail and Rapid Transit, 230(1):283–294, January 2016.
- [44] Briaud, J. L., James, R. W., and Hoffman, S. B.: Settlement of Bridge Approaches:(the Bump at the End of the Bridge)., volume 234. National Academy Press, 1997.
- [45] Monley, G. and Wu, J.: Tensile reinforcement effects on bridge approach settlement. Journal of Geotechnical Engineering, 119(4):749–762, 1993.
- [46] Helwany, S. M., Wu, J. T., and Froessl, B.: {GRS} bridge abutmentsan effective means to alleviate bridge approach settlement. Geotextiles and Geomembranes, 21(3):177 – 196, 2003.
- [47] Li, D. and Davis, D.: Transition of railroad bridge approaches. Journal of Geotechnical and Geoenvironmental Engineering, 131(11):1392–1398, 2005.
- [48] Dahlberg, T.: Railway track stiffness variations consequences and countermeasures. International Journal of Civil Engineering, 8(1):1–12, 2010.
- [49] Zhang, J., Zheng, J. J., , and Lu, Y.: Evaluation of the new technique of geogrid-reinforced and pile-supported embankment at bridge approach. Journal of Bridge Engineering, 19(4):06014001, 2014.
- [50] Paixao, A., Fortunato, E., and Calada, R.: Design and construction of backfills for railway track transition zones. Proceedings of the Institution of Mechanical Engineers, Part F: Journal of Rail and Rapid Transit, 2013.
- [51] Nicks, J. E.: The bump at the end of the railway bridge. Doctoral dissertation, Texas A&M University, 2009.
- [52] Hoppe, E. J.: Guidelines for the use, design, and construction of bridge approach slabs. No. VTRC 00-R4, 1999.
- [53] Shabana, A. A., Chamorro, R., and Rathod, C.: A multibody system approach for finite-element modeling of rail flexibility in railroad vehicle applications. Multi-body Dynamics, 222:115, 2007.

- [54] Rathod, C., Chamorro, R., Escalona, J. L., El-Sibaie, M., and Shabana, A. A.: Validation of a three-dimensional multibody system approach for modeling track flexibility. Multi-body Dynamics, 223:269281, 2009.
- [55] Shabana, A. A.: Computational continuum mechanics.. Cambridge, UK: Cambridge University Press, second edition, 2012.
- [56] Meli, E. and Pugi, L.: Preliminary development, simulation and validation of a weight in motion system for railway vehicles. Meccanica, 48(10):25412565., 2013.
- [57] Kalker, J.: Three-Dimensional Elastic Bodies in Rolling Contact. Kluwer Academic Publ, Dordrecht, 1 edition, 1990.
- [58] Shampine, L. and Gordon, M.: Computer solution of ordinary differential equations: the initial value problem.. San Francisco, CA: W.H. Freeman, 1975.
- [59] Shabana, A. A.: Computational Dynamics. John Wiley & Sons, 2010.
- [60] Cai, C., Shi, X., Voyiadjis, G., and Zhang, Z.: Structural performance of bridge approach slabs under given embankment settlement. Journal of Bridge Engineering, 10(4):482–489, 2005.

## VITA

### Ahmed I El-Ghandour

---

2701 S. Emerald Ave

Chicago, IL 60616

(312) 912-2617

aighandour@gmail.com

### HIGHLIGHTS OF QUALIFICATIONS

- More than 8 years of professional engineering and R&D experience in the field of Finite Element Analysis (FEA)
- Broad expertise in solving problems of structural, thermal heat conduction (transient and steady state), static, dynamic, and nonlinear nature using ANSYS-APDL scripting.
- Experience using FEM and MBS software separately and coupled. Extensive experience in programming using Matlab and good knowledge of Fortran
- Very well trained and motivated to work as an individual and as a team player

### SKILLS

- Modeling and Simulation, Finite Element Analysis (FEA), Computational Mechanics, Engineering Research and Development, Railroad Analysis, Linear and Nonlinear Structural

Mechanics, Structural Dynamics, Numerical Methods, Thermal Analysis, and Multibody System

- PROGRAMMING: MATLAB, FORTRAN, and APDL (ANSYS)
- CAE/CAD Tools: ANSYS (Classic-APDL and Workbench), LS-DYNA, AUTOCAD, SOLIDWORKS and INVENTOR

## **EDUCATION**

- *M. Sc., Mechanical Engineering, University of Illinois at Chicago (UIC), GPA 4.0/4.0. (Dec 2010)*
- *B. Sc., Mechanical Engineering, Cairo University, GPA 3.7/4.0. (May 2004)*

## **EXPERIENCE**

**University of Illinois at Chicago, Chicago, IL**

**Research/Teaching Assistant**

**August 2009-Oct 2016**

- Developed Finite elements (FE/FEA) models for rails and substructure (crossties, ballast, and subgrade) using ANSYS APDL. Work includes coupled FEA codes (ANSYS and in-house code) with multibody dynamic system (MBS) code.
- Built a bridge approach problem to study the stiffness variation effect on the rail deformation and the effect of the dynamic loads on the soil settlement and waves in the surrounding soil.

- Programed a FEA algorithm using MATLAB and implementing the heat elements in this code.
- Coded a MBS algorithm using FORTRAN which was used to implement higher level continuity on beam elements during the masters work.
- Modeled a FE problem to perform thermal analysis by testing the heat conduction for a nano-technology work related.
- Assisted in supervising M.Sc. and undergrad students, helping them with their FE models and graduation projects.

**GE, Global Research Center, Niskayuna, NY**

**Engineering Summer Intern**

**May 2014-Aug 2014**

- Worked with a design and analysis engineering team to design a new circuit breaker.
- Performed a detailed nonlinear finite element analysis using ANSYS workbench.
- Implemented design modifications to the device CAD/CAE 2D and 3D models using SOLIDWORKS to investigate the performance of the device and compared dynamic response of the current and proposed device design.

**SHARMA & ASSOCIATES, INC, Chicago, IL**

**Engineering Summer Intern**

**May 2013-Aug 2013**

- Investigated the VAMPIRE flexible track implementation for railroad models to document the method of stiffness specification in the model.
- Performed and documented in a technical report a detailed sensitivity analysis of a 3D rail car model using VAMPIRE to investigate the effect of track stiffness on the dynamic vehicle performance.

**Cairo University, Cairo, Egypt**

**Research/Teaching Assistant**

**Aug 2004-Jul 2009**

- Built a Nonlinear FEA model to study the deep drawing process of sheet metal using LS-DYNA including contact and deformation nonlinearity.
- Worked on designing an optimization model for the deep drawing process to optimize its main parameters.

**TEMPUS project, Cairo University, Cairo, Egypt**

**Risk Analyst**

**Jul 2004-Jul 2007**

- Worked as risk analyst and assisted in workshops, training courses, and management for buildings.

**Bureau Veritas, Paris, France**

**Engineering Summer Intern**

**Jul 2005-Sept 2005**

- Worked on developing guidelines for designing fire relevant to the shipping environment, and building a suitable extinguisher system (Fire Safety - Maritime Regulations- Different approaches of Design Fire).

**British Petroleum (BP), Cairo, Egypt**

**Engineering Summer Intern,Drilling Department**

**Jul 2004-Sept 2004**

- Worked on developing guidelines for designing fire relevant to the shipping environment, and building a suitable extinguisher system (Fire Safety - Maritime Regulations- Different approaches of Design Fire).

## **PUBLICATIONS**

- P. Yasaei, A. Fathizadeh, R. Hantehzadeh, A. K. Majee, **A. I. El-Ghandour**, D. Estrada, C. D. Foster, Z. Aksamija, F. Khalili-Araghi, and A. Salehi-Khojin. *Bi-modal Phonon Scattering in Graphene Grain Boundaries*. Nano letters,(2015):10.1021/acs.nanolett.5b01021
- **A. I. El-Ghandour**, M. B. Hamper, and C. D. Foster. *Coupled finite element and multibody system dynamics modeling of a three-dimensional railroad system*.

Proceedings of the Institution of Mechanical Engineers, Part F: Journal of Rail and Rapid Transit (2014): 0954409714539942.

- A. Shabana, **A. I. El-Ghandour**, and K. E. Zaazaa. *Study of the Effect of the Spiral Geometry on Wheel/Rail Contact Forces*. Journal of Multi-body Dynamics, 225(2), (2011), 111-125.
- Wifi, T. F. Abdelmaguid, and **A. I. El-Ghandour**. *A Review of the Optimization Techniques Applied To the Deep Drawing Process*. Proceedings of the 37th International Conference on Computers and Industrial Engineering, Alexandria, Egypt, (2007).

## **COURSES TAKEN**

Introductory Finite Element Analysis, Nonlinear Finite Element, Plasticity Theory, Continuum Mechanics, Computational Continuum Mechanics, Numerical Methods in Engineering, Computer Aided Analysis of Multibody Systems I and II, Intermed Vibration Theory, Structural Dynamics.

## **LANGUAGES**

**ARABIC:** Fluent - **ENGLISH:** Fluent - **FRENCH:** Fair.

## AWARDS AND AFFILIATIONS

- First place winner of the 2016 National University Rail Center (NURail) 3-min thesis presentation competition
- Arab American Association of Engineers and Architects Scholarship (2011, 2012, and 2013)
- Schlumberger Scholarship (2005). A scholarship awarded to the best graduation project and academic performance
- Cairo University Scholarship for Academic Distinction (2001 to 2004)
- Active member in Egyptians Abroad for Development (EAD), a non-profit, non-political organization working to serve Egypt in the fields of health, education, and economy.
- Vice-president and co-founder of EAD-UIC Chapter
- Treasurer and Sports Coordinator, the International Club (IC), UIC, 2013
- Taekwondo Instructor since 2010 and a certified Referee in both Egypt and USA.
- Singer at the Middle East Musical Ensemble (MEME)
- American Society of Mechanical Engineers (ASME)
- American Society of Civil Engineers (ASCE)
- Arab American Association for Engineers and Architects (AAAEA)

**LinkedIn:** <https://www.linkedin.com/in/Ahmed-El-Ghandour>